CR 92083

15 MAY 1967

LMSC-A874831
CODE Y-87-67-1

ENGINEERS HANDBOOK

LOW-G PROPELLANT BEHAVIOR

PREPARED UNDER CONTRACT NO. NAS 9-5174

For The
NATIONAL
AERONAUTICS
AND SPACE
ADMINISTRATION
MANNED SPACEFLIGHT CENTER
HOUSTON, TEXAS

LOCKHEED MISSILES & SPACE COMPANY
A GROUP DIVISION OF LOCKHEED AIRCRAFT CORPORATION
SUNNYVALE, CALIFORNIA

15 MAY 1967

LMSC-A874831
CODE Y-87-67-1

ENGINEERS HANDBOOK

LOW-G PROPELLANT BEHAVIOR

PREPARED UNDER CONTRACT NO. NAS 9-5174

Prepared by
H. M. SATTERLEE
M. P. HOLLISTER

For The
NATIONAL
AERONAUTICS
AND SPACE
ADMINISTRATION
MANNED SPACEFLIGHT CENTER
HOUSTON, TEXAS

LOCKHEED MISSILES & SPACE COMPANY
A GROUP DIVISION OF LOCKHEED AIRCRAFT CORPORATION
SUNNYVALE, CALIFORNIA

PREFACE

This handbook is submitted by Lockheed Missiles & Space Company to the National Aeronautics and Space Administration Manned Spacecraft Center in partial fulfillment of the requirements of contract number NAS 9-5174. The handbook treats liquid propellant shape, sloshing behavior, stability, reorientation behavior, draining and vortexing, and heat transfer problems with emphasis on low-g aspects of these problems. The design procedures for passive liquid-retention systems for storable propellants are also included as in a discussion on experimental techniques useful in the study of low-g liquid propellant behavior.

Other reports submitted under this contract include:

"A Study of Liquid Propellant Behavior During Periods of Varying Acceleration" Final Report, LMSC-A874728

"A Study of Liquid Propellant Behavior During Periods of Varying Acceleration" Summary Report, LMSC-A874729

"The Literature of Low-g Liquid Propellant Behavior," LMSC-A874830

The authors wish to acknowledge the contribution in part of the pressurant pull-through analysis in Section 6 by Dr. Gary D. Bizzell. This analysis was prepared in connection with other review work at LMSC and adapted for use in this handbook.

CONTENTS

ILLUSTRATIONS

TABLES

Section 1
INTRODUCTION

This handbook has been prepared to assist engineers working on propulsion and vehicle dynamics of rocket propelled space vehicles to predict the behavior of liquids in rocket propellant tanks. Low-g liquid behavior has been emphisized in preparing this handbook. It is important that the probable behavior of liquids be recognized. Once this is done, propulsion or control system designers need quantitative information about this behavior. It is the central purpose of this handbook to explain clearly how liquids behave in rocket propellant tanks and to provide tools for the solution of the more important types of liquid behavior problems.

The contents of this work have been subdivided according to the types of liquid behavior occurring in the propellant tanks of space vehicles. The following launch and operation sequence description serves to illustrate the categorization of rocket propellant behavior.

- The launching of a space vehicle requires the use of gimballed main engines of the booster to keep the vehicle on course. This results in lateral sloshing of the liquids in all tanks of the vehicle.
- Booster or upper stage engine cutoff is followed by the release of strain energy stored in the walls of propellant tanks. The strain energy is caused by the hydrostatic pressure (in addition to the static pressure caused by tank pressurization) of the tanked liquids. Rapid release of this results in some, although normally slight, axisymmetric motion of the liquid free surface.
- Booster or upper stage engine shutdown also means that the space vehicle is in a state of free fall. Forces acting on the vehicle are greatly reduced and the acceleration of the liquid relative to the vehicle treated as a single-particle results in greatly reduced body forces acting on the liquid. The shape of the liquids in the propellant tanks will change since capillary forces, insignificant prior to engine shutdown, may now be dominant.

- Injection of a space vehicle into low altitude orbit may result in a deceleration drag force on the vehicle strong enough to reorient the liquids to the forward ends of their tanks. It is well known that capillary forces, when dominant, can hold or stabilize liquids in a nonminimum energy location. The location of liquids in propellant tanks subject to small extraneous forces is in question.
- Lateral sloshing of the propellants during ascent caused by operation of an ascent attitude control system implies that considerable kinetic energy may be present. Depending on the timing of engine shutdown relative to the sloshing cycle, this residual kinetic energy can result in extremely high amplitude liquid motion after engine shutdown.
- Operation of an orbital attitude control system will result in the lateral sloshing of liquids under conditions in which surface tension and wetting properties of the liquid control the liquid free surface shape. Baffles in tanks can be expected to have a much different effect on liquid sloshing motion under such conditions.
- Engine restart requires that liquid propellants be located at tank drains. Positioning propellants by means of auxiliary rockets is one of the accepted ways of assuring proper liquid positioning. Operation of such devices generally results first in reorientation of liquid in a wall bound sheet accompanied by the forward migration of a large central bubble. A central transient jet motion counter to the reorientation flow is subsequently observed under many conditions. Entrainment of ullage gas bubbles in liquid collected at the tank drain is also observed. Knowledge of forces imposed by reorientation flows on baffles is important in the baffle design. Detailed knowledge of the overall liquids reorientation behavior of liquids is important to the minimization of impulse propellants required for propellant settling.
- Other methods for holding liquid propellants against tank drains are available. One particularly suited for use with space storable propellants makes use of the surface tension property of the propellants.
- The draining of rocket tanks under low-g conditions presents special problems. Rapid draining of tanks under low-g conditions can result in the

disruption of the free surface over the drain with consequent extrapment of large residual quantities.

- Heat transfer to propellants is not normally as important to the designer of storable rocket systems as it obviously is to the cryogenic system designer. Knowledge of propellant temperatures can be useful, however, in determining pressurant quantity requirements, and is especially important when orbital engine restarts are considered.

The material in this work has been assembled with two major purposes in mind. The first is to provide a theoretical introduction to the fluid mechanics phenomena being treated. The purpose here is to provide a bridge to more detailed works in fluid mechanics which the worker with deeper theoretical interest can use in establishing a full understanding of the liquid behavior being treated here. This handbook is not a text in fluid mechanics. The user should use his own choice of reference for the theoretical development of the basic equations of fluid mechanics. The purpose here is to help in applying available information to problems posed by low-g liquid propellant behavior.

The second purpose is to collect all of the information available about low-g fluid mechanics for the use of propulsion system designers as well as those responsible for development. Details of the solution of theoretical problems are not presented, but rather the methods used are outlined in enough detail to give those less familiar with the techniques of mathematical analysis an appreciation of the steps involved. Compact, closed form solutions are included in some detail and are used primarily to point out the physical significance of the parameters of the solution to more general problems may be obtained therefrom.

An attempt is made to collect for use enough information to determine the force interaction between liquids in motion and their containers. An appreciation of the forces involved is a necessary bridge for communications between the propulsion system designer and the guidance and control system designer.

The following material has been organized into sections each treating a separate subject. Each section is complete with figures and references. An attempt has been made to unify the nomenclature throughout the handbook, but the symbols are defined in-text in each section.

There now exist several summaries about hydrostatics and hydrodynamics in reduced g situations. (See for example Reference 2 in Section 2.) This handbook supplements these works in a manner which, it is hoped, will assist the propulsion system designer. The recent publication of NASA SP106 (The Dynamic Behavior of Liquids in Moving Containers, H. N. Abramson, ed., 1966) renders unnecessary the inclusion of standard, high-g sloshing and other dynamic behavior information in this handbook.

Section 2

PROPELLANT FREE SURFACE SHAPE

The location and shape of a quantity of liquid propellants in ordinary gravitational conditions is intuitively obvious. The liquid in a container seeks a location and shape characterized by minimum potential energy. The interface shape normally observed is a plane perpendicular to the local direction of gravitational body forces acting on the liquid. In earlier days of space vehicle design, the shape of liquid propellants in rocket tanks was the subject of much conjecture. It has since been well established that the wetting characteristics of most propellants will cause them to wet additional tank wall when body force levels are very greatly reduced; The liquid in a rocket propellant tank seeks a location and shape which results in minimum total potential energy for the volume of liquid.

THE DIFFERENTIAL EQUATION AND BOUNDARY CONDITIONS

The shape of the free surface of liquid propellants in most rocket tanks can be determined from the solution of an easily derived differential equation. Consider the geometry in Figure 2-1. Here liquid is located in a container of revolution. The axial symmetry of this problem allows considerable simplification of the differential equation and its derivation. Nevertheless, the example is useful because of the wide applicability of results. The $\bar{r}$, $\bar{z}$ coordinate system is located at the axis of the cylinder where the vertex of the meniscus intersects the axis. The unbalanced vertical component of pressure forces acting across a differential ring in the free surface is balanced by the net vertical component of surface tension forces. This is described as follows:

$$(p_g - p)\, 2\pi \bar{r}\, d\bar{r} = 2\pi\sigma \frac{d}{dr} \frac{\bar{r} f_{\bar{r}}}{\sqrt{1 + \bar{f}_{\bar{r}}^2}}\, d\bar{r}$$

where σ is the surface tension of liquid. After cancellation this reduces to

$$p_g - p = \frac{1}{\bar{r}} \frac{d}{d\bar{r}} \frac{\bar{r}\,\bar{f}_{\bar{r}}}{\sqrt{1 + f_{\bar{r}}^{-2}}} \tag{2.1}$$

The pressure at any radius $\bar{r}$ is given by the following relation.

$$p = p_g - (p_g - p_o) - \rho g \bar{f} \tag{2.2}$$

Substitution of Eq. (2.1) into (2.2) results in the following differential equation

$$\frac{\sigma}{\bar{r}} \frac{d}{d\bar{r}} \frac{\bar{r} f_{\bar{r}}}{\sqrt{1 + \bar{f}_{\bar{r}}^2}} - \rho g \bar{f} - \bar{f}_{\bar{r}\bar{r}}(0) = 0$$

subject to boundary conditions at the axis and at the wall

$$\bar{f}_{\bar{r}}(0) = \bar{f}_{\bar{r}}(R) - \cot(\theta + \varphi) = 0 \tag{2.3}$$

Nondimensionalization of $\bar{r}$ and $\bar{f}$ using

$$r = \bar{r}/R \quad , \quad f = \bar{f}/R$$

results in the following form for this equation and the associated boundary conditions.

$$\frac{1}{r} \frac{d}{dr} \frac{r f_r}{\sqrt{1 + f_r^2}} - Bf - f_{rr}(0) = 0$$

$$fr(0) = f_r(1) - \cot(\theta + \varphi) = 0 \tag{2.4}$$

Here r runs from 0 to 1. The coefficient B to the second term is defined $B = \rho g R^2/\sigma$, where ρ is the density of the liquid. It can be exptected that the shape of the meniscus will be determined by the value of the Bond number and by the edge angle $(\theta + \varphi)$ which is involved in one of the boundary conditions for the differential equation. This equation is nonlinear, and, further, cannot be transformed into one with a closed-form solution. Numerical values must be obtained by numerically integrating the equation.

DISCUSSION OF AVAILABLE SOLUTIONS

Partial results are available in the literature for meniscus shapes in:

- Axisymmetric containers with no internal surfaces such as cylinder, spheres, cones and ellipses such that the meniscus intersects the axis of the tank perpendicularly. The shapes computed cannot be applied where nonaxisymmetric baffles are used. Reynolds [2.1] has performed calculations applicable to many cases of interest. These results in working chart form enable developing meniscus location and wall rise height information and liquid volume for any axisymmetric tank shape. Specific information relative to spherical tanks has been extracted from this work and is presented in Figure 2-2 as an illustration. Liquid depth under the meniscus in a spherical tank and meniscus wall height are presented as a function of normalized liquid volume with tank volume Bond number as a parameter for zero contact angle.
- Annular cylindrical tanks with both inner and outer walls being circular cylinders. Results for contact angles of zero degrees are presented in Figure 2-3 where use height on the outer and inner walls and the maximum depression, all referenced to mean liquid level,are plotted. Computations for other contact angles have been carried out [2.2], but are not included because of their limited utility.

  Note that for small diameter inner cylinders, the central region of the meniscus is not greatly distorted by the presence of the center body. As

the size of the center body grows, the shape of the meniscus spanning the gap becomes more symmetrical about a surface bisecting the gap. This observation applies qualitatively to the shape of the meniscus spanning between a cylindrical center body and any axisymmetric tank, except for the effect of the outer tank shape on the shape of the meniscus.

LIMITING CASES FOR THE MENISCUS SHAPE

A number of additional observations may be made concerning solutions to the equations just given. These involve behavior of the solution for limiting conditions. First, for $B = 0$ the differential equation becomes that for a circle and can be integrated directly to obtain the free surface shape.

$$f = \frac{1}{\cos(\Theta + \varphi)} \left[1 - \sqrt{1 - \frac{r^2}{\cos^2(\Theta + \varphi)}} \right] \tag{2.5}$$

Second, the shape calculated from the differential equation for small Bond numbers departs very little from the shape for a circular arc. For example even for $B = 1$, the departure of the free surface shape at the wall for $0°$ edge angle $(\Theta + \varphi)$ is only about 11 percent. Third, for very large values of B, the differential equation preducts very flat surfaces with small slopes except very close to the wall. Wall rise heights for large Bond number (> 100,say) can be obtained quite adequately using an asymptotic formula developed by Rayleigh.

$$f(1) \sim \frac{2}{\sqrt{B}} \cos(\Theta + \varphi) + \frac{2}{3B} \left[\frac{1 - \cos 3\left(\frac{\frac{\pi}{2} - \Theta - \varphi}{2}\right)}{\sin\left(\frac{\frac{\pi}{2} - \Theta - \varphi}{2}\right)} \right]$$

$B = 0$, of course, occurs in a practical sense when body forces are zero. Small Bond numbers will obtain if the body force levels are small or if the characteristics length

for the problem at hand is small. In the latter case, for example, the characteristic dimension for a capillary surface can be small even though the tank diameter is large. An illustration is found in an annular cylindrical tank, i.e., two concentric cylinders closely spaced. If the separation distance is very small, the section of the meniscus spanning the gap will be nearly circular, even though the tank may be very large and the gravity level high

APPROXIMATIONS TO THE MENISCUS SHAPE

From the foregoing it is evident that free surface shapes for zero or small Bond numbers may be substituted with reasonable accuracy by circles or ellipses[2.3]. For Bond numbers less than 10, a spheroidal surface (ellipsoid of revolution) is quite acceptable for many purposes. The equation for the proper ellipse is obtained by first choosing an ellipse which satisfies the contact angle condition at the tank wall and then matching the hydrostatic pressure difference between the limb of the meniscus and its vertex. Results of this type of analysis are included in Figure 2-4. Compared with the exact solution of the differential equation, the approximation is best for smaller Bond numbers and is in fact exact for $B = 0$. The approximation is also better for larger contact angles.

The agreement between theory and experimental measurements made of meniscuses in small cylinders can be seen in Figure 2-5. Agreement is reasonable in spite of the experimental difficulties associated with measuring the contact angle and the exact intersection point between the meniscus and the cylinder wall (all these being aggravated by refraction at the cylindrical walls of the model).

There now exists a large literature concerning the capillary liquid free-surface shape. Much of the existing literature, though, was prepared before digital computers were available for the numerical integration of differential equations. Thus, the numerical information available until recently was not great. The interested reader is referred to the reference list in Chapter 11 of NASA SP 106[2.4] or to the separated bibliography accompanying this work[2.5].

REFERENCES

2.1 Reynolds, W. C., Sand, M. A., and Satterlee, H. M.: "Capillary Hydrostatics and Hydrodynamics of Low-G," Stanford University, Department of Mechanical Engineering, Report No. LG-3, Stanford, Calif., 1 Sep 1964, p. 36 and p. 52 (Also, Reynolds, W. C. and Satterlee, H. M.: "Liquid Propellant Behavior at Low- and Zero-G," Ch. 11, The Dynamic Behavior of Liquids in Moving Containers, H. N. Abramson, ed., NASA SP-106, 1966, p. 402

2.2 Seebold, J. C., Hollister, M. P., and Satterlee, H. M.: "Capillary Hydrostatics in Annular Tanks," J. Spacecraft, Vol. 4, No. 1, Jan 1967, pp. 101–5

2.3 Satterlee, H. M., and Chin, J. H.: "Meniscus Shape Under Reduced Gravity Conditions," AFOSR/LMSC Symposium on Fluid Mechanics and Heat Transfer Under Low Gravity, Lockheed Missiles & Space Company, Palo Alto, Calif., 24–25 June 1965, pp. 13–15 ff

2.4 Reynolds, W. G., and Satterlee, H. M., "Liquid Propellant Behavior at Low- and Zero-G, Ch. 11, The Dynamic Behavior of Liquids in Moving Containers, H. N. Abramson, ed., NASA SP-106, 1966

2.5 Lockheed Missiles & Space Company, The Literature of Low-G Liquid Propellant Behavior, prepared for NASA Manned Spacecraft Center, Houston, Texas, under Contract No. NAS 9-5174, 12 May 1967

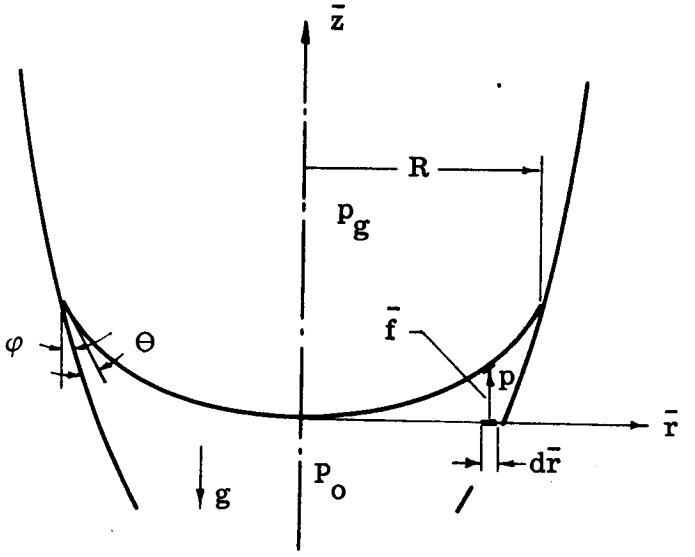

Figure 2-1 Geometry — Meniscus in a Container of Revolution

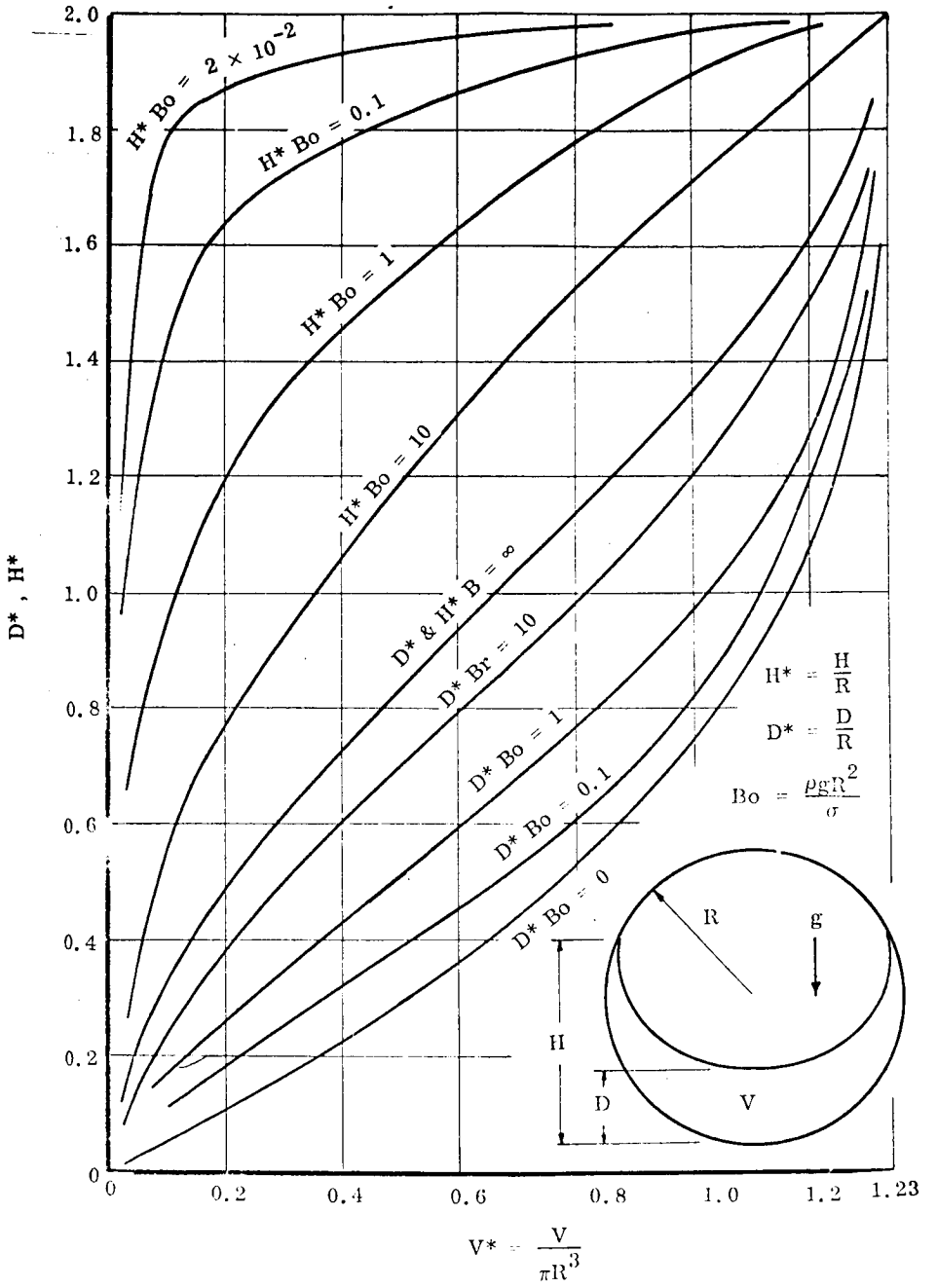

Figure 2-2 Configuration Parameters for Liquid in a Spherical Tank, Contact Angle, $\Theta = 0$

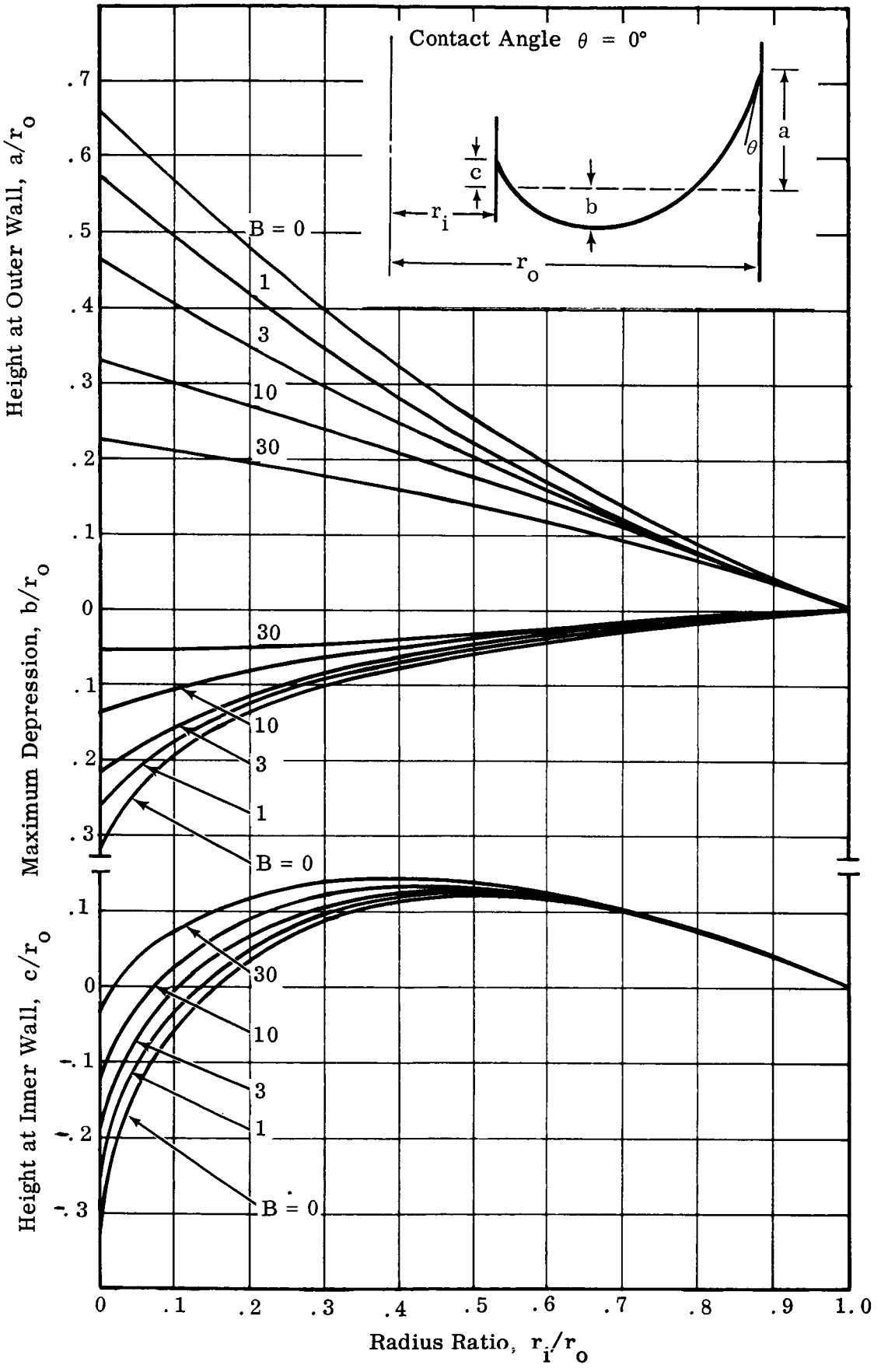

Figure 2-3 Annular Interface Shape Parameters

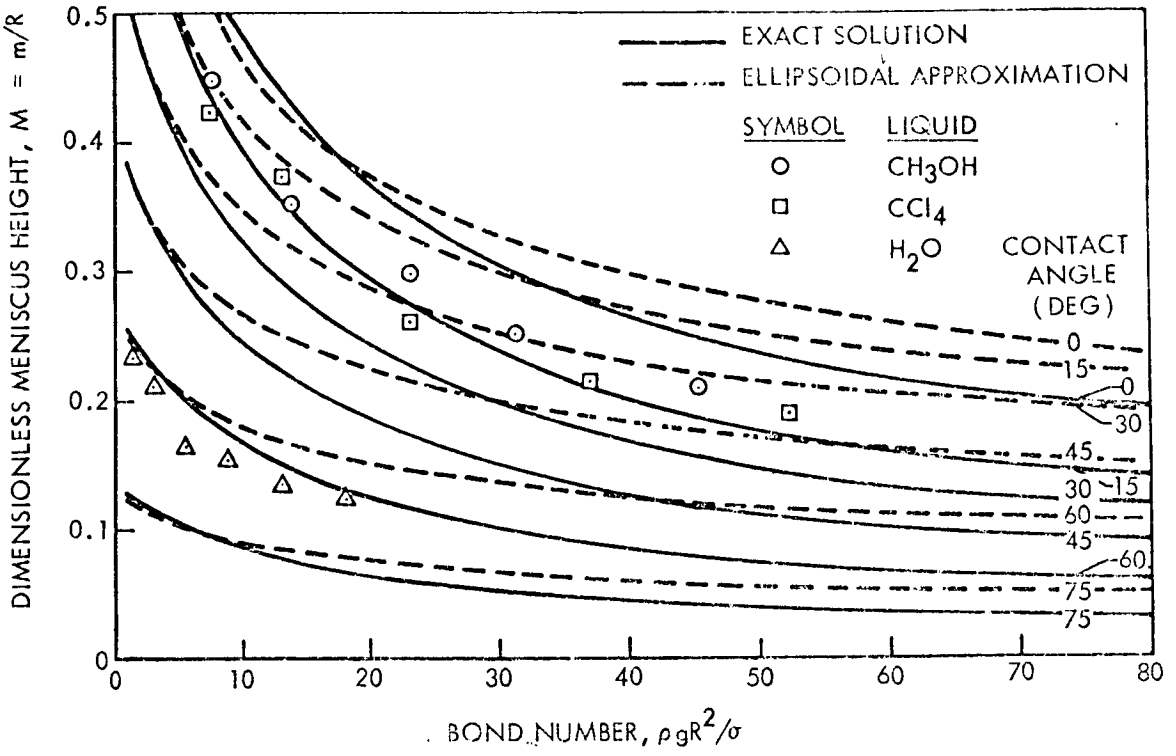

Figure 2-4 Meniscus Rise Height Ratio as a Function of Bond Number and Contact Angle

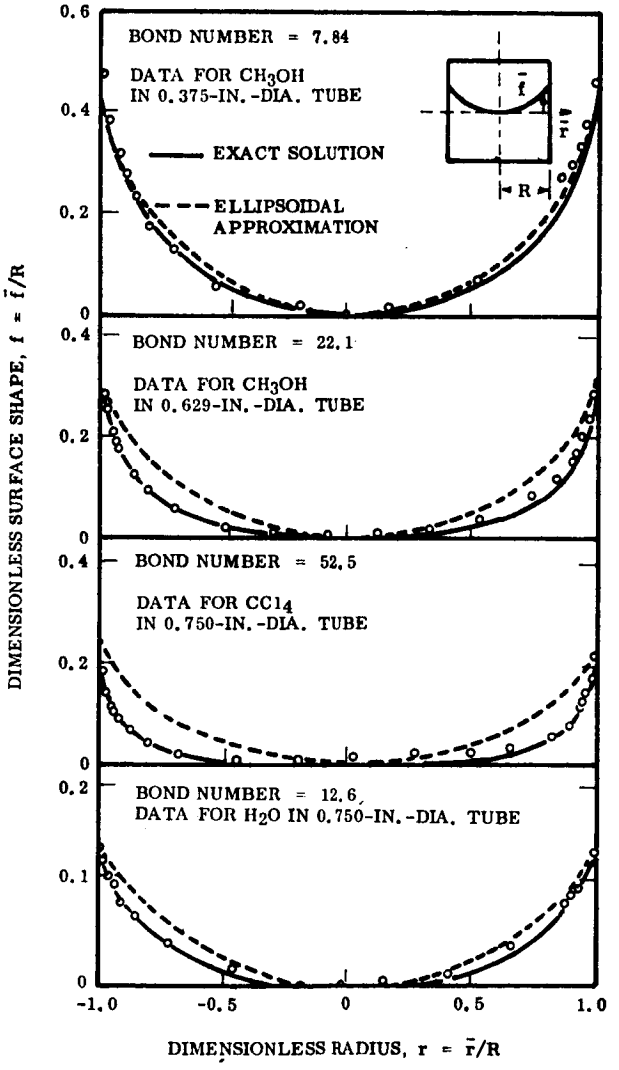

Fig. 2-5 Comparison of Theoretical Meniscus Shapes With Ellipsoidal Approximations and Experimental Data

Section 3
LOW-G LATERAL SLOSHING OF ROCKET PROPELLANTS

The oscillation of liquids in cavities has been a subject of interest to mathematicians and scientists for about 100 years, and its is of special importance today in the design of rocket propelled space vehicles. If a liquid rocket is properly designed, the propellant load comprises a large fraction of the total vehicle mass. Oscillations which take place in liquid propellants, therefore, can be of extreme importance in the design of the propulsion and control systems.

DEVELOPMENT OF THE BOUNDARY EIGENVALUE PROBLEM FOR NORMAL MODE SLOSHING

Liquid propellants used heretofore have been liquids of low viscosity. Most of the theory associated with sloshing has assumed that the liquids are inviscid, and this is a satisfactory assumption for most conditions. Further, the compressibility of most liquids is very low. These facts, in short, make the assumptions of incompressible, inviscid, and irrotational liquid behavior quite reasonable.

The governing relation for sloshing in liquid propellant tanks is thus Laplace's equation, the equation of continuity. The solution to this equation must be determined consistent with appropriate boundary conditions at solid walls and the free surface. The boundary condition at solid walls consistent with the assumption of inviscid behavior is that the velocity of the liquid normal to the tank walls is zero. The pressure at the free surface provides another boundary condition which can be drawn from Bernoulli's equation applied at the free surface. (This equation holds throughout the liquid except that the pressure is known only on the free surface.) When surface tension is important in the sloshing problem, the pressure of the liquid at the liquid-gas interface is related to the gas pressure through the surface tension property of the liquid and the curvature of the interface. This is detailed in the following development.

The geometry used for the formulation of the lateral sloshing problem is shown in Figure 3-1. The polar cylindrical $(\bar{r}, \bar{z}, \theta)$ coordinate system is chosen as being most appropriate for sloshing in containers of revolution. Solid walls are denoted by $\bar{w}$ and the free surface by $\bar{s}$. In general, the liquid meets the wall so as to satisfy the contact angle (Θ) condition at radius R. The magnitude of the downward body body force acting per unit mass of fluid is g.

The governing equation for the problem Laplace's equation, (the equation of continuity) written in terms of a velocity potential φ, is

$$\nabla^2\varphi = \frac{\partial^2\varphi}{\partial\bar{r}^2} + \frac{1}{\bar{r}}\frac{\partial\varphi}{\partial\bar{r}} + \frac{1}{\bar{r}^2}\frac{\partial^2\varphi}{\partial\theta^2} + \frac{\partial^2\varphi}{\partial\bar{z}^2} = 0 \qquad (3.1)$$

with the velocity potential defined by radial, angular, and axial velocity components

$$\begin{aligned} \bar{u} &= \frac{\partial\varphi}{\partial\bar{r}} \\ \bar{v} &= \frac{\partial\varphi}{\partial\theta} \\ \bar{w} &= \frac{\partial\varphi}{\partial\bar{z}} \end{aligned} \qquad (3.2)$$

The zero normal flow velocity condition at solid walls is given by

$$\frac{\partial\varphi}{\partial\bar{n}} = 0 \qquad \text{on } w \qquad (3.3)$$

The boundary condition applied for the free surface may be obtained from the nonsteady Bernoulli equation on

$$\frac{p}{\rho} + (\nabla\varphi)^2 + g\bar{s} = \frac{\partial\varphi}{\partial\bar{t}} \qquad \text{on } \bar{s}$$

The liquid pressure in the free surface is related to the gas pressure above the free surface by the relation

$$p_g - p = \sigma J \tag{3.4}$$

where the total curvature of the free surface J is

$$J = \frac{1}{\bar{r}} \frac{\partial}{\partial \bar{r}} \frac{\bar{r}\, s_{\bar{r}}}{\sqrt{1 + s_{\bar{r}}^2 + \frac{1}{\bar{r}^2} s_\theta^2}} + \frac{1}{\bar{r}^2} \frac{\partial}{\partial \theta} \frac{s_\theta}{\sqrt{1 + s_{\bar{r}}^2 + \frac{1}{\bar{r}^2} s_\theta^2}} \tag{3.5}$$

Without loss of generality, $F(t)$ in the Bernoulli equation can be set equal to a constant; for convenience this will be chosen to be the liquid pressure at the vertex of the equilibrium liquid surface divided by the liquid density, i.e. p_o/ρ. Bernoulli's equation is then

$$\frac{p}{\rho} + (\nabla \varphi)^2 + g\bar{s} + \frac{\partial \varphi}{\partial \bar{t}} = \frac{p_o}{\rho}$$

The use of Equation (3.4) relating liquid and gas pressure can then be used to arrive at the following free surface boundary condition.

$$\frac{\sigma}{\rho} J + (\nabla \varphi)^2 + g\bar{s} + \frac{\partial \varphi}{\partial \bar{t}} = \frac{\Delta p_o}{\rho} \tag{3.6}$$

where Δp is the pressure difference between the gas and the liquid at the vertex of the equilibrium meniscus. The velocity potential in this equation must be related to the motion of the free surface itself by means of a kinematic condition. Consider $\bar{s} = \bar{s}(\bar{r}, \theta, \bar{t})$. The total derivative of $\bar{s}$ with respect to $\bar{t}$ is given by

$$\frac{d\bar{s}}{dt} = \frac{\partial \bar{s}}{\partial \bar{r}} \frac{d\bar{r}}{d\bar{t}} + \frac{1}{r} \frac{\partial \bar{s}}{\partial \theta} \frac{\partial \theta}{\partial \bar{t}} + \frac{\partial \bar{s}}{\partial \bar{t}}$$

Here the total derivatives $d\bar{s}/d\bar{t}$, $d\bar{r}/d\bar{t}$ and $\bar{r}(\partial\bar{s}/\partial\theta)$ are the velocity components $\bar{w}$, $\bar{u}$, and $\bar{v}$, respectively. The definition of the velocity potential may now be employed to obtain the usual form of the kinematic condition

$$\frac{\partial\bar{s}}{\partial\bar{t}} = \frac{\partial\varphi}{\partial\bar{z}} - \frac{\partial\varphi}{\partial\bar{r}}\frac{\partial\bar{s}}{\partial\bar{r}} - \frac{1}{\bar{r}^2}\frac{\partial\varphi}{\partial\theta}\frac{\partial\bar{s}}{\partial\theta} \tag{3.7}$$

The lateral sloshing problem is completely posed by equations (3.1), (3.3), (3.6), and (3.7) subject to an additional constraint relative to the behavior of the contact angle. Although this has not been finally demonstrated, it appears that the contact angle may satisfactorily be described as not varying dynamically, but remaining constant.

It can be seen that foregoing problem is nonlinear. Laplace's equation and the wall boundary condition are linear, but the first two terms in the free surface boundary condition and the kinematic condition are nonlinear. If analysis is limited to small oscillations of the free surface, the velocity squared term can be dropped from the Bernoulli equation and the first term accounting for surface tension effects can be linearized by defining the free surface shape $\bar{s}$ as the sum of the equilibrium surface $\bar{f}$ and a perturbation $\bar{h}$. When this is substituted and the algebra carried out, the free surface boundary condition and the kinematic condition become

$$\frac{\sigma}{\rho}\left\{\frac{1}{\bar{r}}\frac{\partial}{\partial\bar{r}}\frac{\bar{r}\bar{h}_{\bar{r}}}{\sqrt{1+\bar{f}_{\bar{r}}^2}^3} + \frac{1}{\bar{r}^2}\frac{\bar{h}_{\theta\theta}}{\sqrt{1+\bar{f}_{\bar{r}}^2}}\right\} - g\bar{h} - \frac{\partial\varphi}{\partial\bar{t}} = 0 \tag{3.8}$$

$$\frac{\partial\bar{h}}{\partial\bar{t}} = \frac{\partial\varphi}{\partial\bar{z}} - \frac{\partial\varphi}{\partial\bar{r}}\frac{d\bar{f}}{d\bar{r}} \tag{3.9}$$

The condition usually applied to the behavior of the contact angle is that it remain constant, i.e. $\partial\bar{h}/\partial\bar{r} = 0$ at $\bar{r} = R$.

The problem formulated by equations (3.1), (3.3), (3.8) and (3.9) is now linear. However, the container shape and free surface geometry make the solution to this problem quite difficult. Numerical analysis or methods of applied mathematics must be used, both of which require use of digital computer equipment.

DEVELOPMENT OF A MECHANICAL ANALOG FOR NORMAL MODE SLOSHING

The forces and moments caused by liquid sloshing in rocket propellant tanks can be calculated from knowledge of the velocity potential. The pressure at any point in the liquid is given by the unsteady Bernoulli equation.

$$\frac{p}{\rho} + \frac{q^2}{2} + g\bar{z} + \frac{\partial \varphi}{\partial \bar{t}} = C(t)$$

When the liquid is at rest $q = \varphi = \partial\varphi/\partial\bar{t} = 0$. So

$$\frac{p}{\rho} + g\bar{z} = C_1$$

On the equilibrium surface $\bar{f}$ (see Figure 3-1)

$$p = p_g - \sigma \frac{1}{\bar{r}} \frac{\partial}{\partial \bar{r}} \frac{\bar{r}\bar{f}_{\bar{r}}}{\sqrt{1 + \bar{f}_{\bar{r}}^2}}$$

thus

$$\frac{p_g}{\rho} + g\bar{f} - \frac{\sigma}{\rho} \frac{1}{\bar{r}} \frac{\partial}{\partial \bar{r}} \frac{\bar{r}\bar{f}_{\bar{r}}}{\sqrt{1 + \bar{f}_{\bar{r}}^2}} = C_1 \qquad (3.10)$$

When the liquid is sloshing, the pressure in the free surface ($\bar{z} = \bar{f} + \bar{h}$) is

$$\frac{p_g}{\rho} - \frac{\sigma}{\rho}\left\{\frac{1}{\bar{r}}\frac{\partial}{\partial \bar{r}}\left[\frac{\bar{r}\,\bar{f}_{\bar{r}}}{\sqrt{1+\bar{f}_{\bar{r}}^2}} + \frac{\bar{r}\,\bar{h}_{\bar{r}}}{\sqrt{1+\bar{f}_{\bar{r}}^2}^3}\right] + \frac{1}{\bar{r}^2}\frac{\bar{h}_{\theta\theta}}{\sqrt{1+\bar{f}_{\bar{r}}^2}}\right\}$$

$$+ g\bar{f} + g\bar{h} + \frac{\partial \varphi}{\partial \bar{t}} = C(t)$$

Using the immediately preceeding relation,

$$C_1 - \frac{\sigma}{\rho}\frac{1}{\bar{r}}\frac{\partial}{\partial \bar{r}}\frac{\bar{r}\,\bar{h}_{\bar{r}}}{\sqrt{1+\bar{f}_{\bar{r}}^2}^3} + \frac{1}{\bar{r}^2}\frac{\bar{h}_{\theta\theta}}{\sqrt{1+\bar{f}_{\bar{r}}^2}} + g\bar{h} + \varphi_t = C(t)$$

Equation (3.8) can be used here to simplify this to

$$C_1 = C(t)$$

Thus,

$$\frac{p}{\rho} = C_1 - g\bar{z} - \frac{\partial \varphi}{\partial \bar{t}} \tag{3.11}$$

The first two terms on the right side of this equation give the hydrostatic pressure in the liquid, partly contributed by the gravitational body force and partly by the effect of surface tension. The last term on the right gives the dynamic perturbation pressure caused by small amplitude oscillation of the free surface.

Now, the forces and moments caused by the sloshing motion can be calculated. The lateral force exerted can be found by evaluating the integral

$$\bar{F}_x = \int_0^{2\pi} \int_{\bar{\xi}=0}^{\bar{\xi}=\bar{\xi}_0} p \sin\beta \cos\theta \, \bar{r}_w \, d\bar{\xi} \, d\theta$$

$$= -\pi \int_{\bar{\xi}}^{\bar{\xi}} \int_0^{\bar{\xi}_0} \frac{\partial \varphi}{\partial \bar{t}} \sin\beta \, \bar{r}_w \, d\bar{\xi} \qquad (3.12)$$

This integral is obtained because the usual form of the velocity potential for lateral sloshing is $\varphi(\bar{r}, \bar{z}, \theta, \bar{t}) = \varphi(\bar{r}, \bar{z}, \bar{t}) \cos\theta$. The integral involving the first two terms in (3.11), the expression for pressure, vanishes in the integration with respect to θ.

The moment of the dynamic pressure forces on the tank is obtained from the following integral.

$$\bar{M}_y = -\pi \int_{\bar{\xi}}^{\bar{\xi}} \int_0^{\bar{\xi}_0} \frac{\partial \varphi}{\partial \bar{t}} \sin\beta \, \bar{r}_w \, \bar{z}_w \, d\bar{\xi} \qquad (3.13)$$

The velocity potential for these calculations should be expressed in the form

$$\varphi = -\frac{\bar{\omega} \bar{h}_w \varphi(\bar{r}, \bar{z}) \cos\theta \cos\bar{\omega}t}{\left.\frac{\partial \varphi}{\partial \bar{z}}\right|_{\substack{\theta=0 \\ r=R}}} \qquad (3.14)$$

This is obtained through use of (3.9), the kinematic condition, with the requirement that the maximum value of $\bar{h}(R, \bar{t})$ be $\bar{h}_w$. The ratio of these integrals determines the action point of an equivalent force on the tank.

$$\bar{Z} = \frac{\bar{M}_y}{\bar{F}_x} \qquad (3.15)$$

The parameters for a mechanically equivalent spring-mass oscillator can be determined from expressions for the maximum force imposed by and the maximum potential energy stored in the oscillator

$$\bar{F}_x = \bar{k}\,\bar{x}$$

$$\bar{V} = \frac{\bar{k}}{2}\,\bar{x}^2$$

The constant of the equivalent spring is obtained by eliminating $\bar{x}$ between these.

$$\bar{k} = \frac{\bar{F}_x^{\,2}}{2\bar{V}} \tag{3.16}$$

The magnitudeof the equivalent mass in the oscillator is obtained from

$$\bar{\mathcal{M}} = \frac{\bar{k}}{\bar{\omega}^2} = \frac{\bar{F}_x^{\,2}}{2\bar{\omega}^2\,\bar{V}} \tag{3.17}$$

In these expressions, the maximum potential energy can be obtained from the following integral

$$\bar{V} = \frac{\rho}{2} \int_{\substack{\text{Equilibrium} \\ \text{free-surface}}} \varphi \frac{\partial \varphi}{\partial \bar{n}}\, d\Sigma$$

where $d\Sigma$ is an elemental area in the equilibrium surface.

NORMALIZATION OF THE PROBLEM AND THE MECHANICAL ANALOG

For calculation purposes, it is useful to nondimensionalize all of the preceeding relations by first separating time from the problem and then using the following definitions:

$$r = \frac{\bar{r}}{R} \quad , \quad z = \frac{\bar{z}}{R} \quad , \quad f = \frac{\bar{f}}{R} \quad , \quad s = \frac{\bar{s}}{R} \quad , \quad h = \frac{\bar{h}}{R} \quad , \quad \ell = \frac{\bar{\ell}}{R}$$

$$\Phi = \frac{\varphi}{\sqrt{(1 + B)\frac{\sigma R}{\rho}}} \quad , \quad t = \bar{t}\sqrt{(1 + B)\frac{\sigma}{\rho R^3}} \tag{3.18}$$

$$B = \frac{\rho g R^2}{\sigma}$$

The linearized, normal-mode sloshing problem becomes

$$\nabla^2 \Phi = \frac{\partial^2 \Phi}{\partial r^2} + \frac{1}{r}\frac{\partial \Phi}{\partial r} + \frac{1}{r^2}\frac{\partial^2 \Phi}{\partial \Phi^2} + \frac{\partial^2 \Phi}{\partial z^2} = 0 \tag{3.1a}$$

$$\frac{\partial \Phi}{\partial n} = 0 \qquad \text{on } w \tag{3.3a}$$

$$\frac{1}{r}\frac{\partial}{\partial r}\frac{r h_r}{\sqrt{1 + f_r^2}}3 + \frac{1}{r^2}\frac{h_{\theta\theta}}{\sqrt{1 + f_r^2}} - Bh - (1 + B)\omega^2 \Phi = 0 \tag{3.8a}$$

$$\frac{\partial h}{\partial t} = \frac{\partial \Phi}{\partial z} - \frac{\partial \Phi}{\partial r}\frac{df}{dr} \tag{3.9a}$$

The relations for the equivalent spring-mass oscillator become

Maximum Lateral Force:

$$F_x = \frac{\bar{F}_x}{\sigma R} = \frac{\pi(1 + B)\omega^2 h_w}{\left.\frac{\partial \Phi}{\partial z}\right|_{r=R}} \int_0^{\xi_o} r_w \sin \Phi(r_w, z_w)\, d\xi \tag{3.12a}$$

Maximum Moment:

$$M_y = \frac{\bar{M}_y}{R^2} = \frac{\pi (1 + B\ ) \omega_n^2 H_w}{\left.\frac{\partial \Phi}{\partial z}\right|_{r=R}} \int_o^{\xi_o} r_w z_w \sin\beta\Phi (r_w, z_w)\, d\xi \qquad (3.13a)$$

Action Point:

$$Z = \frac{\bar{Z}}{R} = \frac{M_y}{F_x} \qquad (3.15a)$$

Equivalent Spring Constant:

$$k = \frac{\bar{k}}{\sigma} = \frac{\pi^2 (1 + B\ )\, \omega_n^2 \left[\int_o^{\xi_o} r_w \sin\beta\Phi (r_w, z_w)\, d\xi\right]^2}{\iint_{\text{Equilibrium free surface}} \Phi \frac{\partial \Phi}{\partial n}\, d\xi} \qquad (3.16a)$$

Equivalent Mass:

$$= \frac{\bar{M}}{\rho R^3} = \frac{\pi^2 \left[\int_o^{\xi_o} r_w z_w \sin\beta\Phi (r_w, z_w)\, d\xi\right]^2}{\iint_{\text{Equilibrium free surface}} \Phi \frac{\partial \Phi}{\partial n}\, d\Sigma} \qquad (3.17a)$$

A CLOSED FORM SOLUTION

Having posed the dimensionless linear problem for determining normal mode sloshing, it is appropriate to discuss ways in which numerical, and therefore useful, results can be obtained. The most desirable situation, of course, occurs when it is possible to write down closed form solutions to a given problem. It is preferable that such solutions be compact. Unfortunately, closed-form, compact solutions can be obtained in only a very limited number of cases, such as: a) sloshing in flat bottomed channels and b) in flat bottomed cylindrical tanks, both under conditions such that the equilibrium contact angle is 90 degrees. In these cases the equilibrium shape of the liquid is that of a rectangular solid and a right circular cylinder, respectively.

Lateral sloshing in a flat-bottomed, cylindrical tank can be described in a reasonably compact way. The results for this special case are quite useful since they provide a feel for the magnitudes involved in situations with more complex geometries where numerical results can be obtained only with considerable difficulty. The problem statement given by equations (3.1a), (3.3a), (3.8a), and (3.9a) is much simplified. Equations (3.1a) and (3.3a) remain unchanged; however, Equations (3.8a) and (3.9a) become

$$\frac{1}{r}\frac{\partial}{\partial r}(r h_r) + \frac{1}{r^2} h_{\theta\theta} - Bh - (1 + B)\omega^2\Phi = 0 \qquad (3.19)$$

$$\frac{\partial h}{\partial t} = \frac{\partial \Phi}{\partial z} \qquad (3.20)$$

Note here that all the coefficients in the free surface boundary condition are now constants.

The normal mode frequencies can easily be found. The first step requires separation of variables in Laplace's equation to obtain the general form

$$\Phi = \left[C_1 J_m(\lambda_n r) + C_2 Y_m(\lambda_n r)\right]\left[C_3 \cosh(\lambda_n z) + C_4 \sinh(\lambda_n z)\right] \cos m\theta \cos \omega t$$

Where $J_n(\,)$ and $Y_n(\,)$ are respectively Bessel functions of first and second kind of order m . It must be remembered that Φ is a function of time even if it does not appear in Laplace's equation. Hence, the factor $\cos \omega t$ in this relation. An implied boundary condition for this problem is that the velocities of the sloshing liquid and thence the velocity potential be regular (noninfinite) on the axis of the tank. This requires that the coefficient to the Y_n part of the solution be zero. Application of this and the solid wall boundary condition, Equation (3.3a), results in the following form for the velocity potential.

$$\Phi = C J_1(\lambda_n r) \cosh\left|\lambda_n (z + \ell)\right| \cos m\theta \cos \omega t \tag{3.21}$$

where the λ_n's are zeros of the equation

$$J_1'(\lambda_n) = 0 \tag{3.22}$$

Next, this result can be substituted into a combination of equations (3.10) and (3.11) to obtain normal mode oscillation frequencies.

$$\omega_n^2 = \frac{B\lambda_n + \lambda_n^3}{1 + B} \tanh \lambda_n \ell \tag{3.23}$$

Note that there is a whole family of possible solutions. The fundamental, of course, is the one of most practical importance.

Use of a velocity potential of the form of equation (3.21) in equations (3.12a) through (3.17a) yields (for 1st mode)

$$F_{x_{max}} = \frac{\pi h_w \left(B + \lambda_1^2\right) \tanh \lambda_1 \ell}{\lambda_1} \tag{3.24}$$

$$M_{y_{max}} = \frac{\pi h_w \left(B + \lambda_1^2\right) \tanh \lambda_1 \ell}{\lambda_1^2} \quad \frac{1 - \cosh \lambda_1 \ell}{\sinh \lambda_1 \ell} \tag{3.25}$$

$$Z = \frac{\cosh \lambda_1 \ell - 1}{\lambda_1 \sinh \lambda_1 \ell} \tag{3.26}$$

$$k_1 = \frac{(1 + B) \tanh^2 \lambda_1 \ell}{\lambda_1 \left(\lambda_1^2 - 1\right)} \tag{3.27}$$

$$\bar{M}_1 = \frac{\pi \tanh \lambda_1 \ell}{\lambda_1^2 \left(\lambda_1^2 - 1\right)} \tag{3.28}$$

It will be instructive to use these relations to determine the approximate behavior of liquid propellants in a tank of typical size under different gravitational conditions. Consider a 4 ft diameter tank filled to a depth greater than 4 ft. The expressions for natural frequency, lateral force, moment, lateral force action point, spring constant, and equivalent sloshing mass can be simplified. For first mode sloshing $\lambda_1 \cong 1.84$. The expressions are shown in Table 3-I together with the numerical values of the above parameters when the gravitational body force acting on the liquid is zero, $10^{-6} g_o$, and $1\ g_o$.

NUMERICAL SOLUTIONS

The normal mode problem for low Bond numbers has recently been solved by completely numerical means for the hemispherically-bottomed, cylindrical tank geometry [3.1].

From an applications viewpoint, the major results of this study were

- Normal mode lateral sloshing frequencies. First mode sloshing frequency as a function of liquid depth and axial Bond number ($B_\alpha = \rho g R^2/\sigma$) are given in Figure 3-2. Higher eigenvalues are collected in Table 3-II.
- Mechanical analog parameters to simplify the computation of the forced response of the liquid to lateral perturbing accelerations (when the perturbing acceleration frequency, if cyclic, differs from any of the natural frequencies including those listed in Table 3-II. The mechanical analog parameters are presented in Figures 3-3 and 3-4.

Figure 3-5, giving the liquid volume-depth relationship in the tank bottom, is included to aid the use of the information in Figures 3-2 through 3-5 and Table 3-II.

DISCUSSION OF NONLINEAR EFFECTS

It might be hoped that the solution of this type of problem could be extended to include nonlinear effects. These occur because of the presence of the $(\nabla\varphi)^2$ terms in the unsteady Bernoulli Equation, (3.6). But, unfortunately, this has not yet been done. Two problems arise to make this a very difficult thing to do. First, because the free-surface boundary condition is nonlinear, there is no assurance that the angular and time dependence of the velocity potential can be separated as in the linear problem. Because of this, it is not possible to identify coefficients to certain terms in the problem as eigenvalues as in Equation (3.8a) where ω^2 is identified as the eigenvalue. Second, in the linear problem, it is satisfactory to evaluate properties on the equilibrium free-surface $\bar{f}$ because this is equivalent to evaluating them on the moving free surface $\bar{s}$ (in Equation 3.6) to first order in $\bar{h}$ – all that is required by the linear problem. This means that Laplace's equation need only be solved in a domain of fixed shape. In the nonlinear problem, this simplification may not be possible.

There are two possibilities for obtaining solutions. The first involves treating the problem in the form of a three-dimensional initial value problem. Techniques for

carrying out this type of analysis in simpler problems will be briefly described in Section 5 of this Handbook. The second possibility involves determining the nonlinear effects by expanding the velocity potential in a perturbation series. This requires that a small parameter exist. The $(\nabla\varphi)^2$ term probably offers such a parameter when nondimensionalized because adequate results for most purposes are obtained by neglecting this term altogether. The net result of all this is that solution of the nonlinear problem is extremely difficult. Challenge enought is offered by the simpler and more useful problem of normal-mode, linear sloshing in practical container geometries.

DAMPING UNDER LOW-G CONDITIONS

The damping of liquid sloshing motions in rocket tanks is an important subject because without the effective dissipation of such motions sloshing can have an important influence on the structural design of propellant tanks and the operation of spacecraft guidance and control systems. Because of its importance to rocketship design, damping of liquid propellants has received considerable attention. Most of the investigation of damping under high-g conditions has been collected by Silverman and Abramson [3.2].

Most liquid propellants now in use have low viscosity. This results in very low natural damping factors. This is illustrated by the relation reported in the above reference in which the logarithmic decrement for clean cylindrical tanks, expressed in terms of sloshing frequency, is reported to be

$$\delta = 6.10\sqrt[4]{\frac{\nu^2}{R^3 g}}$$

It is seen that damping in small-scale models is much greater than in propellant tanks of ordinary size, but that gravity level has a relatively small effect. Assuming this can be extrapolated to very low g levels, reducing the gravity level to $10^{-6}\, g_o$, for example, increases the log decrement by only a factor of about 30. But, since the log decrement for clean tanks under normal conditions is only 0.004 or less

(for a 4-ft diameter tank, say), it will still be quite small, especially considering the very low natural sloshing frequencies. In short, damping must rely on internal devices such as baffles just as under high g conditions.

Analysis can be applied to most baffle systems to determine their effectiveness. The method first used by Miles [3.3] is an especially useful way of determining damping of baffles under reduced g conditions because of the difficulty of measuring damping in carefully scaled experiments. This method involves estimating the drag force on the baffle by computing the liquid velocity in the tank at the baffle location as if the baffle weren't there, using this to compute the drag force on the baffle using available drag coefficient information for the baffle shape, and then estimating the average rate of energy decay caused by the baffle. The latter is simply the product of the drag force and the liquid velocity. These quantities can all be computed on an elemental basis at one position of the baffle and then integrated over the baffle to obtain the total average rate of energy dissipation.

Consider, as an illustrative example, the ring baffle shown in Figure 3-6. The liquid velocity in a clean tank of identical geometry can be obtained by differentiating the velocity potential

$$\varphi = \frac{\bar{h}_w \, \omega R \, J_1\left(\lambda_1 \frac{\bar{r}}{R}\right) \cosh \frac{\lambda_1}{R}\left(\bar{\ell} + \bar{z}\right)}{\lambda_1 \, J_1(\lambda_1) \sinh \frac{\lambda_1 \ell}{R}} \cos \bar{\omega}\bar{t} \cos \theta$$

The liquid vertical velocity at the wall at depth $\bar{d}$ is

$$w = \frac{\bar{h}_w \, \omega \sinh \frac{\lambda_1}{R}\left(\bar{\ell} - \bar{d}\right)}{\sinh \frac{\lambda_1 \ell}{R}} \cos \bar{\omega}\bar{t} \cos \theta$$

This may be used over the entire baffle width if the width is not a large fraction of the radius. The drag force over an elemental angle of the baffle is

$$dF = \frac{C_D \rho W R \bar{h}_w^2 \bar{\omega}^2 \sinh^2 \frac{\lambda_1}{R}(\bar{\ell} - \bar{d})}{2g_c \sinh^2 \frac{\lambda_1 \bar{\ell}}{R}} \cos^2\theta \cos^2 \bar{\omega}\bar{t}\, d\theta$$

The rate of energy dissipation at this element is

$$\left.\frac{dE}{dt}\right|_{element} = \frac{C_D \rho W R \bar{h}_w^3 \bar{\omega}^3}{2g_c} \left| \frac{\sinh^3 \frac{\lambda_1}{R}(\bar{\ell} - \bar{d})}{\sinh^3 \frac{\lambda_1}{R}\bar{\ell}} \cos^3 \bar{\omega}\bar{t} \cos^3\theta \right| d\theta$$

The average rate of energy dissipation over the entire baffle is determined by integration with respect to time over one cycle and with respect to θ over the interval $(0, 2\pi)$.

$$\overline{\frac{dE}{dt}} = -\frac{\pi \rho W R C_D}{g_c} \bar{\omega} \bar{h}_w \left[\frac{\sinh \frac{\lambda_1}{R}(\bar{\ell} - \bar{d})}{\sinh \frac{\lambda_1}{R}\bar{\ell}}\right]^3 \frac{}{3\pi}^3$$

This is easily related to the damping ratio γ by

$$\gamma = -\frac{\overline{\frac{dE}{dt}}}{2\bar{\omega}\bar{E}}$$

The average energy of the sloshing wave is obtained by averaging the kinetic energy per unit volume over the entire volume, but is equivalently and more easily obtained for this case from the surface integral

$$\bar{E} = \frac{\bar{\omega}}{2\pi} \int_0^{2\pi/\bar{\omega}} d\bar{t} \; \frac{\rho}{2g_c} \int_{\substack{\text{Entire} \\ \text{bounding} \\ \text{surface}}} \varphi \, \frac{\partial \varphi}{\partial n} \, d\Sigma$$

For the geometry in Figure 3-6

$$E = \frac{\rho \bar{h}_w^2 \bar{\omega}^2 \pi R^3}{4g_c} \; \frac{\lambda_1^2 - 1}{\lambda_1^3 \tanh \frac{\lambda_1}{R} \bar{\ell}}$$

A combination of these yields

$$\lambda = 2\left(\frac{4}{3\pi}\right)^3 \frac{\lambda_1^3 \bar{h}_w \sinh^3 \frac{\lambda_1}{R} (\bar{\ell} - \bar{d}) \tanh \frac{\lambda_1}{R} \bar{\ell}}{R^2\left(\lambda_1^2 - 1\right)} C_D$$

The point of all this is that the computed damping ratio γ is a function of tank size and geometry, and the maximum height of the wall wave, and the baffle drag coefficient. Potential flow velocities may now be used to determine the drzg coefficient.

Keulegan and Carpenter (3.8) have indicated that, in an important range, the drag coefficient for ring baffles is given by

$$C_D = 15\left(\frac{w_m T}{W}\right)^{1/2}$$

where w_m is the maximum velocity at the baffle location, W the baffle width, and T the period of the sloshing wave. Now, w_m is directly related to the sloshing frequency and T inversely related; thus P is is independent of the natural frequency. Even outside the range of $0 \leq P = w_m T/W \leq 20$ indicated above, the drag coefficient is still a function only of P and independent of frequency. Since, for the

flat interface geometry of Figure 3.6, the drag coefficient and thence the damping ratio are independent of Bond number.

The net result of this discussion is that baffle dampling coefficients are not dependent on the gravity level. Similar arguments apply to different types of baffles constructed from screens or perforated plates. Thus, the large quantity of information developed about the damping ratio of different types of baffles (such as is collected in NASA SP 106 (3.2) can be used more or less as is. The logarithmic decrement is related to the damping ratio in the conventional way:

$$\delta = 2\pi\gamma$$

and δ is related to the slosh wave decay by

$$\delta = \ln \frac{\bar{h}_{w_n}}{\bar{h}_{w_{n+1}}}$$

where the numerator is the maximum height of the nth oscillation and denominator that of the $n + 1$ st oscillation.

The central point of this illustration is that the damping afforded by a given baffle can be computed for situations for which experiments cannot now be carried out. It is important to have some tool to use in a situation even if the ideal tool is not immediately available.

An experimental study (3.5) of the effect of liquid free-surface curvature attending low-g conditions has indicated that the natural frequency can actually be increased by ring baffles. This occurs as the baffle apparently deflects the flow of liquid up the wall toward the tank centerline causing distortion of the interface on the upward swing of the wave. This effect is similar to that caused by dynamic contact angle variation (often called

"hysteresis") which has been shown to result in an increase of the low-g natural frequency (3.6). The effect of baffle location on natural frequency is shown in Figure 3-7 where the ratio of the natural frequency with the baffle to that without is plotted as a function of baffle depth.

REFERENCES

3.1 Concus, P., Crane, G.E., and Satterlee, H. M.; "Small Amplitude Lateral Sloshing in a Cylindrical Tank With a Hemispherical Bottom Under Low Gravitational Conditions," NASA CR-54700, 20 Jan 1967. Prepared under Contract No. NAS 3-7119 for the NASA Lewis Research Center by Lockheed Missiles & Space Company

3.2 The Dynamics Behavior of Liquids in Moving Containers, NASA SP 106, H. N. Abramson, ed., Ch. 4, 1966

3.3 Miles, J. W. "Ring Damping of Free Surface Oscillations in a Circular Tank," J. Appl. Mech., vol. 25, No. 2, June 1958, pp 274-8

3.4 Keulegan, G. H. and Carpenter, L. H.: "Forces on Cylinders and Plates in an Oscillating Fluid," National Bureau of Standards, report No. 4821, Washington, D.C., 5 Sep 1956

3.5 Hollister, M. P., and Satterlee, H. M.: "A Study of Liquid Propellant Behavior During Periods of Varying Acceleration," Final Report, LMSC-A874728, prepared by Lockheed Missiles & Space Company, Sunnyvale, Calif., under NASA Contract No. NAS 9-5174 for the NASA Manned Spacecraft Center, Houston, Texas

3.6 Satterlee, H. M., and Reynolds, W. C.: "The Dynamics of the Free Liquid Surface in a Cylindrical Container Under Strong Capillary and Weak Gravity Conditions," Stanford University, Department of Mechanical Engineering, Report No. LG-2, Stanford, Calif., Apr 1964, p. 87

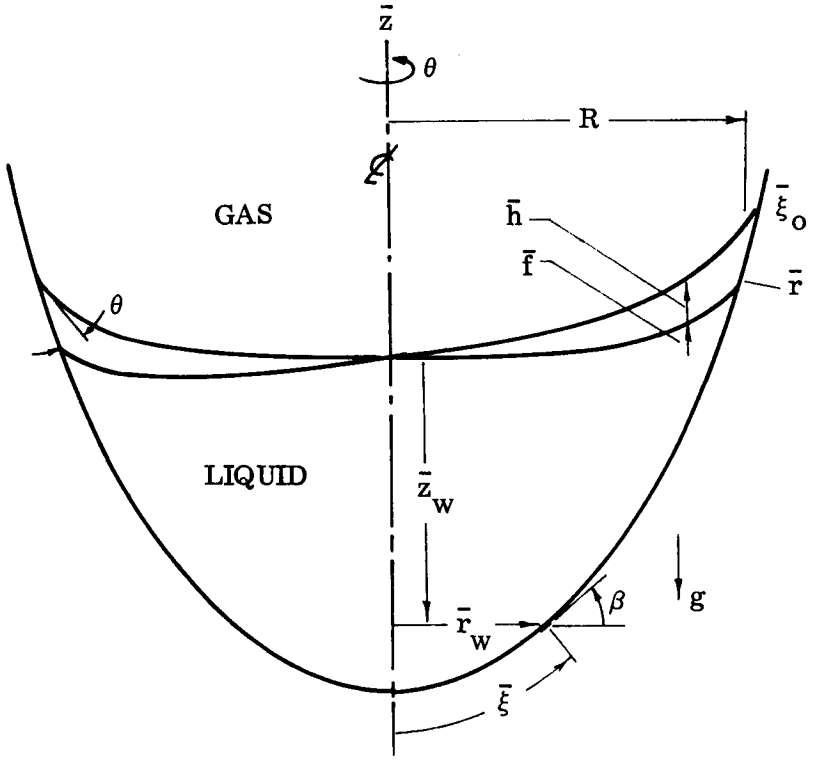

Figure 3-1 Geometry - Lateral Sloshing in an Axisymmetric Tank

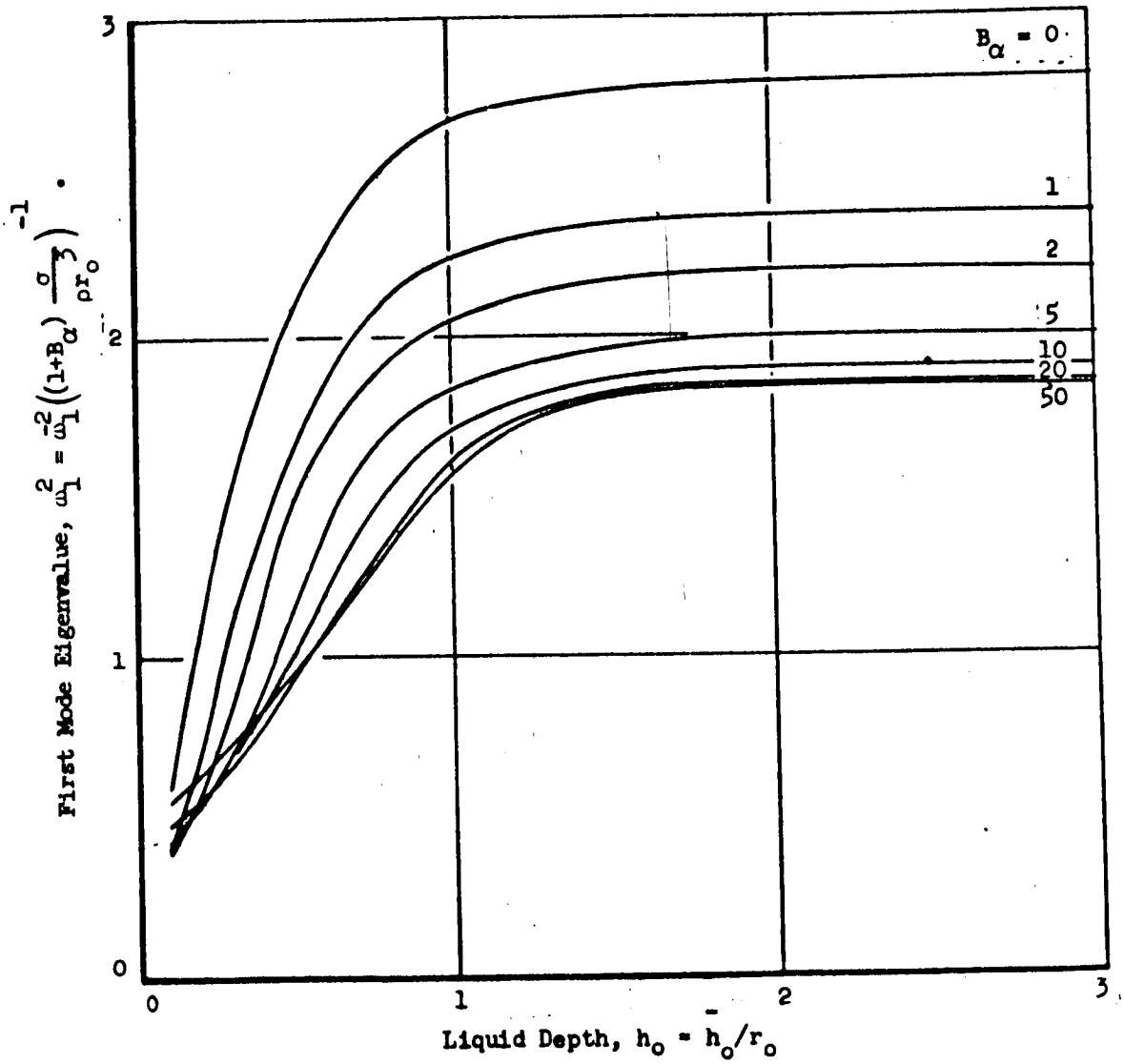

Figure 3-2 First Mode Eigenvalue for Lateral Sloshing in a Cylindrical Tank with Hemispherical Bottom; θ = 5 Degrees

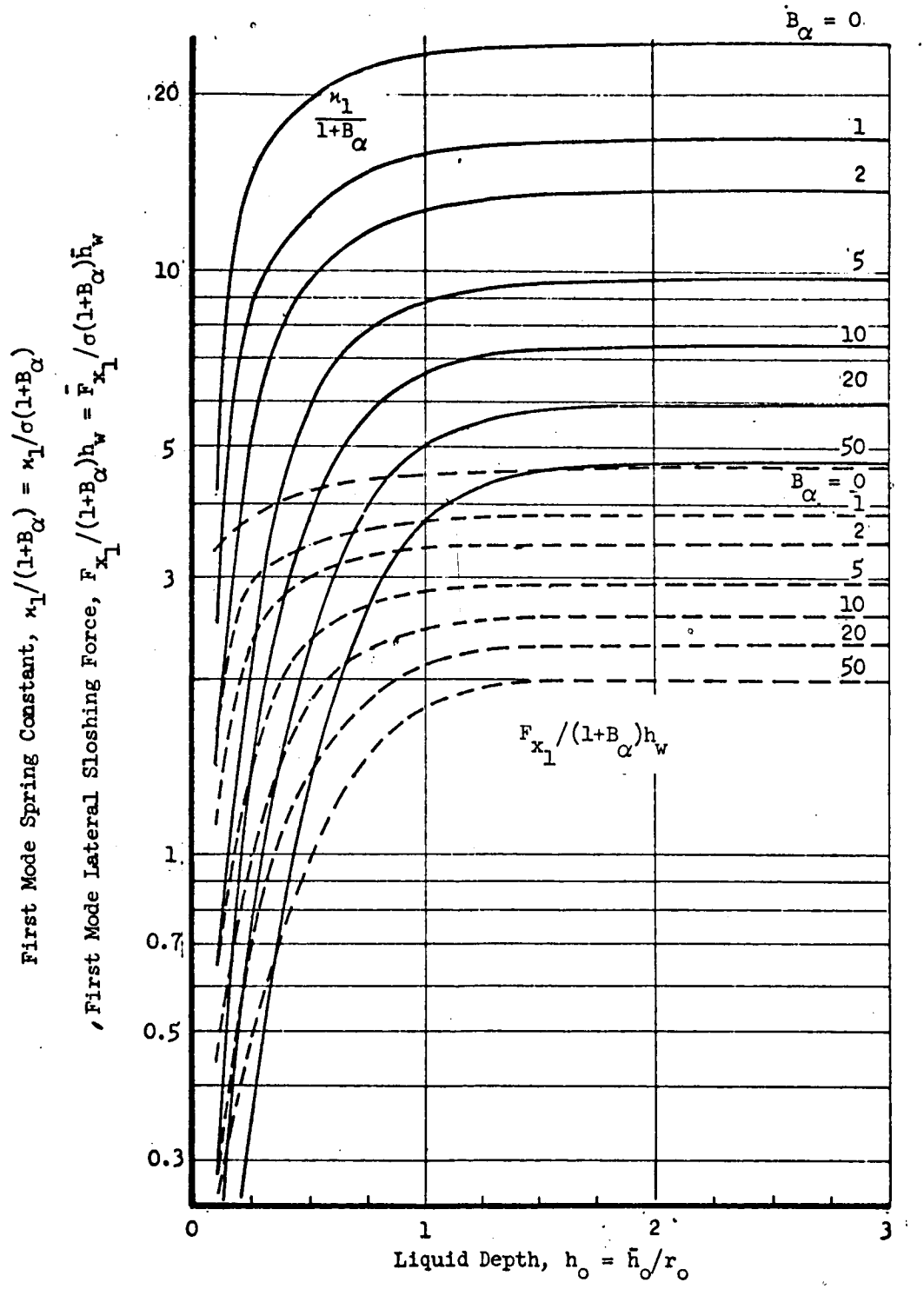

Figure 3-3 First Mode Mechanical Analog Spring Constant and Lateral Force Cylindrical Tank With a Hemispherical Bottom (Θ = 5 Degrees)

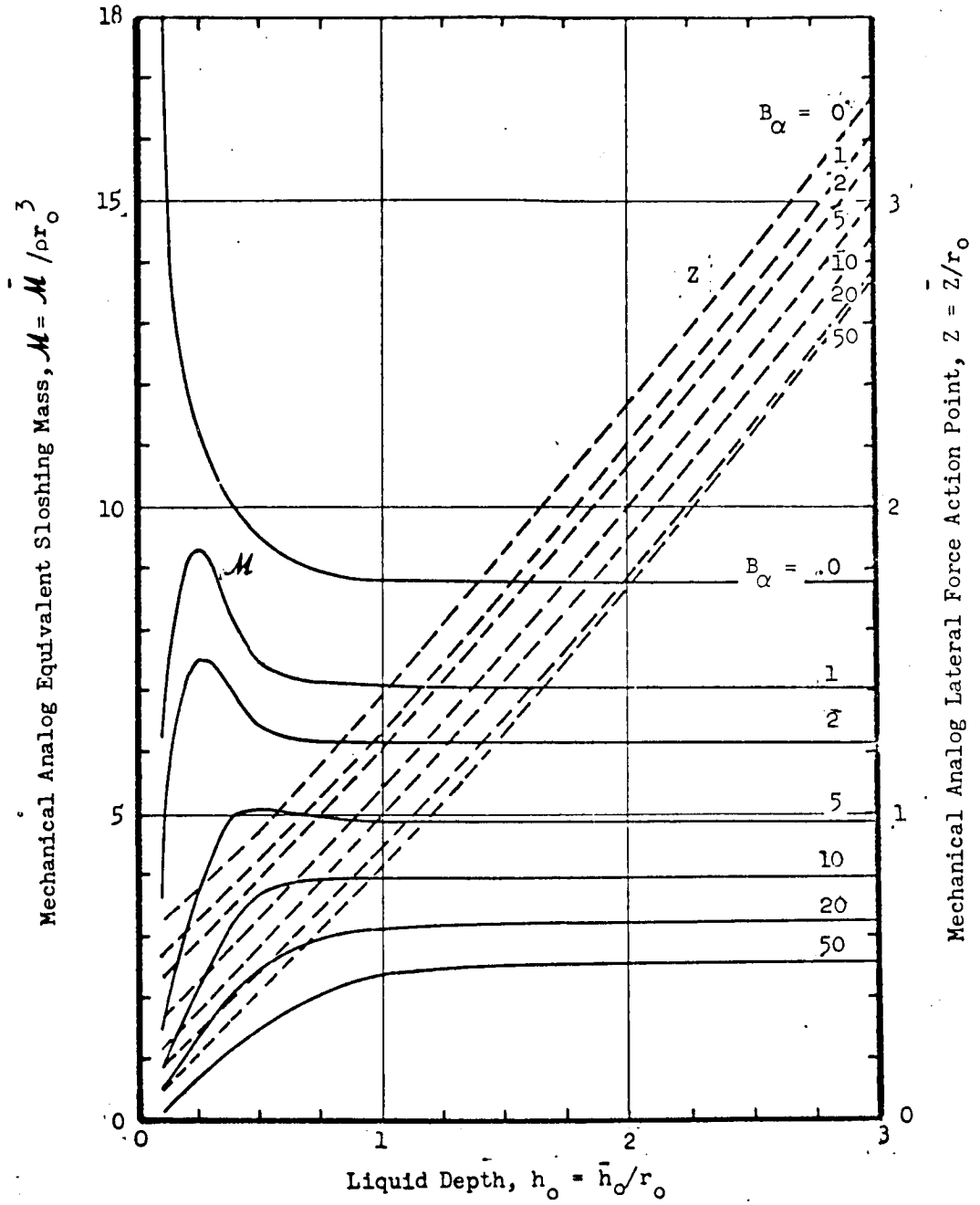

Figure 3-4 First Mode Mechanical Analog Sloshing Mass and Lateral Force Action Point for Lateral Sloshing in a Cylindrical Tank With a Hemispherical Bottom; Θ = 5 Degrees

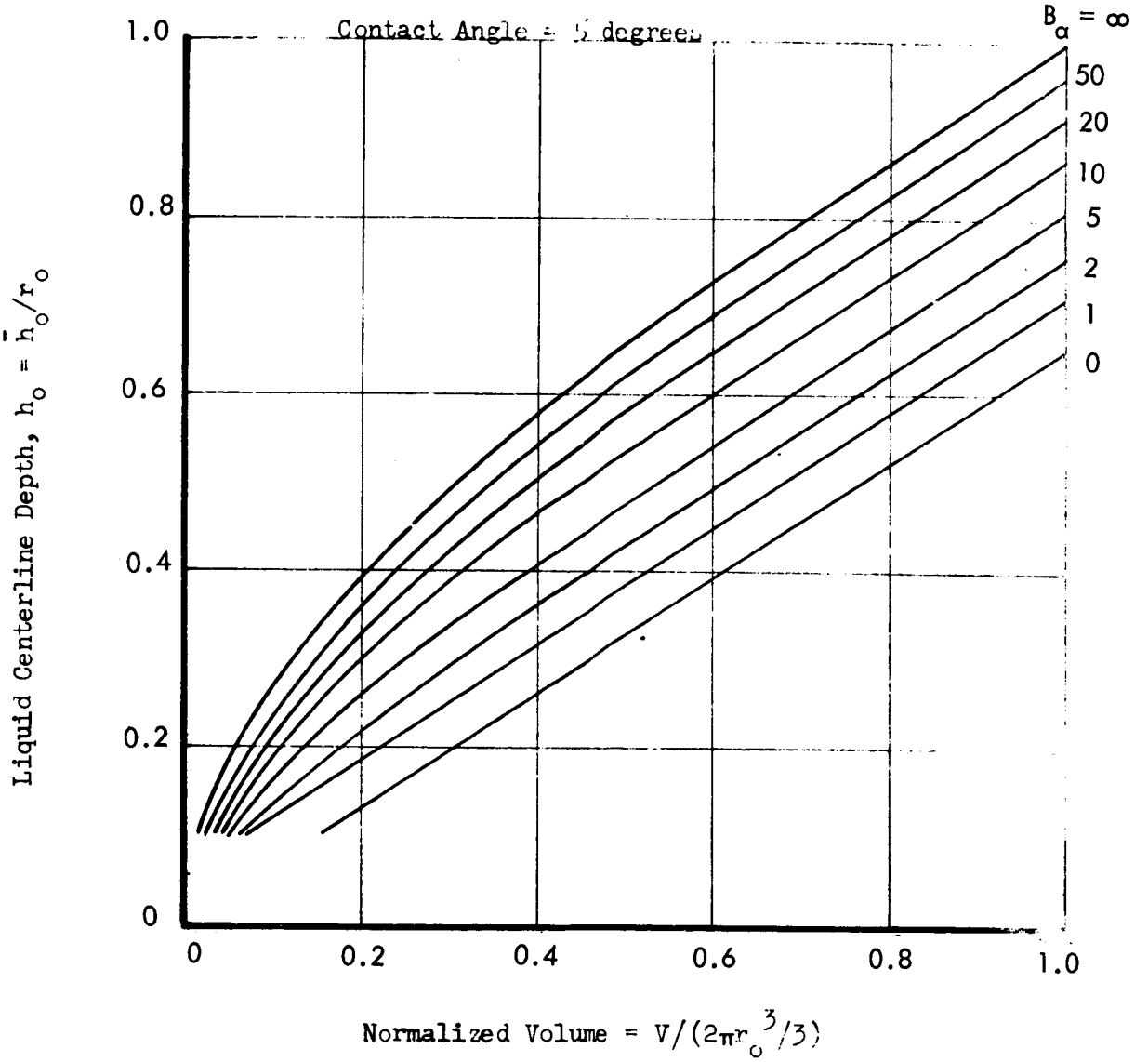

Figure 3-5 Liquid Centerline Depth - Tank Volume Relationship

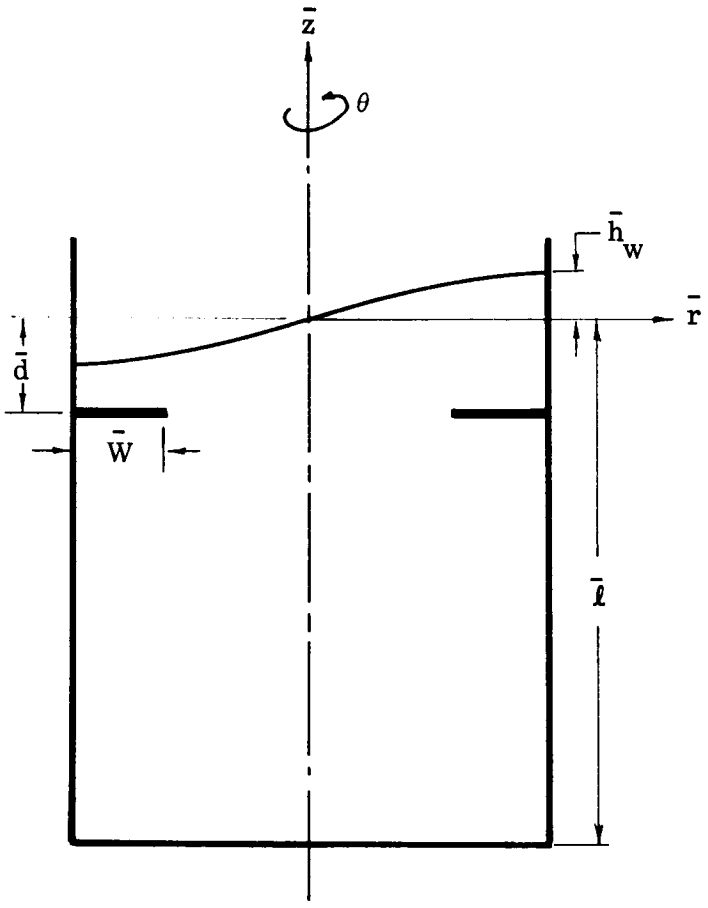

Figure 3-6 Ring Baffle Geometry in a Cylindrical Tank

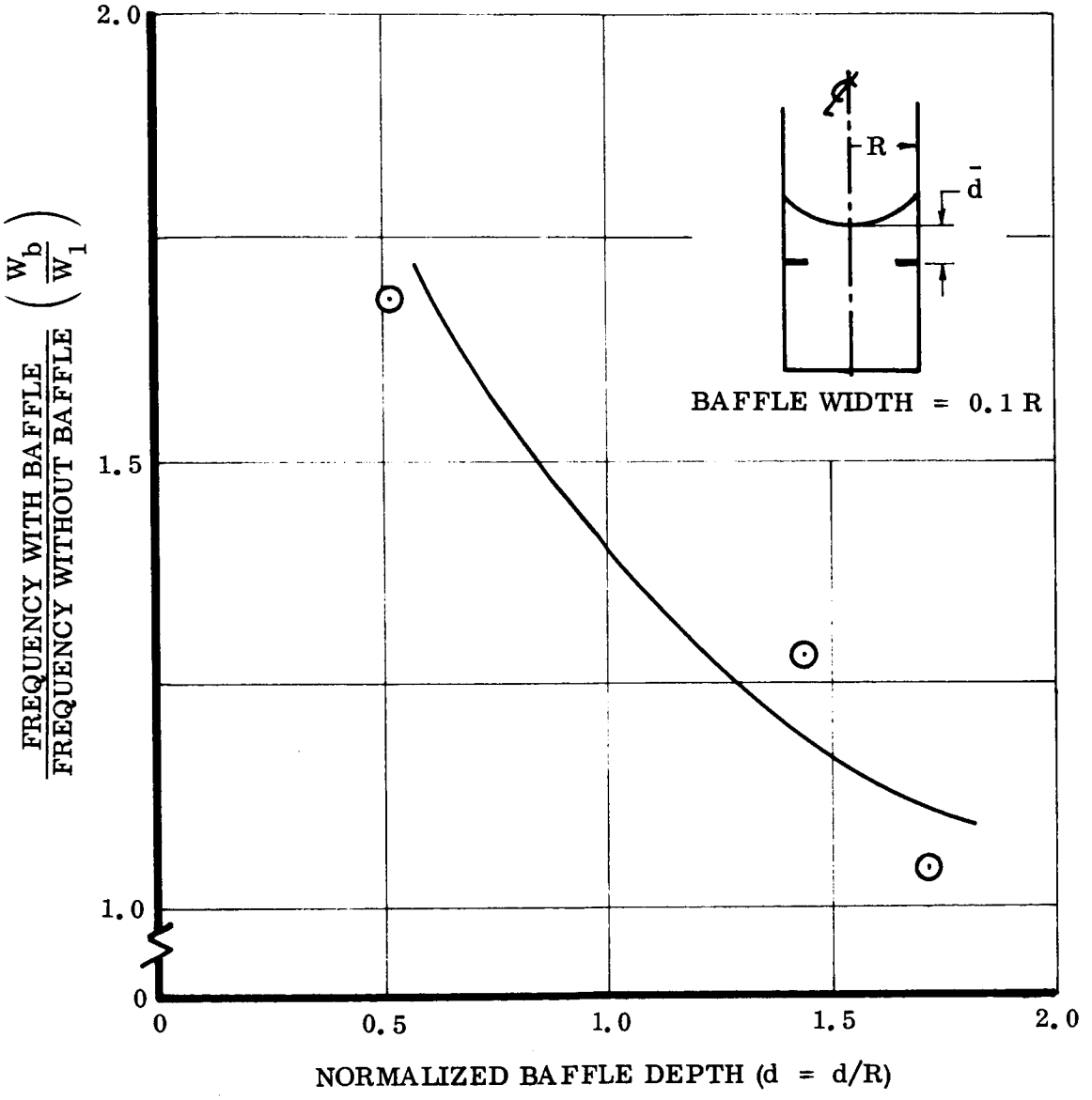

Figure 3-7 The Effect of Ring Baffle Location on Zero-g Sloshing Frequency

Table 3-I

SLOSHING PARAMETERS FOR A 4-FT DIAMETER TANK FILLED TO A DEPTH OF 4-FT

Parameter	Formula (Dimensionless)	ACCELERATION LEVEL (g_o's)/BOND NUMBER ($\rho\alpha R^2/\sigma$)			
		0/0	10^{-6}/0.116	10^{-3}/11.6	1/116,000
$\bar{\omega}_1$ sec^{-1}	$\left(\frac{1.84\ B_\alpha + 6.26}{1 + B_\alpha}\right)^{1/2}$	3.01×10^{-2}	3.12×10^{-2}	5.9×10^{-2}	5.6
$\frac{\bar{F}_x}{\bar{h}\omega}$ Dyne/cm	$1.71\ B_\alpha + 5.79$	144.8	149.8	640	49.5×10^5
$\frac{\bar{F}_x}{\bar{h}\omega}$ #/ft		.0099	.0125	.0439	338
$\bar{Z}_1$ *cm	$\frac{1}{1.84}$	32.8	32.8	32.8	32.8
$\bar{Z}_1$ ft		1.17	1.17	1.17	1.17
$\bar{k}_1$ $\frac{Dyne}{cm}$	$0.713\ (1 + B\alpha)$	17.8	19.6	225	2,120,000
$\bar{k}_1$ $\frac{\#}{ft}$		0.00122	0.00134	0.0154	146
$\mathcal{M}_1$ gm	1.42	1.04×10^5	1.04×10^5	1.04×10^5	1.04×10^5
$\mathcal{M}_1$ lb		473	473	473	473

*Below free-surface

Table 3-II

LATERAL SLOSHING EIGENVALUES FOR CYLINDRICAL TANK WITH HEMISPHERICAL BOTTOM (Θ = 5 Degrees)

Bond No. $B_\alpha = \rho g_\alpha r_o^2/\sigma$	Depth $h_o = \bar{h}_o/r_o$	Eigenvalues $\omega_k^2 = \bar{\omega}_k^2[(1+B_\alpha)\sigma/\rho r_o^3]^{-1}$ k = 1	2	3	4	5
0	3	2.81	34.6	137	353	723
	2	2.80	34.6	137	353	723
	1	2.69	34.0	136	353	723
	1/2	2.11	31.5	131	349	721
	1/4	1.33	24.8	113	314	675
	1/10	0.596	12.5	63.6	197	465
1	3	2.38	26.2	95.8	239	480
	2	2.38	26.2	95.8	239	480
	1	2.25	25.8	95.7	239	480
	1/2	1.65	23.6	92.0	235	477
	1/4	0.981	16.7	74.1	203	432
	1/10	0.403	12.5	73.0	239	578
2	3	2.21	22.4	78.3	191	380
	2	2.20	22.4	78.3	191	380
	1	2.07	22.1	78.3	191	381
	1/2	1.49	20.2	75.6	188	378
	1/4	0.717	11.8	54.2	154	338
	1/10	0.397	12.7	74.2	240	not produced
5	3	2.00	17.0	55.4	131	255
	1	1.85	16.8	55.3	131	255
	1/2	1.17	14.1	50.8	124	245
	1/4	0.615	9.93	45.7	129	279
	1/10	0.408	11.8	67.3	214	502
10	3	1.90	13.3	40.4	92.1	176
	2	1.90	13.3	40.4	92.2	177
	1	1.72	13.2	40.3	92.1	177
	1/2	1.02	10.4	35.1	83.5	164
	1/4	0.604	8.74	38.3	104.1	219
	1/10	0.434	10.6	58.2	180.5	417
20	3	1.85	10.2	28.6	62.5	117
	1	1.62	10.1	28.5	62.3	117
	1/2	0.941	8.11	25.5	58.9	114
	1/4	0.629	7.62	30.8	80.1	165
	1/10	0.475	9.34	48.1	144	325
50	3	1.84	7.54	18.2	36.7	65.2
	2	1.83	7.55	18.3	36.8	65.5
	1	1.58	7.48	18.2	36.6	65.1
	1/2	0.939	6.40	17.5	37.3	68.7
	1/4	0.701	6.41	22.1	52.7	103
	1/10	0.549	7.77	35.7	101	218

Section 4
LIQUID PROPELLANT LOCATION AND STABILITY

INTRODUCTION

The location of liquids in rocket propellant tanks under low gravitational conditions has, as with the shape of the liquid surface under low-g condition, been the subject of much investigation over the last few years. It is desirable to know where liquid propellants are under reduced gravitational conditions, and how best to get them where they need to be at specified times. In fact, this information is more important than that of the shape of liquid masses under reduced g conditions discussed in Section 2. Discussion of this topic has been delayed to this section because the ideas involved draw naturally on the materials presented in Section 2 and 3.

One periodically encounters liquid handling systems which are dominated by surface tension effects. A liquid-filled thermometer (e.g., mercury-in-glass) is a good example. The liquid located in the capillary always remains adjacent to the bulb end regardless of the attitude of the thermometer. This suggests that surface tension forces are somehow causing the liquid to remain in the bulb end of the thermometer even though gravitational body forces may act to displace the liquid to the other end. A corollary to this is that, under low g conditions, when surface tension forces dominate liquid behavior, liquid propellants in rocket tanks may be similarly affected, and that the liquids may be stabilized by surface tension away from more desirable locations. The purpose of this section is to indicate why this can happen and to show how the effect can be calculated.

Consider the classic example used to illustrate stable equilibrium shown in Figure 4-1. The ball is acted upon by a downward gravitational force. The ball located at point A is in a position where its gravitational potential energy is at least minimum locally.

Displacement of the ball from point A at the bottom of the valley will result, in the absence of mechanical dissipation, in cyclic motion of the ball about point A. Relocation of the ball to point B located at a ridge results in the ball being in a position of maximum gravitational potential energy. Displacement of the ball in one direction or the other from point B does not result in oscillation about this point, but rather results in the ball rolling away from point 3.

Before considering the stability of liquid propellants under low gravitational conditions, it is useful to examine the stability of another mechanical system whose stability is dependent upon the value of the gravitational acceleration relative to other parameters. Consider the mechanical system shown in Figure 4-2. A mass, W, is located between the vertical walls of the system by two horizontal springs and by a weightless rigid vertical link pinned at both ends. The differential equation describing small motions of the mass W about its equilibrium position $x = 0$ is easily derived with the aid of Newton's second law: the unbalanced force acting on the mass is equal to the mass times its acceleration.

$$\frac{W}{g_c} \ddot{x} = - kx + \frac{Wg}{\ell g_c} x \tag{4.1}$$

This can be arranged as follows:

$$\ddot{x} + p^2 x = 0 \tag{4.2}$$

Where

$$p^2 = \frac{kg_c}{W} - \frac{g}{\ell} \tag{4.3}$$

It can be stipulated that the solution to this differential equation describes cyclic motion about the equilibrium position $x = 0$ as long as p^2 is greater than zero. But p^2 is dependent upon the value of the mechanical gravitational acceleration relative to other

parameters of the system. The important lesson here is that the system is stable if it is able to oscillate. If the system is unstable it cannot oscillate; a small displacement will grow in time. When the vibration frequency is exactly zero, the system is neutrally stable, neither stable nor unstable. This condition, of course, separates stable conditions from unstable conditions.

The example of a mechanical system with gravity-dependent stability has little to do with the stability of liquids in rocket propellant tanks except to illustrate a principle. A more cogent example is available in the behavior of a small amount of liquid trapped in a small diameter tube. Consider the liquid shown in the small tubes in Figure 4-3.

Liquid is shown in a stable condition on the left and unstable on the right. The equilibrium location of the liquid in the tube on the left is determined by the small pressure difference which exists between the gas pressure above and below the slug of liquid. However, the lower free surface is stabilized by the surface tension property of the liquid. This can be illustrated by performing a simple experiment. If the diameter of the tube is increased, a diameter will be reached beyond which surface tension is no longer capable of stablizing the liquid surface, and the liquid and gas will begin to exchange positions with the liquid running down the walls and the gas rising in the center, as shown on the right. All other things being equal, the size of the tube has determined the stability of the system. The conditions of this experiment can be modified slightly by installing the small cylinder in a centrifuge with a small quantity of liquid located in the same manner as before. As the speed of the centrifuge is increased, an acceleration will be reached beyond which the liquid is destabilized as on the right in Figure 4-3. In this experiment, the effective level of gravitational acceleration has determined the stability of the system. It can be concluded then, that for a given liquid, increasing size and/or g-level eventually results in destabilizing the liquid surface.

THE STABILITY OF THE LIQUID GAS INTERFACE

The stability of the free surface in liquid propellant tanks against adverse accelerations can be determined in two ways. The small vibration method just illustrated provides perhaps the easiest way to an understanding of the limit of stability. Here the small amplitude lateral sloshing frequency of the surface is determined. Those conditions resulting in a zero sloshing frequency determine the limit of stability.

A more fundamental approach, however, is based upon the fact that, from a mathematical viewpoint, the stability of a conservative mechanical system is assured if, and only if, the total potential energy of the system is minimized. This is consistent with the second law of thermodynamics which requires that a stable system isolated from its surroundings must have maximum entropy.

The question of stability, however, cannot be attacked until the shape of the meniscus has been determined. The shape of the liquid whose stability limit is to be determined can be found according to Section 2. Consider the liquid in the cylindrical container of rotation shown in Figure 3-1. We will now use the small vibration analysis developed in Section 3 to determine the stability of the liquid to an adverse acceleration – one such that the body forces acting on the liquid are directed from more dense liquid toward a less dense material (say, a gas). An adverse acceleration would be opposite to the convention adopted in Figure 3-1 and would tend to make the liquid run out of the container in an upward direction. The stability of the liquid can be determined by solving for the sloshing frequency in the problem posed by Equations (3.1a), (3.3a), (3.8a) and (3.9a), setting this equal to zero, thus determining the Bond number which makes the system neutrally stable.

This process is best illustrated by examining the closed-form solution of the special case examined in Section 3. The Bond number for neutral stability is best obtained by solving for the frequency of vibration in Equation (3-23) and equating this to zero.

$$\omega_n = 0 = \frac{B\lambda_n + \lambda_n^3}{1 + B} \tanh \lambda_n \ell \tag{4.4}$$

The critical Bond number is

$$B_{cr} = -\lambda_n^2$$

The lowest value of this is the one of importance, and this is

$$B_{cr} = -3.39$$

Note that the depth of the liquid in the tank does not affect the stability of the free surface.

There is another useful viewpoint for this problem which results in an easier way of performing stability calculations. This can be observed by re-examination of Equation (3.19), the free surface boundary condition for the simple sloshing problem just used in the preceding illustration. If it is assumed beforehand that the frequency is zero, (3.19) becomes

$$\frac{1}{r}\frac{\partial}{\partial r}(rh_r) + \frac{1}{r^2}h_{\theta\theta} - Bh = 0 \tag{4.5}$$

This is a linear partial differential equation with the boundary condition drawn from the contact angle condition for the sloshing problem

$$\left.\frac{\partial h}{\partial r}\right|_{r=1} = 0 \tag{4.6}$$

The fact that this equation is linear enables reduction of the solutionof Equation (4.5) to the solution of two ordinary differential equations by the familiar process of separation of variables.

Setting

$$h(r, \theta) = \eta(r)\,\tau(\theta) \tag{4.7}$$

(4.6) can be reduced to

$$\eta_{rr} + \frac{1}{r} - \left(\frac{\mu^2}{r^2} + B\right)\eta = 0 \tag{4.8a}$$

$$\tau_{rr} + \mu^2\,\tau = 0 \tag{4.8b}$$

Where (4.8a) is subject to boundary conditions

$$\eta(0) = \eta_r(1) = 0 \tag{4.9}$$

Equation (4.8a) is Bessel's differential equation. The boundary conditions (4.9) can be met only if $\mu^2 > 0$ and $B < 0$. With this, the problem is reduced to solution of (4.8a) subject to (4.9). Now -B is an eigenvalue of this problem. Solutions must be found for (4.8a, 4.9), and these occur only for certain values of -B.

The solutions are of the form

$$\eta = J_\mu\left(\sqrt{-B}\,r\right) \tag{4.10}$$

where $J_\mu(\ )$ is the Bessel function of first kind of order μ. Eigenvalues for this occur (for $\mu = 1$) only when $-B = -3.39, -28.5, -72.8, \ldots$; and only the smallest of these occurring for $\mu = 1$ is important (this number being the smallest nontrivial eigenvalue for $\mu \geq 0$).

The process just outlined gives us another and easier way of determining the critical Bond number for meniscuses of more complicated shape. The basic idea is to simultaneously solve the nonlinear differential equation for the free surface shape (2.4)

$$\frac{1}{r}\frac{\partial}{\partial r}\frac{rf_r}{\sqrt{1+f_r^2}} - Bf - f_{rr}(0) = 0 \tag{4.11}$$

subject to

$$f(0) = f_r(1) - \cot(\theta + \varphi) = 0 \tag{4.11a}$$

and the linear free surface boundary condition for the sloshing problem (3.8a) with the frequency set equal to zero.

$$\frac{1}{r}\frac{\partial}{\partial r}\frac{rh_r}{\sqrt{1+f_r^2}^3} + \frac{1}{r^2}\frac{h_{\theta\theta}}{\sqrt{1+f_r^2}} - Bh = 0 \tag{4.12}$$

subject to

$$h(0) = h_r(1) = 0 \tag{4.12a}$$

Equation (4.12) is linear, although with nonconstant coefficients, and the technique of separation of variables is still applicable. Equation (4.11) and the first boundary condition on (4.12) (i.e., $h(0) = 0$) limit the use of these equations to cylinders or cones which do not contain bodies of revolution along the axis as in annular tanks. The equations and/or boundary conditions can easily be modified to allow extension to other cases. The first of the boundary conditions (4.12a) may be modified to account for constant contact angle condition at a circular cylindrical or conical inner body, i.e.,

$$h_r(r_i) = 0 \tag{4.12b}$$

Both boundary conditions on (4.12) become more complex where meridians of the inner and outer surfaces are curved.

AVAILABLE SOLUTIONS

By this time the results of stability calculations for many geometries are available in the literature. Reynolds, et al.[4.1] have presented the most extensive exposition of this subject. Selected results from this work and others available at this time are summarized as follows:

Circular Cylinders. The solution to Equations (4.11) and (4.12) for this case was first computed by Seebold[4.2]. The stability limit for this simple geometry is presented as a function of contact angle in Figure 4-4. Note that the closed form solution presented as an illustration is included in this case.

Annular Cylinders. The problem for the cavity formed by concentric circular cylinders is the same as that just above except that the boundary conditions for (4.11) and (4.12) are replaced by

$$-f_r(r_i) = f_r(1) = \cot\theta \tag{4.11b}$$

$$h_r(r_i) = h_r(1) = 0 \tag{4.12b}$$

Results of computations by Seebold, et al.[4.3] are given in Figure 4-5.

Rotating Circular Cylinders. The stability of liquid in solid body rotation with angular velocity ω with a cylindrical container about its own axis has been computed by Seebold[4.4] and is given in Figure 4-6. The differential equation for the free surface

shape (4.12) is modified by the addition of a single term resulting in

$$\frac{1}{r}\frac{d}{dr}\frac{r f_r}{\sqrt{1 + f_r^2}} - Bf - f_{rr}(0) + \Omega^2 r^2 = 0$$

where $\Omega^2 = \rho R^3 \omega^2/2\sigma$. In this case, the boundary conditions (4.11a) and the stability equation (4.12) and its boundary conditions (4.12a) remain unchanged.

Cones. The solution to (4.11) and (4.12) for this case is presented in Figure 4-7. The solution here depends only upon the edge angle and the radius of the contact circle measured from the axis of the capillary shape. These results can be used for bubbles or drops where the edge angle defined in the figure is normally negative.

Annular Cones. The results of partial computation of the limit of stability in a conical cavity with a circular cylindrical center body coaxial with the cone is given in Figure 4-8. The volume of liquid stabilized is plotted against the Bond number based upon the radius of the central cylinder with total cone angle as a parameter for a contact angle of 5 degrees.

Spherical Cavities (Including Annular Spherical Cavities): Spherical cavities without center bodies have a zero limit of stability. That is, the slightest adverse acceleration will displace the liquid to another location in the tank. When center bodies are present, however, liquid can be stabilized against an adverse acceleration. Results of partial calculations[4.5] are presented in Figure 4-9. These calculations are also limited to a 2-1/2-degree contact angle and to cylindrical bodies concentric with a diameter of the sphere. The critical Bond number based upon tank radius is plotted against the tank fill fraction with the ratio of cylindrical standpipe radius to tank radius as a parameter.

General Contains of Revolution (Without Center Bodies). Reynolds[4.1] has developed a general criterion for the limit of stability of liquids in surfaces of revolution. The reader is referred to the Reference 4.1 for details. (This material is also presented in NASA SP-106[4.6].)

REFERENCES

4.1 Reynolds, W.C., Saad, M.A., and Satterlee, H.M., "Capillary Hydrostatics and Hydrodynamics at Low-g," Stanford Univ., Dept. Mech. Engr, Rpt. No. LG-2, Stanford, Calif., Sept. 1, 1964, pp 34 ff

4.2 Seebold, J.G., Private Communication, Dec. 1963

4.3 Seebold, J.G., Hollister, M.P. and Satterlee, H.M., "Capillary Hydrostatics in Annular Tanks," Jour. of Spacecraft and Rockets, Vol. 4, No. 1, Jan. 1967, pp. 101–105

4.4 Seebold, J.G. and Reynolds, W.C., "Configuration and Stability of a Rotating Axisymmetric Meniscus at Low-g," Stanford Univ., Dept. Mech. Engr., Rpt. No. LG-4, Mar. 1, 1965

4.5 Seebold, J.G., "The Stability of Meniscuses in Spherical and Conical Tanks With Cylindrical Standpipes," Lockheed Missiles & Space Co., Independent Development Program, 1966 (Unpublished)

4.6 "The Dynamic Behavior of Liquids in Moving Containers," NASA SP-106, H. N. Abramson, ed., 1966, 1. 406

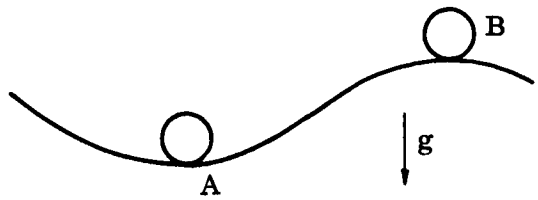

Figure 4-1 Equilibrium of a Ball

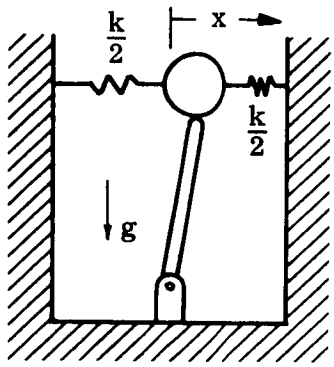

Figure 4-2 Mechanical System With Gravity-Dependent Stability

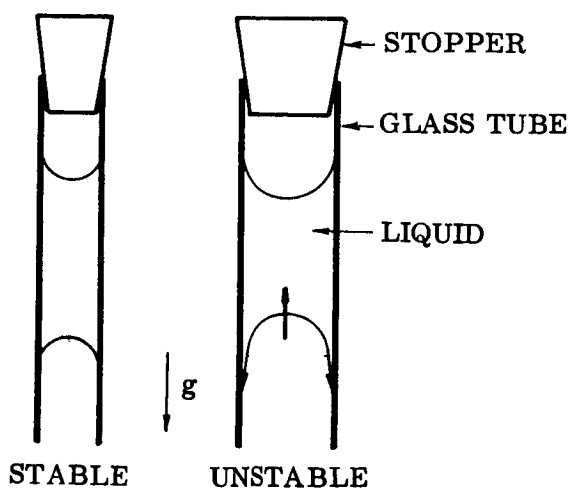

Figure 4-3 Meniscus Stability

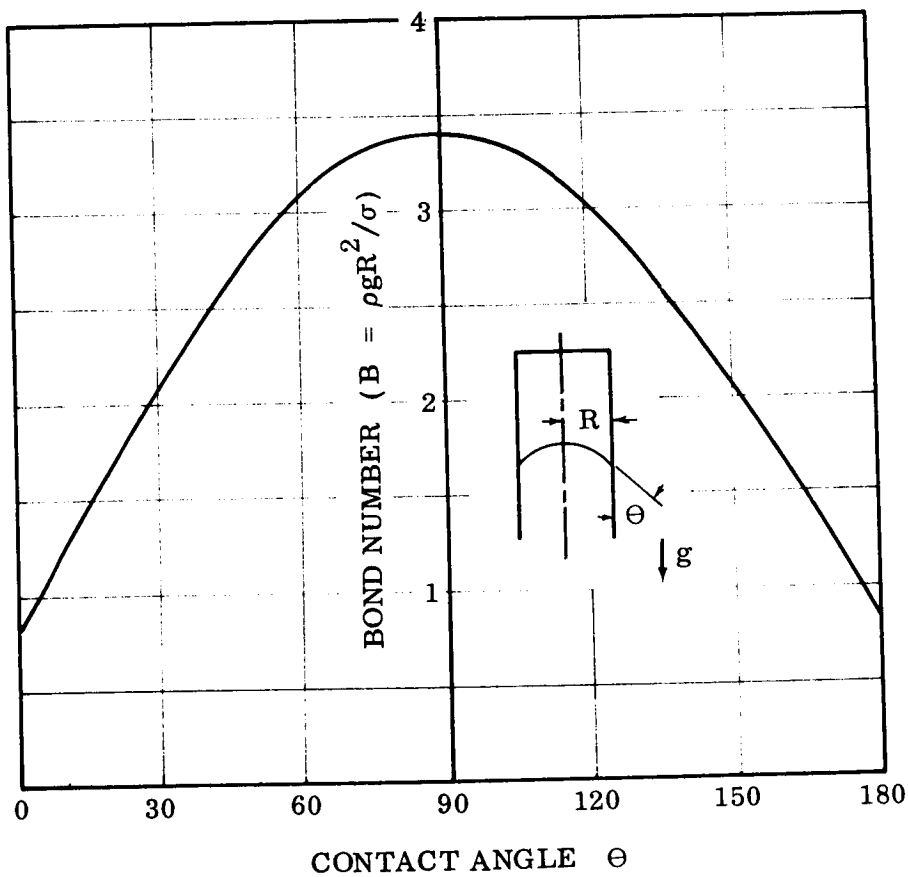

Figure 4-4 Meniscus Stability in a Circular Cylinder

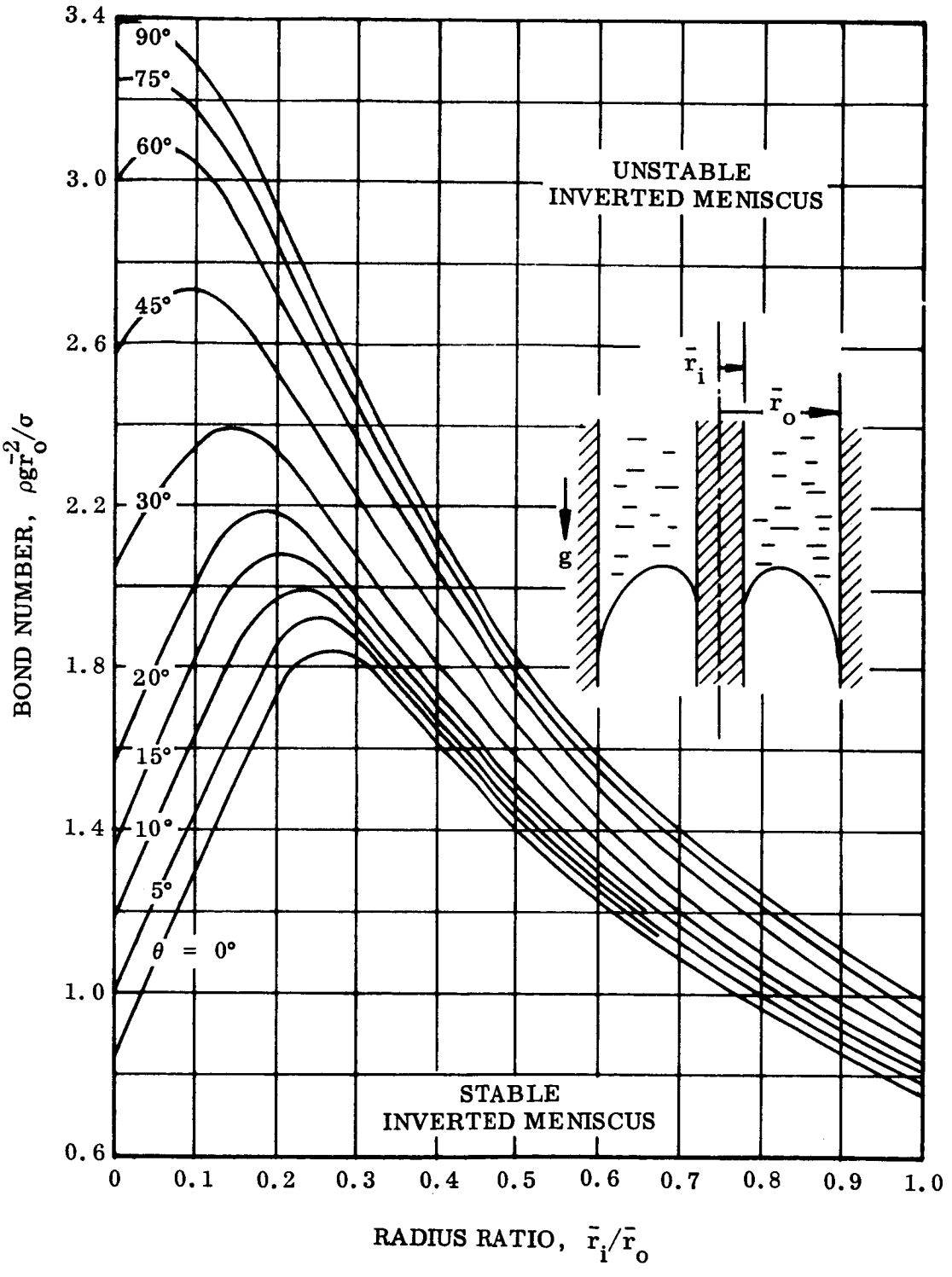

Figure 4-5 Stability of an Inverted Annular Meniscus

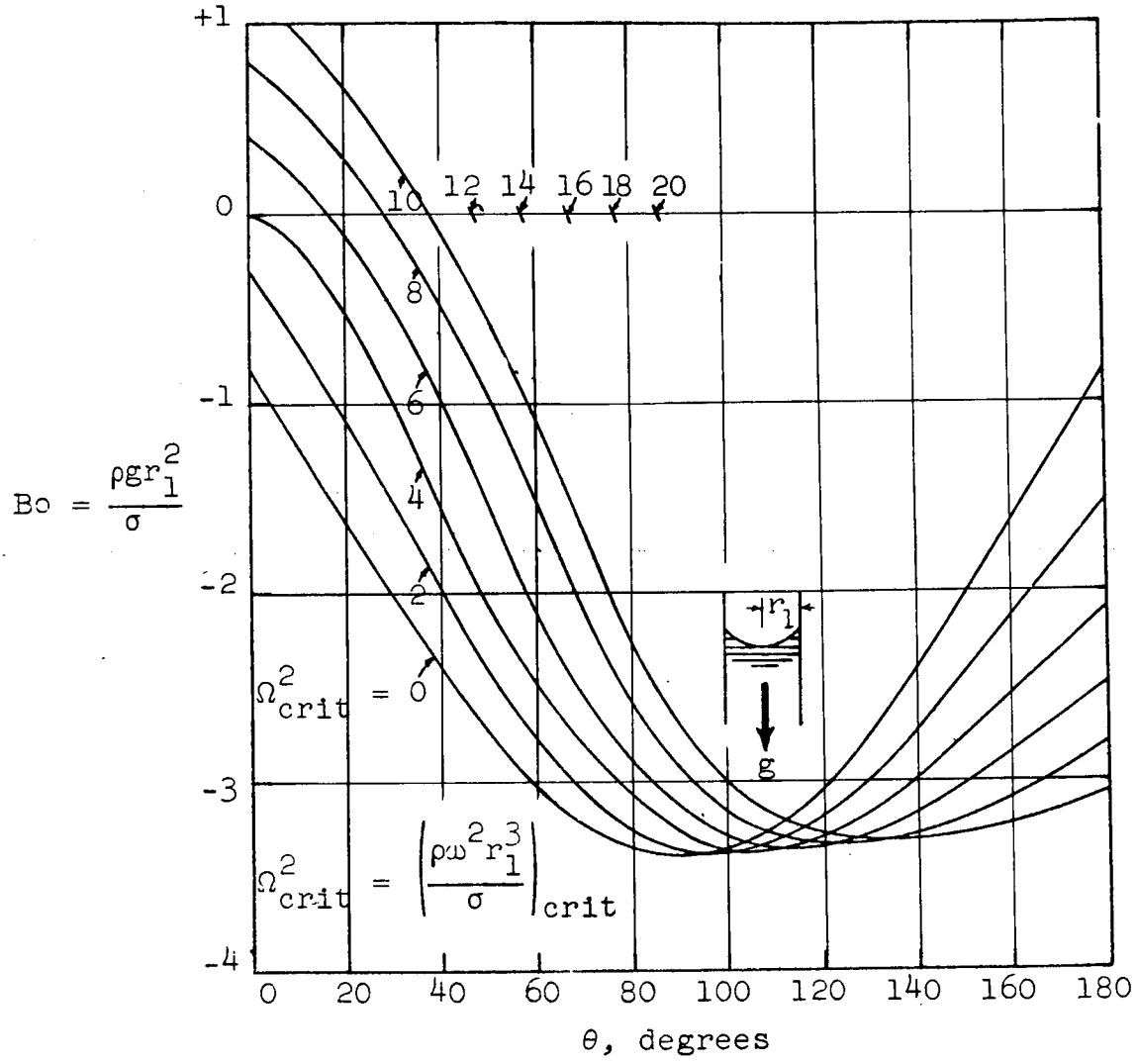

Figure 4-6 Stability Map

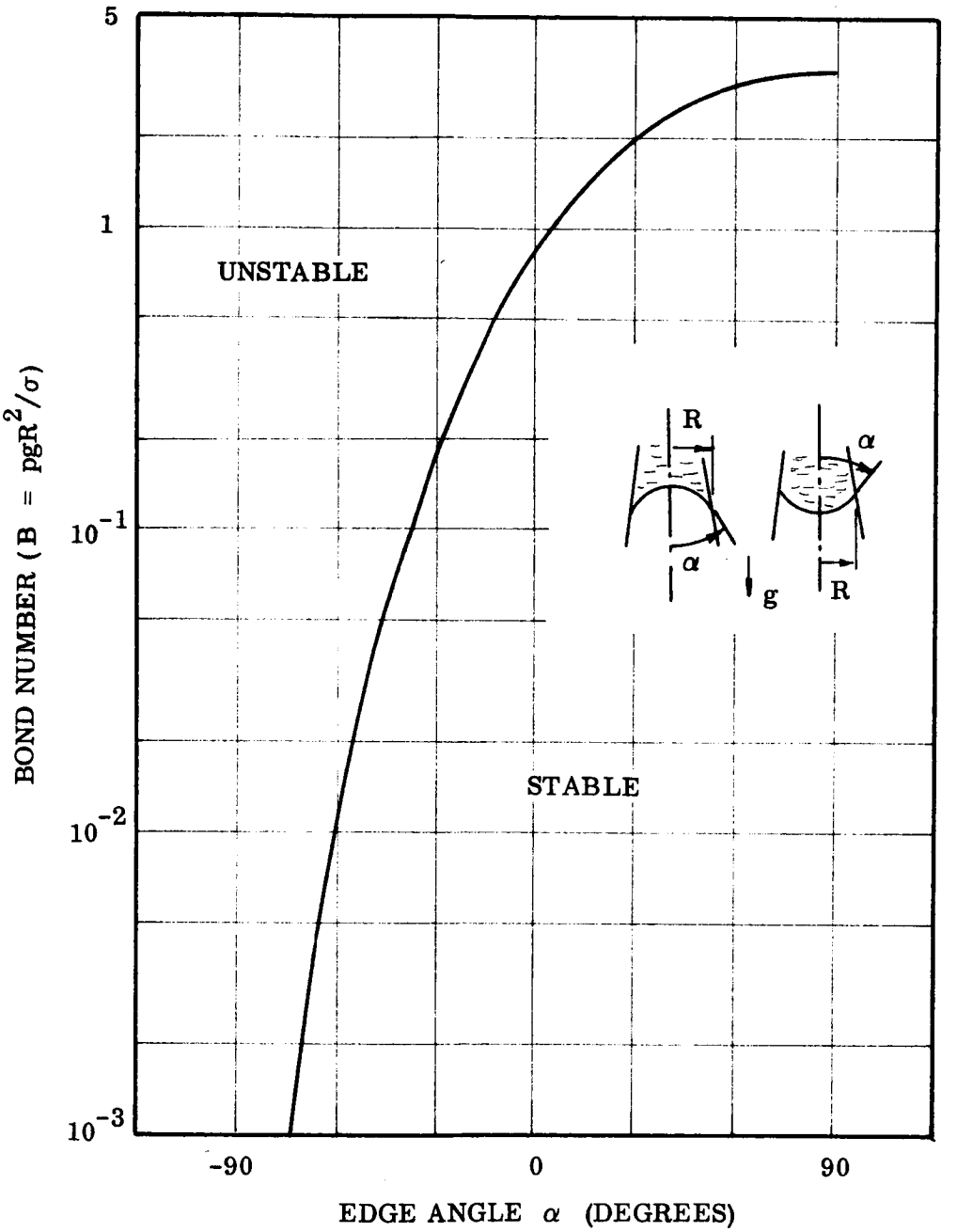

Figure 4-7 Stability of a Meniscus in a Conical Container

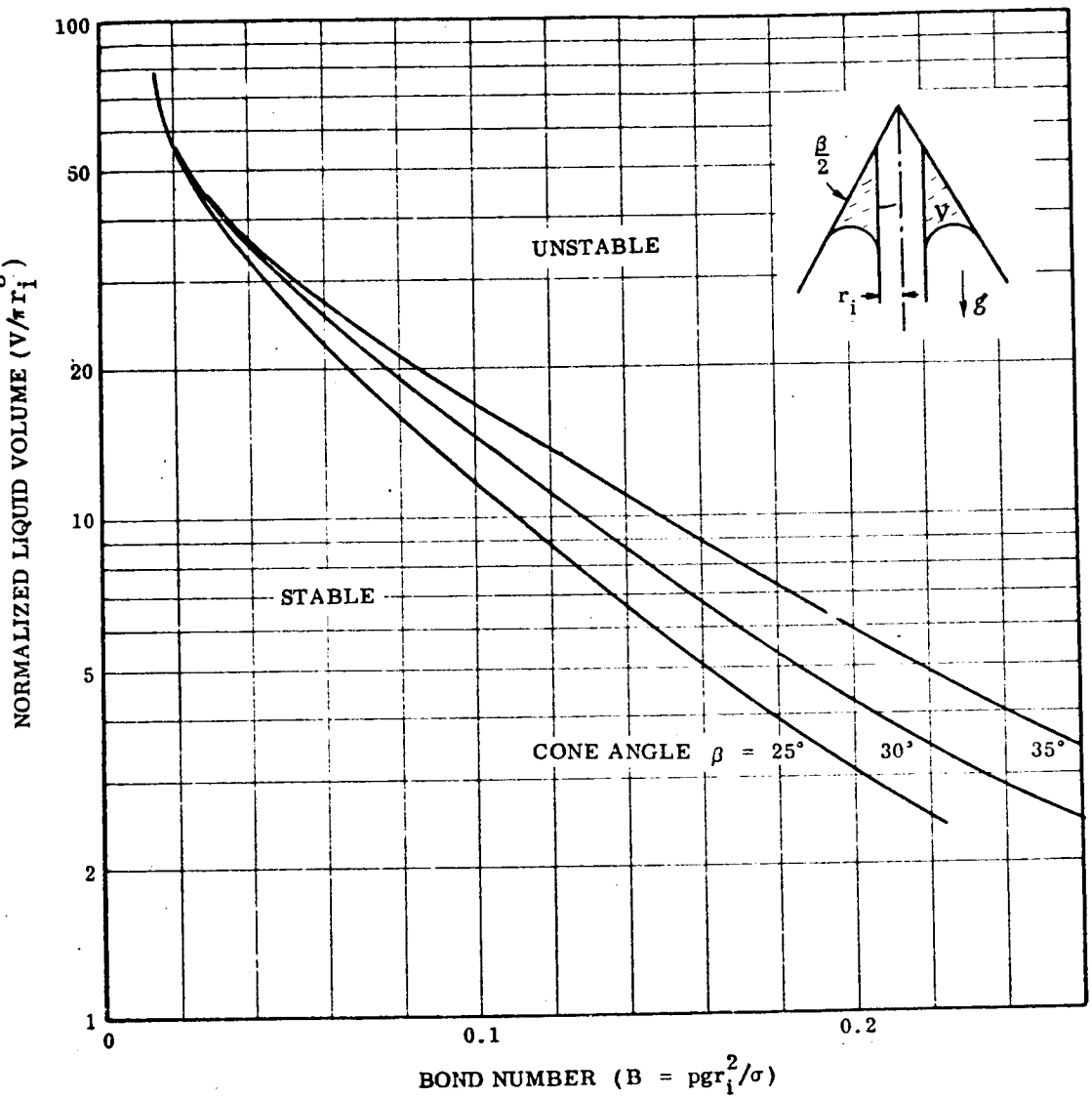

Figure 4-8 Stability of a Meniscus in an Annular Cone

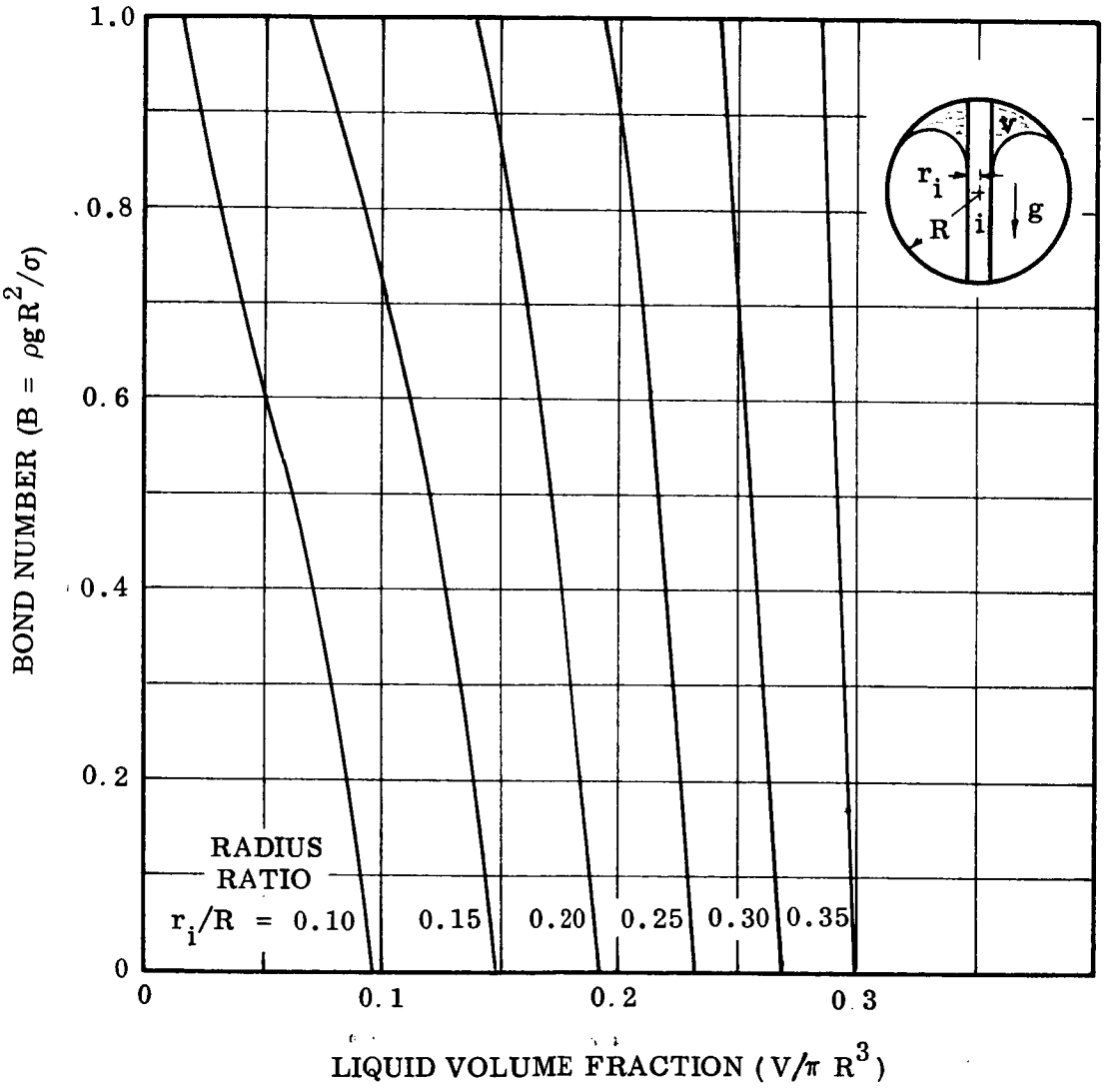

Figure 4-9 Meniscus Stability in a Spherical Tank with Cylindrical Standpipe

Section 5
LIQUID REORIENTATION AND ULLAGE ENTRAINMENT

INTRODUCTION

The operation of a sophisticated space vehicle system may require maneuvers which will place liquid propellants at the wrong ends of their respective tanks. Subsequent operation of the propulsion system requires that the liquids be oriented at the drain end. It is important, therefore, to know how the liquid propellants behave during liquid-settling maneuvers so that these will have a minimum effect on the efficiency of the spacecraft. This section of the Handbook will describe the basis for a theoretical treatment of the problem, outline methods for implementing the theoretical treatment, and indicate the results of analysis as well as experiments which have been carried out.

A brief description of a settling maneuver and the resultant liquid behavior will establish a basis for the discussion to follow. Consider the rocket propellant tank shown in Figure 5-1a. The tank has been in free fall for a period of time with the propellant collected in the end opposite the drain. Further, the interface has the spherical cap-shape characteristic of free-fall conditions. At a given time, an axial force is applied to the tank as shown in Figure 5-1b. When the liquid-tank system is viewed from a coordinate system fixed with respect to the tank, it appears as if the liquid is acted upon by a body force directed oppositely to the applied force. In response to this body force, the liquid begins to run down the tank wall forming a wall sheet surrounding a central bubble which rises toward the upper end of the tank (Figure 5-1c). As the wall sheet enters the tank bottom and impinges upon itself it may, depending upon preceding conditions, produce a central jet of liquid which can rise to the liquid still remaining in the upper end of the tank (Figure 5-1d). Formation of such a jet is usually a very dissipative process and the jet soon dissapears into the pool of liquid being collected in the tank bottom. The wall sheet, as it joins the collecting pool, carries ullage gas

with it which is mixed in the form of small bubbles with the collected liquid (Figure 5-1d). These eventually rise to the surface of the collecting pool as long as the settling acceleration is maintained. Meanwhile, the central bubble approaches the tank top, and as it does so, it can ordinarily be expected to slow down.

Different behavior from that just described can be expected depending upon the departure of operation conditions from the preceding conditions:

- Should the tank be acted upon by a force opposite to the settling force prior to the settling process, the interface will be flattened. Application of the settling thrust may, depending on the settling acceleration level, result in the formation of a central drop in addition to the wall sheet flow. Such drops have been observed to eventually wash off on to one side of the tank, but most propellant tanks are short enough that this does not occur before the wall sheet and the central drop impact the tank bottom.
- Significant transverse liquid motion prior to the settling maneuver will cause the liquid to slide predominately down one side of the tank.
- Very low settling accelerations do not result in the entrainment of ullage gas in the collecting liquid pool.
- Baffles have a very marked influence on the flow patterns in the tank. The nature and extent of the effect depends on the detail baffle design.

This description points out a number of details about settling liquid motions which require quantitative discussion. First, the position histories of the reorienting wall sheet and the central bubble and the average thickness of the wall sheet are desired. The position history of the wall sheet is needed to determine the minimum time for a settling maneuver using secondary propulsion. The position history of the central bubble determines when equipment such as venting devices will be free of liquid. Second, the height, volume, and life of the rebound jet affect vehicle dynamics. Third, the quantity and size of ullage gas bubbles entrained in the collected liquid influence the time required to settle them out, thereby affecting total impulse propellant requirement for the settling maneuver.

MATHEMATICAL PROBLEM FORMULATION FOR AXISYMMETRIC REORIENTATION

The first of the basic phenomena associated with liquid reorientation to be examined is the initial formation of the wall sheet and the central bubble. The mathematical problem describing the initial stages of the axisymmetric reorientation of a liquid from one end its tank toward the other can be easily formulated. Consider the liquid in the tank pictured in Figure 5-2. Based upon the assumptions that the liquid is inviscid and incompressible and that its motion is irrotational, the motion of the liquid can be determined from the solution of the boundary/initial value problem derived as follows. The governing equation is Laplace's equation, the equation of continuity. In terms of the velocity potential, this may be written in polar cylindrical coordinates

$$\varphi_{\bar{r}\bar{r}} + \frac{1}{\bar{r}} + \varphi_{\bar{z}\bar{z}} = 0 \text{ in } D \tag{5.1}$$

where the velocity potential is defined by the following equations for the radial and axial velocity components.

$$\bar{u} = \varphi_{\bar{r}} \ , \ \bar{w} = \varphi_{\bar{z}} \tag{5.2}$$

The solution to Laplace's equation must satisfy a zero normal flow condition at solid walls.

$$\frac{\partial \varphi}{\partial \bar{n}} = 0 \text{ on } w \tag{5.3}$$

The solution is further constrained by a boundary condition drawn from the nonsteady Bernoulli equation applied to the free surface together with a kinematic condition identical to the one developed in the preceding section on lateral sloshing. The general nonsteady Bernoulli equation is

$$\frac{p}{\rho} + \frac{1}{2}(\nabla\varphi)^2 + \alpha(t) g_\alpha \bar{z} + \frac{\partial \varphi}{\partial \bar{t}} = F(\bar{t})$$

The pressure difference across the interface caused by curvature of the free-surface is

$$p_g - p = \sigma\left\{\frac{1}{\bar{r}}\frac{1}{\partial\bar{r}}\frac{\bar{r}\,\bar{f}_{\bar{r}}}{\sqrt{1+\bar{f}_{\bar{r}}^2+\frac{1}{\bar{r}^2}\bar{f}_\theta^2}}+\frac{1}{\bar{r}^2}\frac{\partial}{\partial\theta}\frac{f_\theta}{\sqrt{1+\bar{f}_{\bar{r}}^2+\frac{1}{\bar{r}^2}\bar{f}_\theta^2}}\right\}$$

$$= 2\sigma\,\bar{H}$$

Substitution of this into the preceding equation and evaluation at $\bar{f} = 0$ when the velocity potential is zero yields

$$F_o = \frac{p_g}{\rho} - \frac{2\sigma\,\bar{H}_o}{\rho} + g_\alpha\,\bar{f}_o$$

Here, subscript zero refers to the initial condition at $\bar{t} = 0$. The free surface boundary condition then becomes

$$\frac{2\sigma\,\bar{H}}{\rho} - \frac{1}{2}(\nabla\varphi)^2 - \alpha(t)g_\alpha\bar{f} - \frac{\partial\varphi}{\partial\bar{t}} = \bar{F}(t) \qquad (5.4)$$

The right hand side of this equation is an arbitrary function of time. The kinematic condition is, using the nomenclature defined by Figure 5-2,

$$\frac{\partial\bar{f}}{\partial\bar{t}} = \frac{\partial\varphi}{\partial\bar{z}} - \frac{\partial\bar{f}}{\partial\bar{r}}\frac{\partial\varphi}{\partial\bar{r}} \qquad (5.5)$$

The time dependent solution to this problem is determined from the application of initial conditions regarding the location and velocity of the free surface.

$$\bar{f}(\bar{r}\ ,\ 0) = \bar{f}_o(\bar{r}) \quad \text{on} \quad \bar{f} \qquad (5.6)$$

$$\bar{u}_o(\bar{r}) = \frac{\partial \varphi}{\partial r}\left[\bar{r},\ \bar{f}_o(\bar{r}),\ 0\right] = \bar{w}_o(\bar{r}) = \frac{\partial \varphi}{\partial z}\left[\bar{r},\ \bar{f}_o(\bar{r}),\ 0\right] = 0 \text{ on } \bar{f} \qquad (5.7)$$

The first of these boundary conditions gives the location of the interface at $\bar{t} = 0$; the second indicates that the liquid is initially at rest.

Numerical treatment of the problem just posed is made most convenient by nondimensionalization of the equations. The coordinated in equations (5-1 through 5-7) are normalized by dividing distances by a convenient length, say the radius of the tank R_o shown in Figure 5-2. Normalization is completed by dividing the velocity potential and time by

$$\left[R^3 g_\alpha (1 + \beta)\right]^{1/2} \text{ and } \left[\frac{R}{g_\alpha (1 + \beta)}\right]^{1/2}$$

respectively where $\beta = \sigma/\rho g_\alpha R^2$, the reciprocal of the Bond number based on the maximum acceleration. The distance R and acceleration g_α can be any value but are conveniently taken as the tank radius and the maximum value of the axial acceleration such that r and α range from zero to unity.

Laplace's equation (5.1) and the boundary conditions at solid walls (5.3) remain unchanged by this normalization as do the kinematic condition and the initial conditions.

The complete problem statement in dimensionless form is as follows.

$$\Phi_{rr} + \frac{1}{r}\Phi_r + \Phi_{zz} = 0 \text{ in } D \qquad (5.1a)$$

$$\frac{\partial \Phi}{\partial r} = 0 \text{ on } w \qquad (5.3a)$$

$$2\frac{\beta}{1 + \beta} H + \frac{1}{2}(\nabla\Phi)^2 - \frac{\alpha(t)}{1 + \beta} f - \frac{\partial \Phi}{\partial t} = 0 \qquad (5.4a)$$

$$\frac{\partial f}{\partial t} = \Phi_z - f_r \Phi_r \tag{5.5a}$$

$$f(r) = f_o(r) \text{ on } f \tag{5.6a}$$

$$u_o(r) = w_o(r) = 0 \text{ on } f \tag{5.7a}$$

The mathematical problem just posed appears straightforward. One might imagine that the solution to Laplace's equation could be found which satisfied almost any boundary conditions. Such is not the case, unfortunately; the problem set up in the preceding paragraphs offers considerable numerical difficulties. The most straightforward way of attempting a solution is to expand the velocity potential in a series of spatial functions each term multiplied by a time dependint coefficient. The spatial functions are chosen so as to satisfy Laplace's equation in the interior of the liquid. The series is then substituted into the boundary conditions and the resultant expressions evaluated at enough points on the boundary of the domain occupied by the liquid to enable evaluation of the coefficients to the series at any given point in time. Next, the series is used to determine the velocity of particles in the free surface at the given point in time. These are used to predict the location of the free-surface of the liquid at the next time step.

Sophisticated computing schemes may involve the repetition of enough of these steps to enable the correction (in the numerical sense) of truncation errors introduced by the preceding (or predictor) portion of the calculation.

In the recent past, a number of attempts (5.1, 5.2) have been made to compute reorientation motions in the manner just outlined. The process used in one of these is repeated in enough detail to illustrate the procedure.

The method used to approximate the solution of the foregoing problem is as follows. In brief, the velocity potential is represented in the form of a series

$$\Phi (r, z, t) = \sum_n C_n(t) \Psi_r (r, z) \tag{5.8}$$

where the functions $\Psi_r(r, z)$ satisfy Laplace's Equation (5.1) (and possibly some of the boundary conditions included in 5.3). The time dependent coefficien ts $C_n(t)$ are determined numerically by an orthonormalizing computation in order to satisfy those boundary conditions which are not naturally satisfied by $\Psi_r(r, z)$.

For the flat-bottomed cylindrical container shown in Figure 5-3, the velocity potential satisfying Equations (5.1) and (5.3) has the representation, determined by separation of variables,

$$\Phi(r, z, t) = \sum_n C_n(t) J_o(\lambda_n r) \frac{\cosh(\lambda_n z)}{\cosh(\lambda_n H)} \tag{5.9}$$

where $J_o'(\lambda_n) = 0$ determines the numbers λ_n, $n = 1, 2, \ldots,$. The time variation of the velocity potential $\Phi(r, z, t)$ [i.e., of the coefficients $C_n(t)$] is determined by requiring that the representation (5.9) satisfy the boundary condition (5.4a); i.e., that

$$\sum_{n, m} \frac{dC_n}{dt}(t) F_n(r, t) = \hat{\Phi}(r, t) \tag{5.10}$$

where

$$\hat{\Phi}(r, t) = \frac{f}{1+\beta} + \frac{\beta}{1+\beta} \frac{1}{r} \frac{d}{dr} \frac{r f_r}{\sqrt{1 + f_r^2}} - \frac{1}{2} [\nabla \varphi(r, f, t)]^2 \tag{5.11}$$

and where

$$F_n(r, t) = J_o(\lambda_n r) \frac{\cosh[\lambda_n f(r, t)]}{\cosh(\lambda_n H)} \tag{5.12}$$

This can be satisfied approximately by determining the coefficients $C_n(t)$ numerically by some orthonormalizing computation [cf. Davis and Rabinowitz[5.3], for a general description of orthonormalizing methods]. The method developed to determine the first few coefficients $C_n(t)$, $n = 1, \ldots, N_o$ is outlined below. Basically, it amounts to following the motion of the free surface on the $\theta = 0, \pi$ plane. The derivatives $dC_n(t)/dt$ may be determined from Bernoulli's equation i.e., from

$$\sum_{n=1}^{N_o} \frac{dC_n}{dt}(t)\, F_n(r, t) = \hat{\Phi}(r, t) \tag{5.13}$$

by the orthonormalization technique used by Moore and Perko (5.1). The functions $\hat{\Phi}(r, t)$ and $F_n(r, t)$ are defined in (5.4a) and (5.10) respectively. The predicted surface shape at $t + \Delta t$ follows from the kinematic equation (5.5a) as

$$\begin{aligned} f(r, t + \Delta t) &= f(r, t) + f_t(r, t)\,\Delta t \\ &= f(r, t) + [\varphi_z - f_r \varphi_r](r, t)\,\Delta t \end{aligned} \tag{5.14}$$

Having computed the predicted coefficients and surface shape, one then proceeds to the correction step of the modified Euler method to move ahead one increment of time. The time dependent coefficients $C_n(t)$, $n = 1, \ldots, N_o$ and the motion of the free surface $f(r, t)$ are determined in this way. The computation scheme is outlined in Figure 5-4.

OBSERVATIONS BASED ON AVAILABLE ANALYSIS AND EXPERIMENTS

Results of the calculations carried out by the computation scheme just described which are most important to the description of the reorientation of liquids in rocket propellant

tanks are summarized as follows together with the results of other analysis and experiments:

- The liquid wall sheet formed as the liquid begins to run down the tank wall from its initially hemispherical shape accelerates with the body force acting on the liquid. Small scale experiments performed in drop tower experiments have indicated that the wall sheet accelerates at about 0.70 to 0.87 times the rate of a freely falling body. The discrepancy between experiments and the results of this type of theoretical treatment may possibly be laid to the fact that the analysis neglects the viscous property of the liquid. This seems proper in the interior of the liquid because the analysis of other aspects of the reorientation phenomenon agree to a much better degree with experiments. The difficulty apparently lies in neglecting the boundary layer formed adjacent to the tank wall. Larger scale experiments designed to explore other aspects of reorientation liquid behavior indicate that the viscous boundary layer has a much smaller effect on the acceleration of the leading edge of the reorienting wall sheet. The small scale of drop tower experiments and the relatively larger scale experiments required for other purposes (such as exploring liquid rebound) leave a gap which cannot easily be filled with available experimental facilities. Consequently, there is now no experimental evidence one way or the other indicating that the slowness of wall wave leading edges in small drop tower experiments is due solely to the necessary small scale of drop test models.
- The thickness of the wall sheet formed in the initial stages of reorientation is strongly influenced by the shape of the liquid prior to the application of the settling acceleration. When the motion starts from a spherical cap interface the wall sheet thickness δ is given by

$$\delta = 0.165 \sqrt{\frac{R^3}{x}}$$

where R is the radius of the tank and x is the axial distance from the vertex of the rising bubble.

This expression was derived by Taylor[5.4] in the steady state analysis of the rise of large bubbles in cylinders.

The central bubble which forms upon the application of settling acceleration to a liquid with an initially spherical cap interface shape finally attains the rise velocity developed by Taylor* and even earlier by Dimitrescu[5.5]

$$v_b = 0.46\sqrt{gR}$$

The time required to achieve this velocity is approximately given by

$$t = \sqrt{\frac{g}{R}} \text{ for } B_R > 10$$

A precise value for this length of time is not available from the analysis because the results reported here were obtained by extrapolating the calculation from the computation scheme past the point in time when they became unstable. Results of the extrapolation do, however, agree quite well with experimental observations.

As the reorientation proceeds, the initial wall sheet enters the bottom of the tank, assuming, for the moment, that there are no obstructions in the tank such as baffles. The bottoms on most liquid propellant tanks are segments of spheroids. This geometry effectively reduces the flow area for the wall sheet, and, because of this, the wall sheet grows thicker. Upon reaching the center of the tank bottom, the liquid impacts upon itself resulting in a rather violent splash or geyser (often called rebound). As the flow proceeds, the tank bottom begins to fill and the wall sheet flows then into a growing pool of liquid. Ullage gas is entrained by the wall sheet as it flows into the collecting pool. The numerical characteristics of the phenomona just outlined are described below to the extent that experimental evidence allows.

---

*Op. cit.

Reorientation such that the Weber number

$$W = \frac{R\, V_R^2}{\sigma/\rho} < 2$$

results in essentially no geyser[5.6]. The velocity V_R may be estimated for this purpose from $V_R \approx \sqrt{2gh}$ where h is the distance travelled by the wall wave leading edge until the initial impact. The geyser resulting from reorientation Bond numbers of the order of 3000 have been examined experimentally under standard gravitational conditions. It is observed that the geyser initially rebounds a significant percentage of the tank length and may approach the location of the liquid in the tank prior to the application of the settling acceleration. The diameter of the geyser during this initial portion of its life averages 0.3 to 0.4 the radius of the tank. The growth and decay of the geyser is shown in Figure 5-5. It may be concluded that during the growth of the geyser the liquid is exerting a greater force on the bottom of the tank than is exerted after the geyser has subsided.

Ring baffles and internal tank stiffeners, commonly employed in propellant tanks, can have a marked influence on the character of the reorientation flow. Baffles severely complicate the reorientation flow pattern and can result in a flow which is initially pulsating. The processes involved in such a pulsating flow are as follows:

> At all but perhaps very low reorientation Bond numbers and high fill levels, the wall sheet thickness is of the order of the width of these baffles and structural numbers. The wall flow encountering one of these previously unsubmerged obstacles is deflected radically inward toward the tank center (see Figure 5-6a), causing a thickening of the sheet and eventual impingement upon itself at the tank center. The angle of deflection is determined by the ratio of the wall sheet thickness to the baffle width. Impingement of the deflected flow at the tank centerline partitions the ullage volume and

temporarily prevents further reorientation of the gas "below" the sheet of propellant spanning the tank. Two propellant streams issue from the impingement area in opposite directions along the tank axis, one continuing into the tank drain and the other returning toward the tank top in a recirculation pattern (Figure 5-6). Because the liquid spans the tank cross section at the baffle, the reorientation flow is temporarily interrupted. At some point the liquid flow passing the baffle is stopped (Figure 5-6c) and the interface spanning the baffle fails again (if the Bond number is still large enough) allowing further interchange of liquid and the gas in Volume 2 (Figure 5-6c). It should be noted that the stability limit for this second interface condition at the baffle can be higher by nearly an order of magnitude than that for the "clean" cylindrical tank geometry with small contact angle.

The collection of liquid in a pool at the tank bottom is accompanied by the entrainment of a certain amount of ullage gas in the liquid. The wall sheet carries the gas into the liquid where it forms into a large number of small bubbles.

Experiments[5.5] performed with water as the test fluid indicate that there is a Weber number minimum entrainment condition given by

$$W_{e_i} = 0.50\ Re^{2/3}$$

with $W_{e_i} = u_i\, Q'\, \rho_\ell / \sigma$ and $Re = Q'/\nu$

where u_i, Q', ρ_ℓ, σ, and ν are respectively the minimum entrainment wall sheet velocity, liquid wall sheet flow rate, liquid density, surface tension and kinematic viscosity. Conditions resulting in the Weber number less than the critical quantity given here apparently do not produce ullage entrainment.

These same experiments indicate that the volumetric rate of ullage gas entrainment P' is given by

$$P' = 0.0009\ F_r$$

with $F_r = (u_\ell - u_i)^2/2g\ t_\ell$ where u_ℓ, g, and t_ℓ are the liquid velocity, local acceleration and wall sheet thickness.

Further, the minimum and maximum bubble diameter may be prediced by:

Minimum diameter:

$$\frac{D_{min}\ u_i^2\ \rho_\ell}{\sigma} = 1.59\left(\frac{\rho_\ell}{\rho'}\right)^{1/3}$$

Maximum diameter:

$$\frac{D_{max}\ u_i^2\ \rho_\ell}{\sigma} = 15.9\left(\frac{\rho_\ell}{\rho'}\right)^{1/3}$$

In these relations ρ' is the density of the gas being entrained. All of the foregoing relations for gas entrainment are considered valid when the gravity level does not vary too much from 1 g_o, say $0.1\ g_o \leq g \leq 10\ g_o$, and where the Froude number based on liquid wall sheet velocity is limited to a few hundred, i.e. $Fr = u_\ell^2/2g\ t_\ell < 200 - 300$.

REFERENCES

5.1 Perko, L. M., and Moore, R.E.: "Inviscid Fluid Flow in an Accelerating Cylindrical Container," J. Fluid Mech., Vol. 22, June 1965, pp. 305-20

5.2 Concus, P., Crane, G. E., and Perko, L. M.: "Inviscid Fluid Flow in an Accelerating Axisymmetric Container," Conference on Fluid Mechanics and Heat Transfer Under Low Gravity, sponsored by AFOSR and LMSC and held at Lockheed Missiles & Space Company, Palo Alto, Calif., 24-25 June 1965

5.3 Davis, P. J., and Rabinowitz, P.: "Advances in Orthonormalizing Computation," Advances in Computers, Vol. 2, Academic Press, New York, 1961

5.4 Davies, E. M., and Taylor, G.I.: "The Mechanics of Large Bubbles Rising Through Liquids and Through Liquids in Tubes," Proc. Royal Society, Vol. 200, Series A, pp. 375 ff.

5.5 Dimitrescu, Th.: "Zeitschr fur Angew" Math. u. Mech., Vol. 23, 1943, p. 139. (Referenced by L. Prandtl in Essentials of Fluid Dynamics, Hafner, New York 1952, p. 330)

5.6 Salzman, J. A. and Masica, W. J.: "Experimental Investigation of Liquid Propellant Reorientation," NASA TM D-3789, Jan 1957

5.7 Lockheed Missiles & Space Company, A Study of Liquid Propellant Behavior During Periods of Varying Acceleration, LMSC-A874728, prepared for NASA Manned Spacecraft Center, Houston, Texas, under NASA Contract NAS 9-5174, 29 Apr 1967

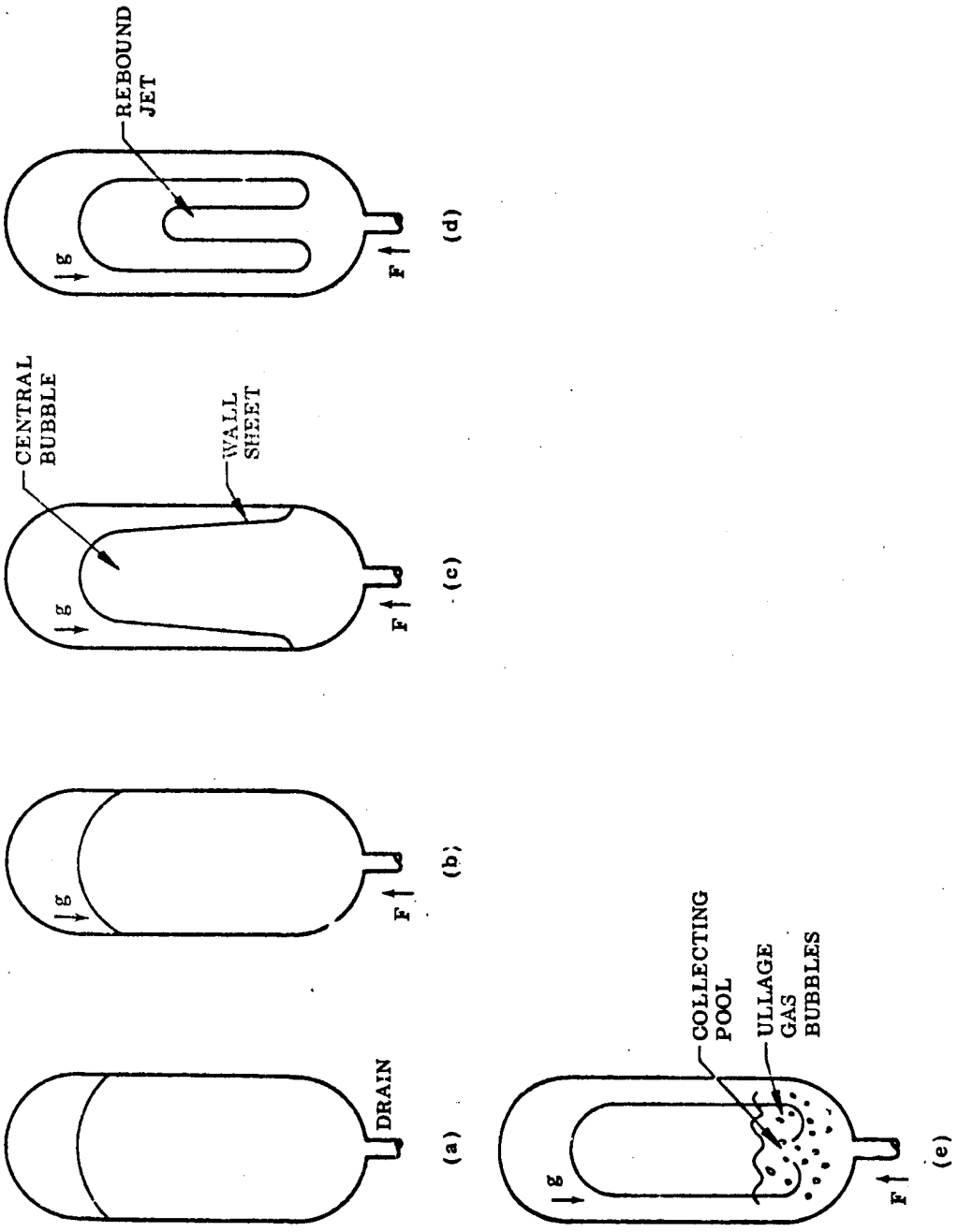

Figure 5-1 Liquid Reorientation Processes

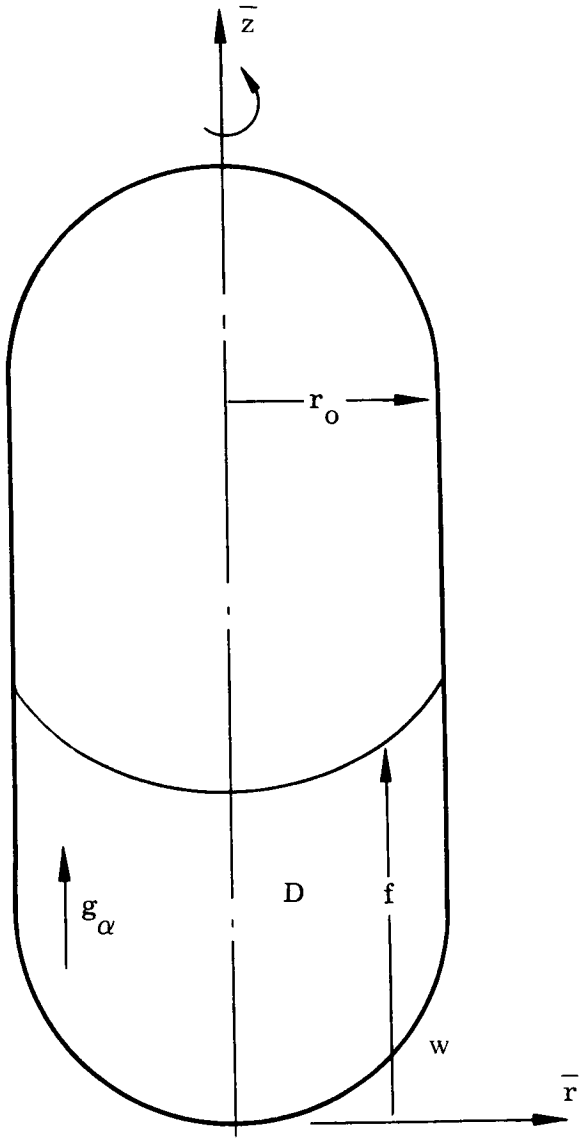

Figure 5-2 Liquid Reorientation in a Propellant Tank

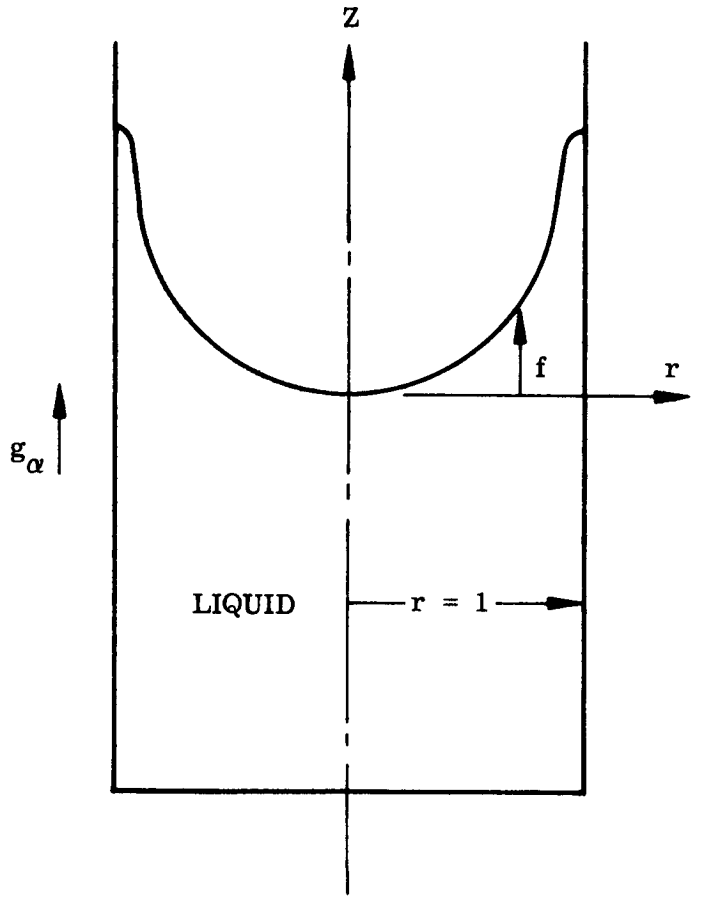

Figure 5-3 Geometry for Liquid Reorientation in a Flat-Bottomed Cylinder

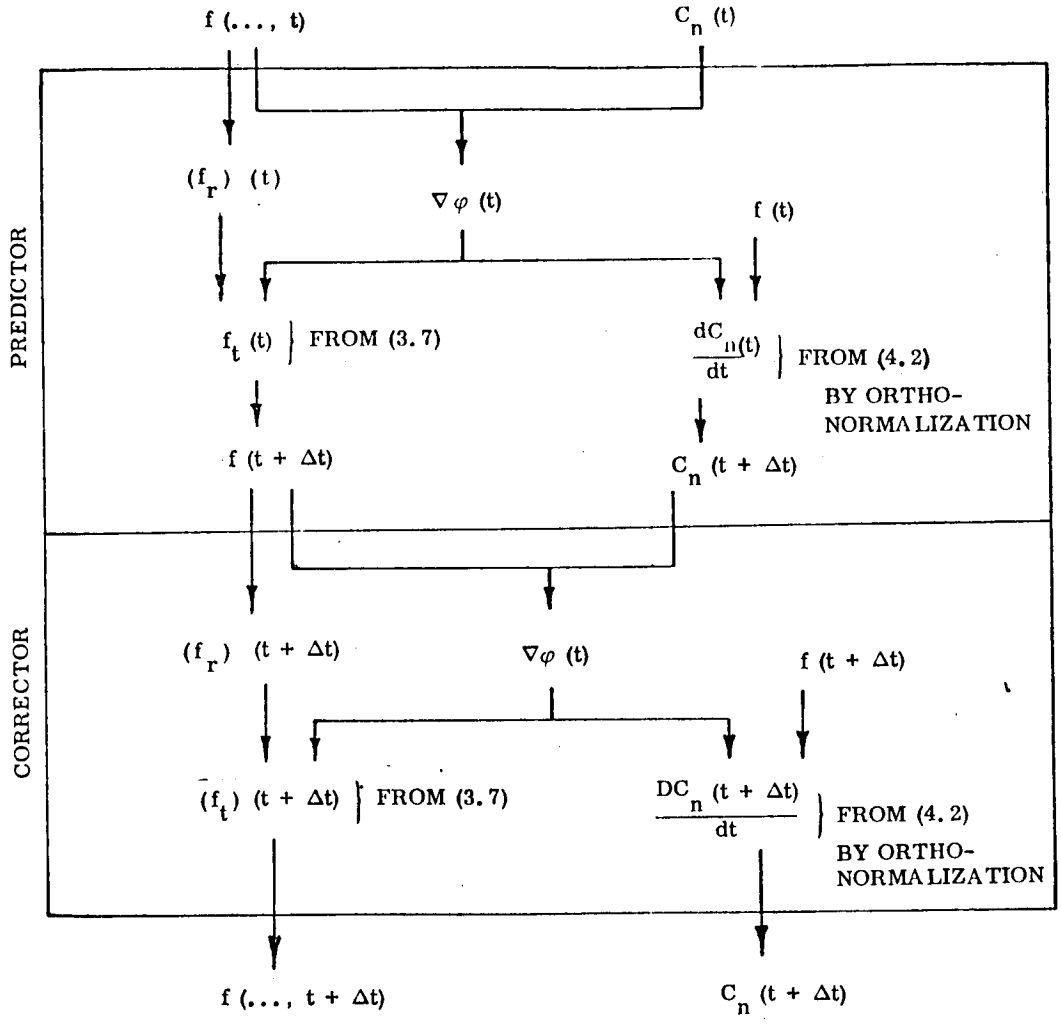

Figure 5-4 Computation Scheme for Separation of Variable Approach

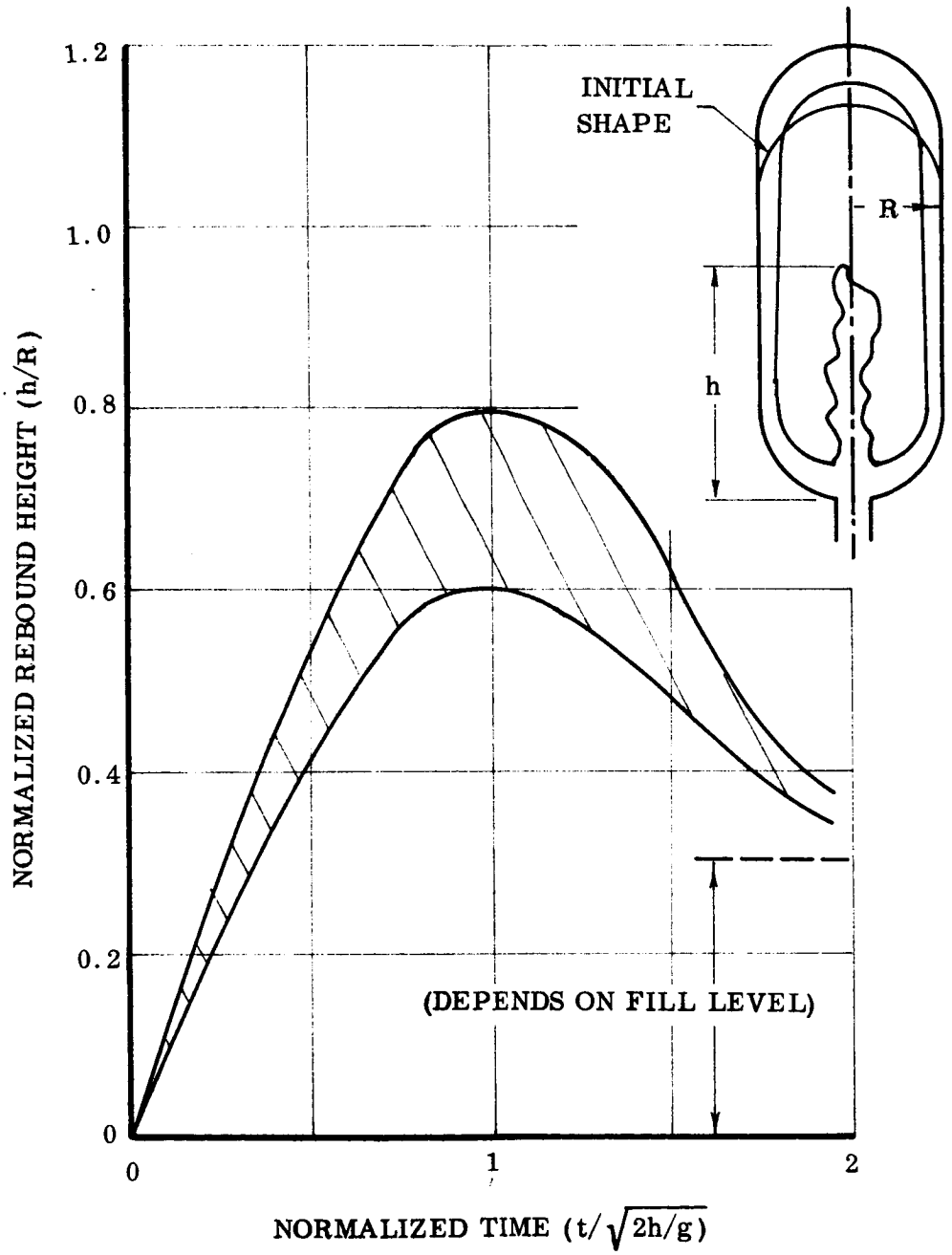

Figure 5-5 Geyser Growth and Subsidence

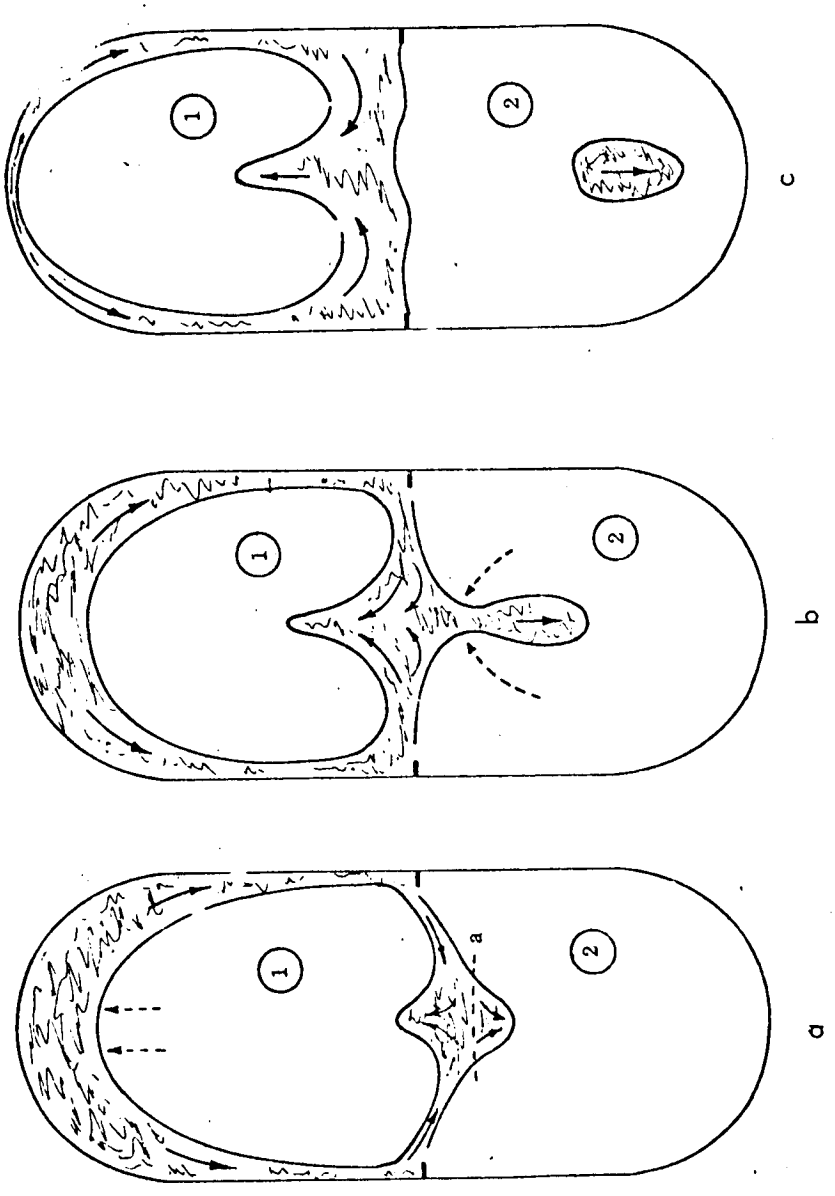

Figure 5-6 The Effect of a Ring Baffle on Reorientation Flow

Section 6
PASSIVE LIQUID RETENTION

INTRODUCTION

This section is concerned with the discussion and analysis of passive propellant retention systems. The fundamental theory governing the operation of such systems will be derived and discussed together with various aspects affecting the proper operation of a passive retention system.

The considerations of this section shall be limited to "passive" propellant retention systems. These are devices having no moving parts which rely for operation on a combination of container geometry and propellant capillary properties (surface tension, density and wetting characteristics) to accomplish the positioning and retention of propellant masses in the presence of upsetting body forces due to vehicle maneuvers. Thus, excluded from consideration are those propellant management systems employing bladders, bellows, pistons, ullage rockets, valves, and dielectrophoretic forces. Although for certain specific applications a positive expulsion device such as a bladder or bellows may be more desirable, in general, the above listed system share in varying degrees the disadvantages of large system weights, higher part count (and hence lower reliability), and material compatibility problems with rocket propellants currently employed. This is particularly true when these systems are employed in large propellant tanks for booster and upper stage vehicles. With the increased understanding of the behavior of capillary systems, passive retention systems for spacecraft have become accepted as the most generally desirable means of controlling propellant location. Reference (6.1) reports the results of a survey of most of the techniques employed for liquid propellant control and expulsion including those active systems listed above. The advantages and disadvantages of these systems are discussed. Those interested are referred to this source for more information regarding positive expulsion techniques.

The basic function of a spacecraft propellant retention system is to position all or a part of the liquid propellant in a partially filled tank at the tank outlet and supply propellant on demand to the propulsion system (or to another tank in the case of a resupply tanker operation). This must be accomplished in the presence of the vehicle acceleration environment during its mission. Vehicle accelerations result from such sources as attitude control thrust, aerodynamic drag, secondary propulsion systems operation, docking, crew movements, solar pressure, gravity gradients, etc. The table below lists rough order of magnitudes for these accelerations for a typical vehicle mass of approximately 20,000 lbm.

Source (Not Orbit Dependent)	a/g_o
Attitude control, RCS, etc.	10^{-3}
Centripetal due to roll rates (L = 4 ft)	10^{-6}

Source (Orbit Dependent)	Sun	Earth	Moon
Aerodynamic drag	–	1×10^{-6}	–
Radiation pressure	1×10^{-9}	–	–
Centripetal due to orbital rate	4×10^{-14}	10^{-6}	7×10^{-7}
Gravity gradient	8×10^{-15}	3×10^{-5}	1×10^{-7}

Because of the inertia of the propellants, the vehicle accelerations result in a body force tending to move the liquid mass relative to the tank. If motion is to be prevented this body force must be opposed by some other force of equal magnitude. In this case, that force is produced by the surface tension at the liquid-gas interface, often referred to as a capillary force.

CAPILLARY STABILIZED SYSTEMS

Pressure Supported Systems

Reynolds [6.2] has proposed the terms "pressure supported" and "capillary supported" to describe two classes or modes of the stabilization of liquid masses in containers against gravitational forces by the action of surface tension forces. The first of these concepts can be illustrated with aid of the diagram of a tank partially filled with liquid shown in Fig. 6-1(a). If the tank is accelerated in the y direction normal to the static equilibrium liquid-gas surface with magnitude α, the entire mass of liquid tends to "fall" away from its original position to the other end of the tank much like a piston. The retention of this mass in its original position is dependent on two criterion.

One is the balance of forces on the liquid in the y direction. Thus:

$$\Sigma F_y = 0 \qquad \text{for static } y \text{ equilibrium}$$

$$p_g \pi R^2 - \pi \int_0^R \rho \alpha \, h(r) \, dr - p_\ell (y)_{y=0} \pi R^2 = 0$$

or

$$p_g - p_\ell = \frac{1}{R^2} \int_0^R \rho \alpha \, h(r) \, dr$$

This criterion should be considered in cases where p_g approaches the propellant vapor pressure such that the permissible value of $p_g - p_\ell$ approaches zero. For storable propellant systems this is generally of secondary importance relative the following consideration. The term "pressure supported" is derived from this consideration.

The other criterion in this case is concerned with the relative ability of surface tension to prevent the unstable growth of a deformation of the liquid-gas interface which would allow an exchange of liquid and gas across the equilibrium surface location. The criterion is stated in terms of the Bond number B for interface stability. This subject is discussed in Section 4 and will not therefore be repeated here. Propellant mass and tank geometry combinations satisfying the above two conditions are said to "stabilized in the pressure supported sense."

Capillary Supported Systems

In most instances, however, the net acceleration vector of a propellant tank is not always directed in the manner stated above but will either have a component parallel to the liquid surface or will be directed entirely normal to the axis of symmetry of the equilibrium surface. This is illustrated in Figure 6-1a by the acceleration vector β. In this case, the stabilization of the liquid is in the capillary supported sense. The hydrostatic pressure variation across the tank diameter, $\rho\beta\,(2R)$, is counterbalanced by a surface tension force associated with the distortion of the interface shape.

Analysis of this mode due to its asymmetry and nonlinearity has not yielded a stability criterion. Experimentation reported in Reference 6.3, however, indicates a Bond number stability limit for right circular cylindrical tanks with no internal hardware, thus

$$B\big|_{\text{stable}} = \frac{\rho\beta R^2}{\sigma} \leq 1$$

for transverse acceleration components in clean tanks.

Since the locational stability of liquid masses in both of the above cases is largely governed by the stability of the liquid-gas interface which in turn is highly dependent on the characteristic container dimension, L , the technique most generally employed is to reduce this dimension. This can be accomplished with little loss in tank flow area

by placing a screen grid or perforated plate surface at the liquid-gas interface position. This stabilization surface is illustrated in Figure 6-1b. For the liquid at this screen grid surface, the characteristic dimension L now becomes r which is much smaller than R, resulting in interfacial stability to much higher acceleration levels.

For the pressure supported capillary stabilized surface

$$B\Big|_{\text{stable}} = \frac{\rho \alpha r^2}{\sigma} \leq 0.8$$

in each screen or perforated plate opening where r is the effective hole radius.

Again, since in most cases all or a component of the net acceleration vector will be parallel to all or some portion of a stabilization surface, attention will be turned to the stability criterion for this case. This criterion is a form of capillary supported stability and can be illustrated as follows.

Consider a container enclosing a mass of liquid that has a density, ρ, and surface tension, σ, against the surrounding gas as shown in Figure 6-2. The local accelera tion, β, acts in the direction shown. On one side of the container at its extreme top and bottom a distance, h, apart are located holes of radius r. The hole radius is small compared to the local hydrostatic pressure variation so that the liquid-gas interface can be considered spherical with radius R (i.e., hole Bond number. $\frac{\rho g r^2}{\sigma} < 0.1$). The system contact angle is indicated as θ. Writing the pressure drops across the curved liquid-gas interface at the upper and lower holes in accordance with the Laplace relations where r_1 and r_2 are the principle radii of curvature of the liquid-gas interface.

$$p_o - p_a = \sigma \left(\frac{1}{r_1} + \frac{1}{r_2} \right)_a \qquad (6.1)$$

where

$$\Phi = \varphi \text{ (contact angle, contact angle hysteresis, containment surface geometry).} \qquad (6.8)$$

A theoretical upper limit for the value of Φ for circular holes is 4 since this represents one full bubble pressure based on hole radius at the top and one full drop pressure at the bottom based on hole radius. This amounts to an inverstion of wetting between holes and is, of course, difficult to obtain in a practical situation. In this line of thinking, for a perfectly wetting combination ($\theta = 0$) a Φ value of 2 would indicate one "bubble pressure" based on hole radius with no aid to continament furnished by the "lower" holes. In (6.7) it is understood that the distance h must be measured parallel to the direction of β and be the maximum wetted distance along this line of action.

Experiment reported in Reference (6.4) show that Φ is a weak function of the parameters indicated in equation (6.8) varying between 1.5 and 3.5. For the purposes of setting an unconditional stability limit then, the following would apply:

$$\frac{\rho \beta r h}{\sigma} \leq 1 \qquad (6.9)$$

The above stability limit consideration was also reported by Jetter [6.5] and verified by a series of experiments.

CAPILLARY SUPPORTED RETENTION SYSTEM DYNAMIC BEHAVIOR

Retention System Refill

During the operation of passive retention system, the volume within the system may become partially emptied of liquid. This can occur as the result of an acceleration exceeding one of the above stability limits allowing pressurant gas to enter the volume

$$p_b - p_o = \left(\frac{1}{r_1} + \frac{1}{r_2}\right)_b = \frac{2\sigma}{R_b} \tag{6.2}$$

the hydrostatic pressure difference between holes is

$$p_b - p_a = \rho\beta h \tag{6.3}$$

combining (6.1), (6.2), and (6.3) yields

$$\frac{\rho\beta R_a h}{\sigma} = 2\left(1 - \frac{R_a}{R_b}\right) \tag{6.4}$$

From the geometry of the liquid-gas interface in the upper hole

$$r = R_a \cos\theta \tag{6.5}$$

$$\frac{\rho\beta r h}{\sigma} = 2\left(\cos\theta + \frac{r}{R_b}\right) \tag{6.6}$$

The development of an analytical relation beyond this point is dependent on more explicit knowledge of the detailed influence of hole geometry including burns and other edge deformities, contact angle, and contact angle hysteresis on the shape and size of the liquid gas interface in the containment surface holes. Rather than attempt this, all the known parameters can be grouped on the left hand side of the equation as was done in (6.6) leaving those aspects about which accurate assumptions cannot be made to the right hand side as a nondimensional constant for the particular system, a constant which can be examined experimentally. Thus, we may write:

$$\frac{\beta r h}{\sigma/\rho} \leq \Phi \tag{6.7}$$

in exchange for the loss of liquid or by necessity and design as during an engine startup sequence. This is illustrated in Figure 6-3. Shown in (a) is a partially empty propellant tank containing a simple propellant retention device consisting of a perforated metal sheet spanning the tank above the outlet enclosing a volume bounded by the tank walls and the retention surface. The main body of propellant has been disoriented previously and is located at the opposite end of the tank, leaving one side of the containment surface in partial or total contact with the pressurant gas. Engine restart (Figure 6-3b) results in a withdrawal of propellant from the retention volume. As it takes a finite time for the propellants to arrive at the drain end under the resulting vehicle acceleration, α, pressurant gas is drawn into the retention volume. The main body of propellants then arrive and begin flow past the retention surface to meet the engine demand (Figure 6-3c). The gas within the retention volume must be expelled prior to the next engine start or the possibility exists that a portion of this gas will be ingested at the subsequent restart causing engine malfunction.

As will be shown analytically below, once propellant is oriented so as to cover the retention surface, a portion of this pressurization gas will remain trapped with the retention volume (as in Figure 6-3c) unless provision is made in the system design to vent this gas volume.

Refill Under Engine Thrust

Consider Figure 6-4 which is a diagram of a portion of a passive propellant retention system such as might be employed at the drain. As the reorienting propellant approaches the retention system, the liquid level inside retention volume is at some initial height h_i greater than the final height h_f with pressurant above it at p_o pressure. The flow rate, w, to the engine will, of course, be very much less than the propellant flow entering retention system region. Thus, h_i will begin to diminish as the propellant level rises. Due to the large propellant flow rate outside the retention surface, this surface will become quickly submerged. The level in the retention volume will continue to rise until the gas pressure in the retention system is p_v.

where

$$p_v = p_o + \rho\alpha(H + h_f)$$

and

$$h_f = h_c + h_L$$

for h measured down from the retention system top to be reduced below h_f, gas would have to be expelled past the retention surface against the capillary bubble pressure p_c. We may define

$$h_o = \frac{\Delta p_c}{\alpha\rho}$$

This an another form of the capillary supported stability criterion.

$$\frac{\alpha\rho h_o r}{\sigma} = 2$$

Therefore

$$h_o = \frac{\sigma}{\alpha\rho r}$$

Flow thru the retention surface results in a pressure loss which is reflected as an additional head differential h_L relative to the pressure outside the surface.

Thus,

$$h_L = C_L \frac{\rho v_s^2}{2g_c}$$

where

v_s is propellant velocity in the retention surface holes

C_L a loss coefficient. In general $C_L \approx 1.2$, and

g_c is the conversion factor from mass to force units.

The above consideration illustrates the fact that pressurant gas drawn into a passive retention system is not expelled when the exterior portion of retention surface becomes wet. Note particularly that retention surfaces normal to vehicle thrust axis having no value for h_f are particularly poor from this standpoint since at all points along the surface the liquid pressure in the exterior exceeds the interior trapped gas pressure.

Means for eliminating or reducing the trapped volume include configuring the retention surface so as to vent to main ullage pressure, or configuring the containment surface so the volume associated with the entrapment height, h_f, is small. A conical retention surface shape is an example of the latter. These are illustrated in Figure 6-5.

Refill Under Capillary Forces

The refill considerations above apply to those conditions resulting in the submergence of a retention system by the bulk of the propellant. If the retention system is large enough or the propellant level in the tanks low enough his may not occur. If this condition results in a portion of the retention surface becoming dry, allowing gas pressure communication between gas in the retention volume and the ullage pressurant gas, then, during a period of zero or low gravity, the retention system can refill itself under the action of surface tension forces if properly designed. This is illustrated in Figure 6-6 which shows a representative retention system placed over the tank drain consisting of a right circular cylinder with a screen mesh connecting the base to the tank wall closed off across the top by another screen mesh. The propellant is assumed to wet the tank materials perfectly (i.e., contact angle near zero). In

(a) the retention system is partially full. The gas in the reservoir has pressure communication to the ullage pressurant via the screen at the top. Following a reduction of the acceleration level such as at main engine shut off, the propellant interfaces interior and exterior to retention system will assume the characteristic capillary dominated curved interface shape. From the Laplace relation we can determine the pressure change across each interface as a function of the surface curvature:

For the retention system

$$p_o - p_2 = \sigma\left(\frac{1}{r_1} + \frac{1}{r_2}\right)$$

$$\approx \frac{2\sigma}{2}$$

For the tank

$$p_o - p_1 = \sigma\left(\frac{1}{\mathcal{R}_1} + \frac{1}{\mathcal{R}_2}\right)$$

Noting that

$$2\mathcal{R}_1 = R - r$$

and that $\mathcal{R}_2$, (the other principal radius of curvature for this annular meniscus,)is very large so that

$$\frac{1}{\mathcal{R}_2} \to 0$$

we have

$$p_o - p_1 = 2\sigma\left(\frac{1}{R - r}\right)$$

combining the above to eliminate p_o yields

$$p_1 - p_2 = 2\left(\frac{1}{r} - \frac{1}{R - r}\right)$$

In the absence of a vehicle acceleration, the above relation states that the propellant will flow into the retention system in response to the capillary pressure difference if

$$\frac{1}{r} > \frac{1}{R - r}$$

in the local region of the retention system.

Considering the effect of a small axial acceleration component, α , that produces a hydrostatic pressure variation, we write

$$p_1 - p_2 = \rho\alpha\ (h_2 - h_1)$$

For complete system refill by capillary action in the presence of a positive acceleration, α ,

$$\Delta p \text{ (capillary)} \geq \Delta p \text{ (hydrostatic)}$$

or

$$2\sigma\ (\frac{1}{r} - \frac{1}{R - r}) \geq \rho\alpha\ (h_2 - h_1)$$

setting $(h_2 - h_1)_{max.} = H$

where H is the height of the retention system, we have

$$\alpha \leq \frac{2\sigma}{\rho H}\ (\frac{1}{r} - \frac{1}{R - r}) \qquad (6.10)$$

for complete capillary refill.

The rate of system refill is a function of the driving forces on the liquid mass and the dissipative forces, all of which are strongly dependent on the particular system geometry. The transient process of retention system refill can be expressed in terms of a differential equation in refill height, h, derived from Newton's Second Law thus:

$$F_{CAP} + F_{HYDRO} - F_{DISSIP} = m(t)\,\ddot{h}(t)$$

F_{CAP} is the force due to the capillary pressure differential and is a function of tank and retention system geometry, system wetting characteristics and surface tension.

$$F_{CAP} = f(\sigma, \theta, R, r)$$

Acceleration induced body forces, F_{HYDRO}, are dependent on the propellant density, ρ, local acceleration, α, and height differences, h.

$F_{DISSIPATIVE}$ is a function of the propellant velocity, $\dot{h}$, flow area ratio and geometry and propellant viscosity μ.

The propellant mass, m(t), engaged in the system refill will be time varying in value, being a function of h.

The comments above point out the essential aspects of retention system refill under surface tension and small body forces. Details of a partincular system design must be considered in applying these in an analysis. Siegel (6.6) discusses these aspects in an analysis and experimental investigation of a simple capillary system.

Partial or Total Propellant Retention

Retention system design depends on whether it is necessary to control with the passive system all or a specific smaller volume of the propellants. An important consideration in this case is the stability criterion for capillary supported systems,

$$\frac{\rho g r h}{\sigma} = 1 \text{ for unconditional stability,}$$

since upsetting accelerations other than those aligned with the thrust axis will occur and must be considered. The two alternatives are illustrated in Figure 6-7. In order to keep the gross retention system dimension "h" at a low value so that the permissable upsetting acceleration may remain large, total propellant control generally results in large retention system surface areas and weights relative to the tank weight. In this regard, total retention of all remaining propellant is not attractive for large propellant tanks, but may be acceptable for smaller tank sizes associated with attitude control or secondary propulsion systems.

The approach with partial propellant control is to retain at the tank outlet sufficient propellant to assure engine start and settling of the bulk of the propellant. This provides a minimum volumetric requirement for the retention system in order to prevent pressurant gas entering the engine feed line.

$$V_{r.s.}\Big|_{min} = V_{s.t.} + V_s + V_{p.t.} + V_{r.f.}$$

where

$V_{r.s.}$ = propellant volume to be retained

$V_{s.t.}$ = volume required for engine start transient

V_s = volume required to settle bulk of propellant

$V_{p.t.}$ = volume required to provide a liquid level above the drain to prevent "pull-through" or suction dip

$V_{r.f.}$ = volume associated with any inability to completely refill the system.

The above breakdown is somewhat arbitrary but provides a list of those aspects which must be considered in an analysis of a partial retention system.

The engine start transient is characterized by propellant withdrawal from the retention volume under low gravity conditions building up to rated thrust and high acceleration condition. This volume of propellant is that necessary to fill passages downstream of valves, thrust chamber fuel or oxidizer leads, turbine flow (for pump fed engines), etc., and is dependent upon the particular engine system. Also, since the flow occurs initially under very low gravity conditions, the tendency for pressurant pull-through (or suction dip) is extreme. Thus, the tendency of the propellant surface to follow large velocity potential gradients in the absence of gravity potential gradients must be considered in the shape of the retention system.

Depending upon such factors as tank shape and internal hardware geometry, fill level, and reorientation Bond number, a finite amount of time is required for the wave front of the bulk propellant to arrive at the retention system. During this period the additional propellant volume V_s is withdrawn from that in the retention system.

Just prior to the start of refill of the retention system by the reorienting propellant, the propellant level in the system may be low, thus placing the interface close to the tank outlet. Under these conditions, pull-through or suction dip is again possible. The volume of propellant, $V_{p.t.}$, is that which then cannot be drained or scavenged from the tank bottom, but must be provided to prevent pull-through.

Finally, due to the considerations discussed above regarding refill, it may not be possible with a particular design to completely refill the retention system following the initial engine restart with deoriented propellants and volume $V_{r.f.}$ must be provided to prevent propellant depletion in the retention system during a subsequent start.

CONCLUSIONS

This section has presented those considerations and design criteria generally essential to the analysis and design of a passive propellant retention system. Summarized, these are:

1. Interfacial Stability, Pressure Supported:

$$\frac{\rho g R^2}{\sigma} \leq \Phi_1 ; 0.8 \leq \Phi_1 \leq 2$$

for most common tank geometries and propellants

2. Interfacial Stability, Capillary Supported:

$$\frac{\rho g r h}{\sigma} \leq \Phi ; 1 \leq \Phi \leq 3$$

3. Retention System Refill
4. Volume Size for Partial Retention System

Beyond these fundamental considerations the particular configuration of a passive propellant retention system is highly dependent on the specific mission and vehicle system to which this technique is applied. In this respect, it must be emphasized that no particular passive retention system is the best for all applications. In view of a general desire to minimize system weight and design complexity, however, a partial retention system is more suitable than a total retention system. This approach results in a small retention system size, making it possible to provide a design stable under a wide variety of upsetting acceleration levels as well as resulting in minimum vehicle weight increments.

REFERENCES

6.1 Bell Aerosystems Company, "Development of Expulsion and Orientation Systems for Advanced Liquid Rocket Propulsion Systems," Tech. Doc. Report No. RTD-TDR-63-1048, AF Contract No. AF04(611)-8200, Jul 1963

6.2 Reynolds, W. C., Saad, M.A., and Satterlee, H. M., "Capillary Hydrostatics and Hydrodynamics at Low-g," Stanford, Calif., Sep 1964

6.3 Masica, W. J., Petrash, D. A., and Otto, E. W., "Hydrostatic Stability of the Liquid-Vapor Interface in a Low-Acceleration Field," NASA TN-D-2267, May 1964

6.4 Hollister, M. P., "Propellant Containment Utilizing Screen Mesh and Perforated Plate Surfaces," LMSC-A665481, Lockheed Missiles & Space Company, Dec 1964

6.5 Jetter, R. I., "Orientation of Fluid Surfaces in Zero Gravity Through Surface Tension Effects," Proceedings, American Astronautical Society, Physical and Biological Phenomena Under Zero Gravity Conditions, Second Symposium, Los Angeles, Calif., 18 Jan 1963

6.6 Siegel, R., "Transient Capilary Rise in Reduced and Zero-Gravity Fields," ASME, Trans., Ser. E., J. Appl. Mech., Vol. 28, Jun 1961

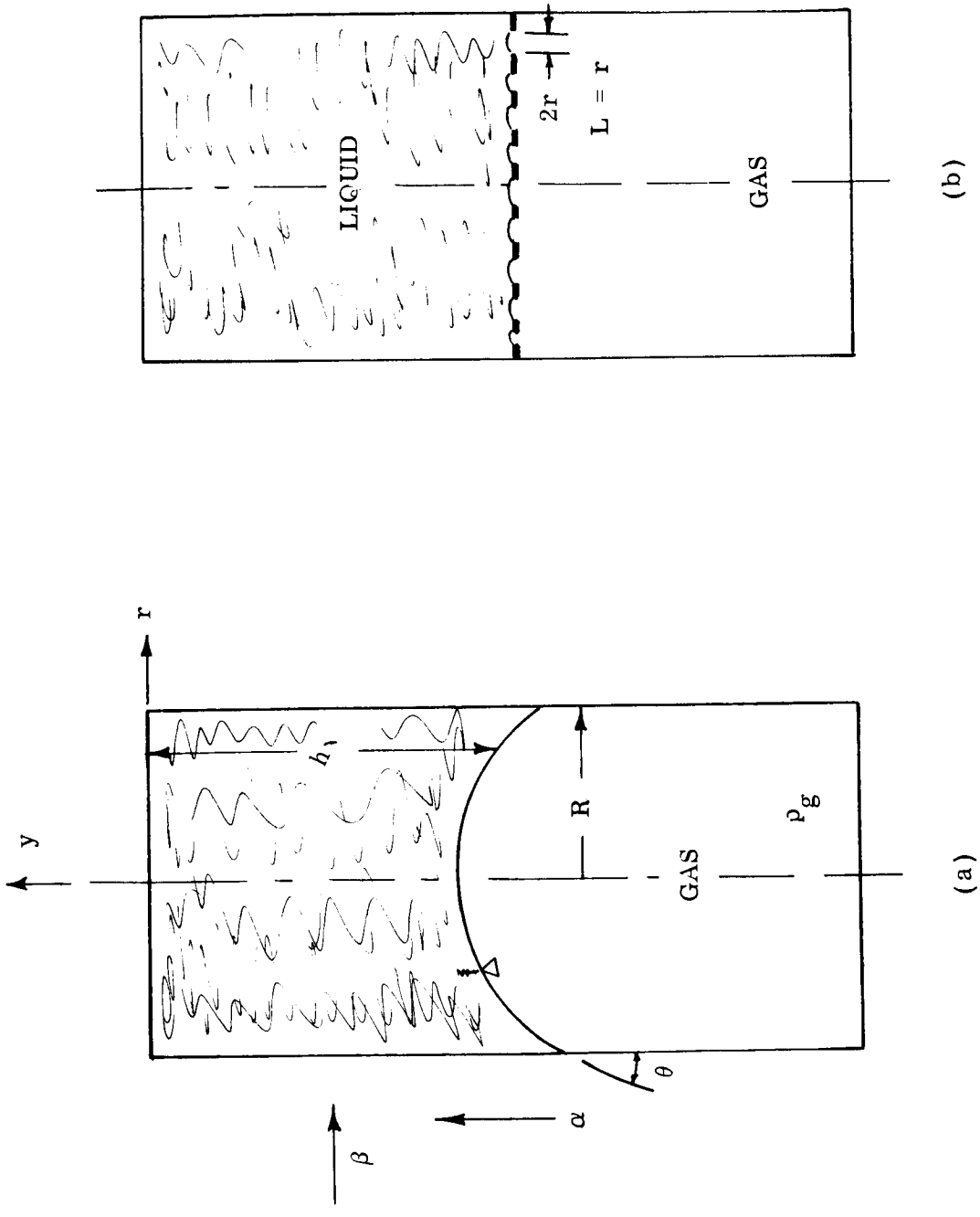

Figure 6-1 Pressure Supported and Capillary Supported Containment

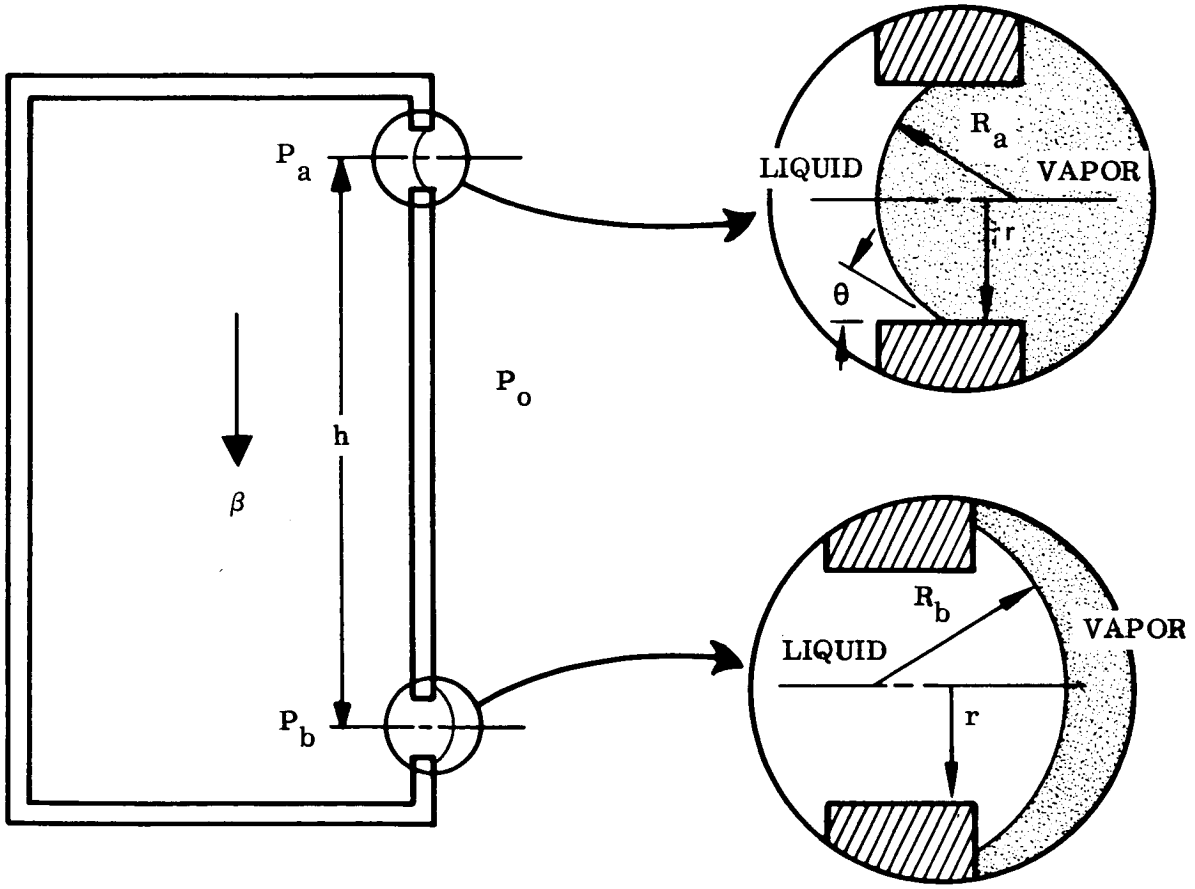

Figure 6-2 Capillary Supported Containment

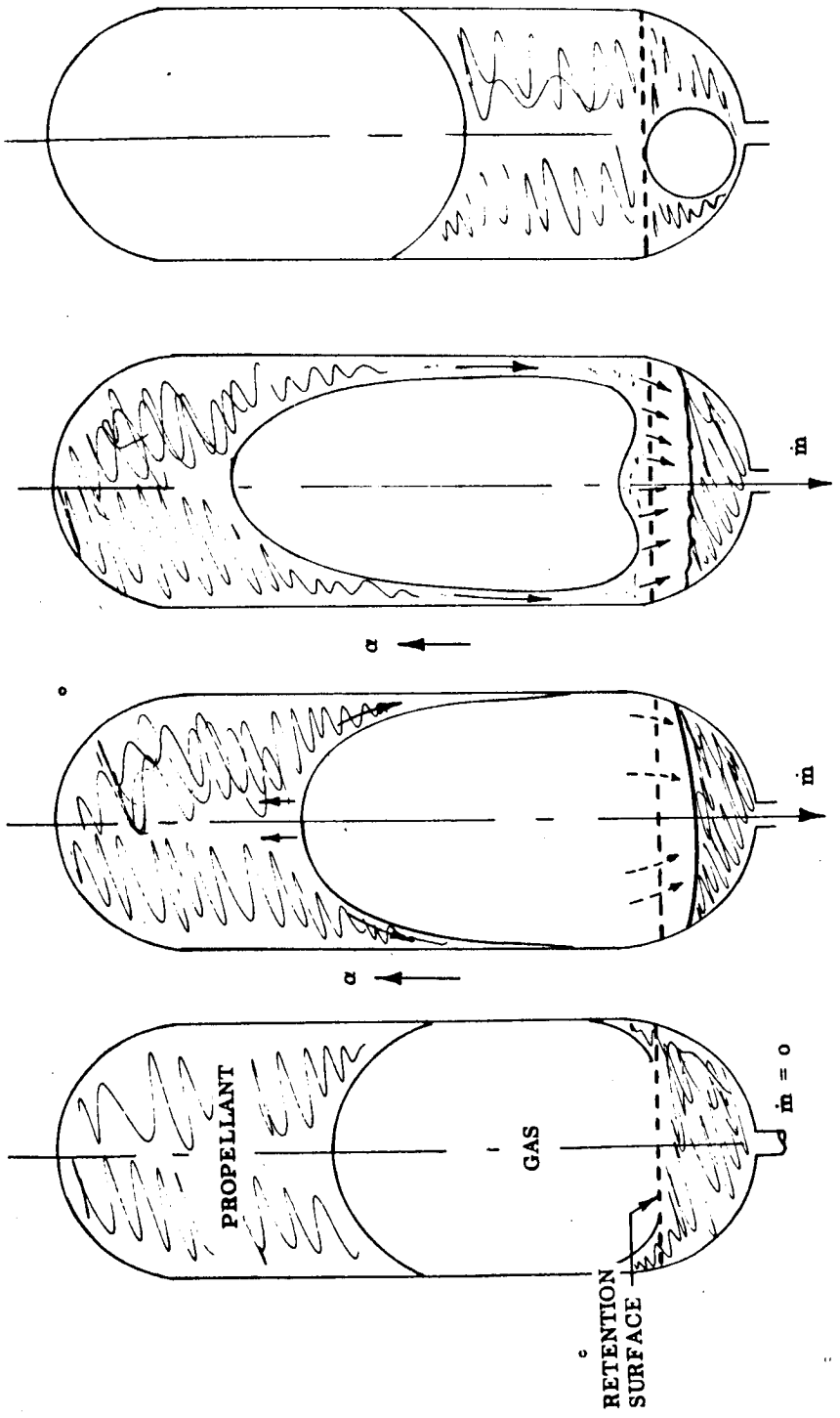

Figure 6-3 Entrapment of Gas By Capillary Containment System

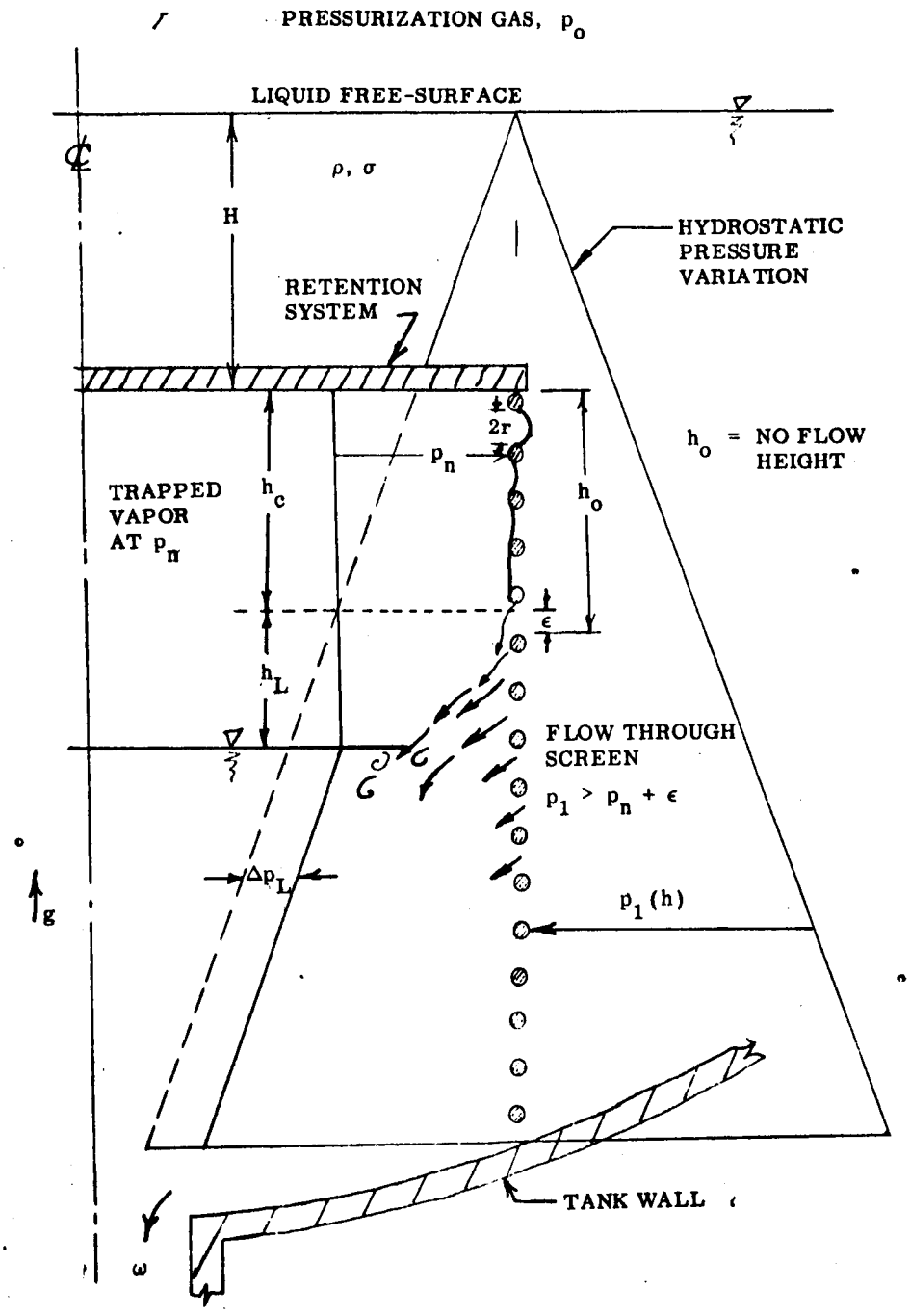

Figure 6-4 Geometry — Containment System Refill Analysis

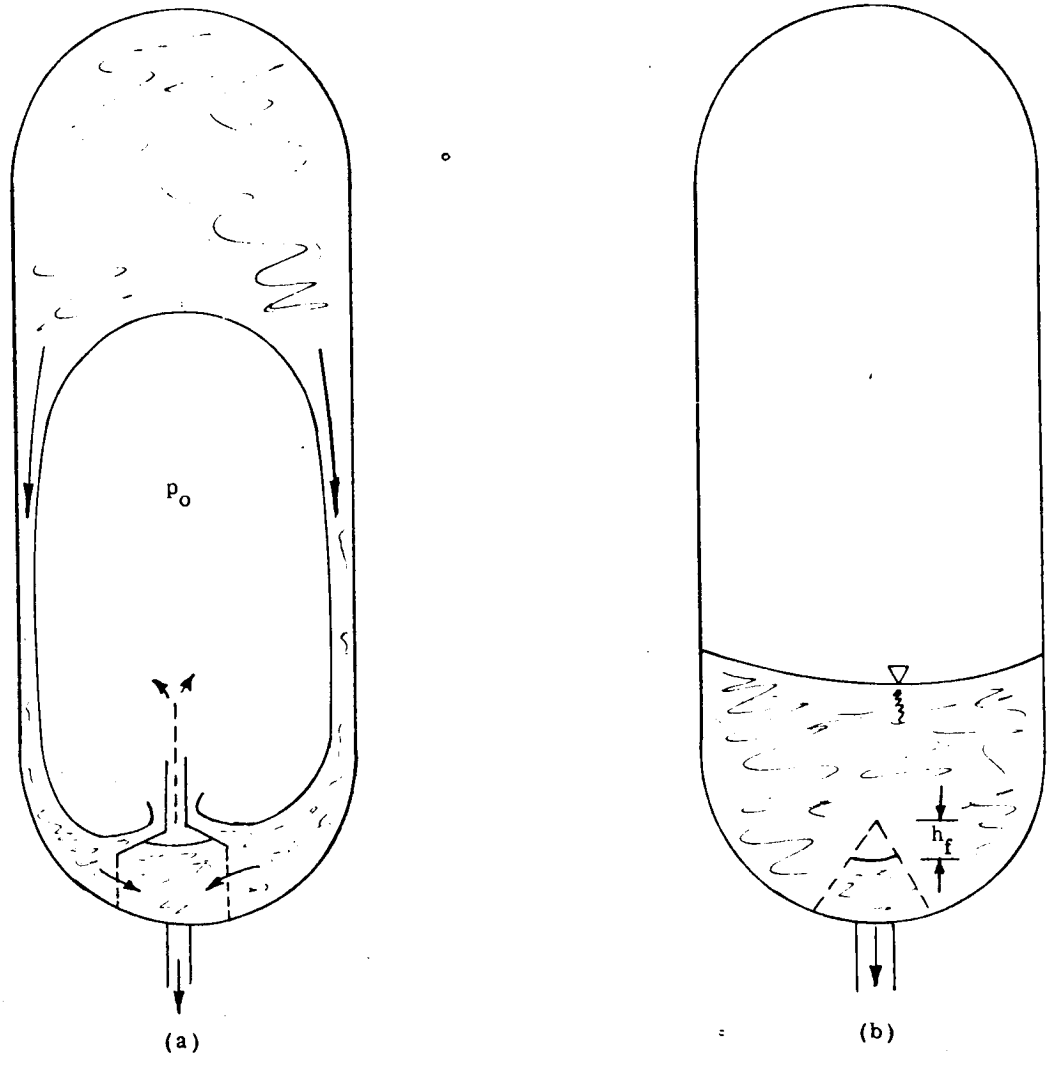

Figure 6-5 Containment Systems With and Without Clearing Tube

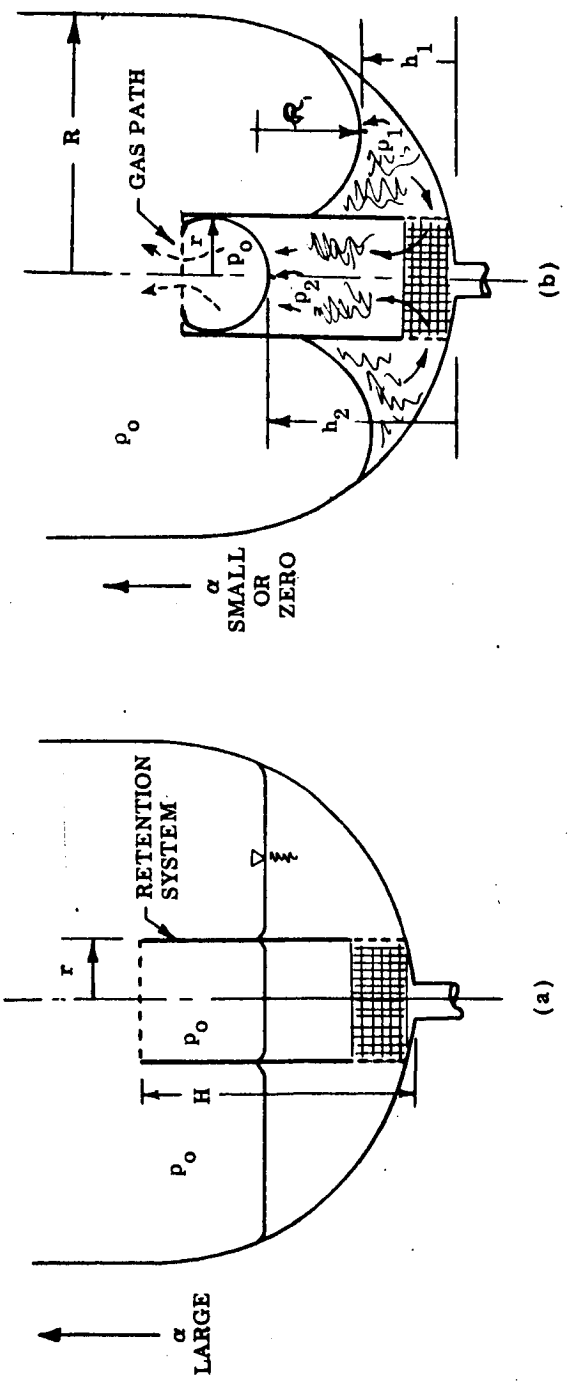

Figure 6-6 Capillary Refill of a Containment System

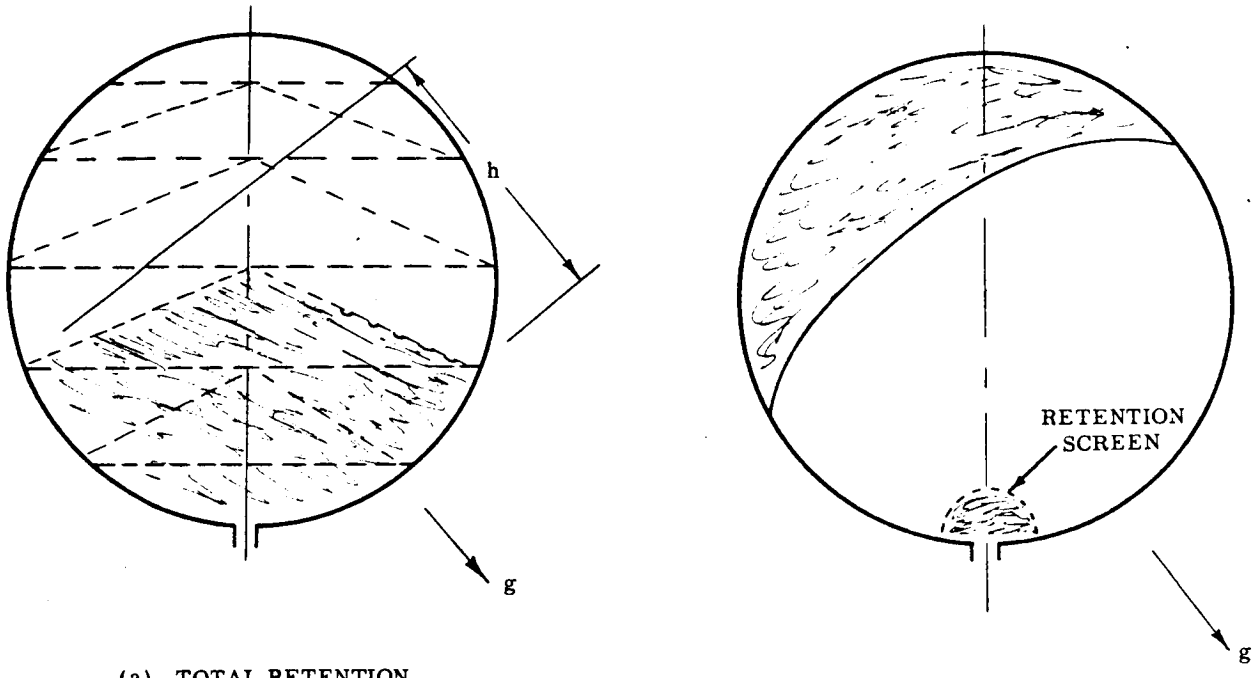

(a) TOTAL RETENTION

(b) PARTIAL RETENTION

Figure 6-7 Total and Partial Capillary Retention Systems

Section 7
LOW-G PROPELLANT TANK DRAINING PROBLEMS

Increasingly sophisticated space missions have already required that liquid propellants be supplied to rocket motors under reduced gravitational conditions. To date, most such situations have occurred during the use of small or secondary propulsion systems. These devices are normally characterized by small total impulse (and, therefore, small tanks) and by low propellant-flow rates. The most expedient solution has been to positively expel propellants from small tanks, using bladders or diaphragms in the tanks.

The draining of large tanks, however, presents problems of much greater magnitude. Bladders or bellows add considerably to the weight of large tanks (at least in theory, since no large tanks have yet been built utilizing such systems). Further, the reliability of such devices greatly reduces their attractiveness if only from the part count viewpoint.

The advent of space exploration will require operation of propulsion systems fed from large tanks. The great size of many projected space vehicle systems probably will result in the operation of such systems under reduced gravitational conditions. Further, some contemplated missions envision transfer of propellants or other liquids from a tanker to a receiver in space under near zero-g conditions. It can be expected that such operations will produce special problems, or, at least, will aggravate situations met under more familiar high-g conditions.

Two problems may be expected in conjunction with the draining of tanks under low-g conditions: vortex formation and pressurant blow-through. The first problem presents a familiar phenomenon, occurring during the draining of almost any container of liquid. The second is not found in very many everyday situations, but only those in which tanks are drained very rapidly and in which vortex formation is somehow avoided. These two problems will be discussed in turn.

VORTEX PROBLEMS IN LOW-G

The vortexing of liquids in propellant tanks is of great importance, if only because vortexes must be avoided at all costs. Maintenance of engine thrust-level and possibly the engine mixture ratio are dependent on being able to drain the propellant tanks in a predictable manner. This is certainly not possible if vortexes appear during the draining process. A serious vortex motion will result in a depression of the liquid surface over the tank drain to the extent that gas actually enters the drain. When this occurs, the flow cross-section of the drain for liquid is reduced and the liquid flow rate is lowered.

One of the major difficulties encountered in the vortexing problem is that analysis is of little help. Most of the palliatives have been developed empirically; experiments have also developed most of the information about vortexing in propellant tanks.

From a qualitative standpoint, vortexes appear eventually if there is some residual circulation in the liquid in the tank. The practical impossibility of avoiding some circulation means that vortexing is always possible. Further, the inception of a vortex is not at all predictable. Experimental observation (7.1) indicate certain general trends about the probability of vortexing. These trends include the following:

- The probability of vortex formation increases with the magnitude of liquid circulation at the start of the draining process and the time to vortex inception is reduced.
- The probability of vortex formation is strongly influenced by tank shape. For example, vortexes form more readily in conical than in flat bottomed tanks.
- Off-center drains reduce the severity of vortex motion. A vortex may start but may also be swept away by the circumferential motion of the liquid.

The net result of all this is that corrective appliances must be installed in the tank bottom. Some studies have been undertaken to determine the best types of vortex suppressors. The exact choice should be made on the basis of model tests in the tank in question. The choice cannot be made until tank development is started. It may be said, however, that cruciform baffles installed over the drain are effective in reducing

vortex formation and severity. Horizontal baffles located over the drain are also effective. Both types can be made of perforated material or screens as a means of weight minimization.

The foregoing treatment has said nothing about vortex formation under reduced gravitational conditions. In order to make some judgement about the similarities and differences between vortexing under reduced-g and normal, high-g conditions, we may examine the Euler equations of motion in polar cylindrical coordinates. This is justifiable because vortex motion can be considered to be irrotational except in a central rotation core. The equations in the r, θ, and z coordinates are as follows.

$$\left.\begin{aligned} \frac{Du_r}{Dt} &= -\frac{1}{\rho}\frac{\partial p}{\partial r} + \frac{u_\theta^2}{2} \\ \frac{D(ru_\theta)}{Dt} &= 0 \\ \frac{Du_z}{Dt} &= \frac{1}{\rho}\frac{\partial p}{\partial z} - g \end{aligned}\right\} \qquad (7.1)$$

where

$$\frac{D}{Dt} = \frac{\partial}{\partial t} + u_r\frac{\partial}{\partial r} + ru\ \frac{1}{r}\frac{\partial}{\partial \theta} + u_z\frac{\partial}{\partial z}$$

p is the pressure

ρ is the liquid density

q is the local body force per unit mass

The only difference between application of these equations in a low-g condition compared to more normal high-g conditions is found in the equation for the z direction.

There is nothing the r and θ direction equations to indicate that a vortex would start more quickly under reduced-g conditions. Once started, though, it is clear from

the z-equation that the amplitude of the resulting free-surface disturbance would result in a different flow pattern in the tank.

If it is true that anti-vortex devices are required under high-g conditions, it is obviously doubly true under reduced-g conditions.

PRESSURANT BLOWTHROUGH PROBLEMS

Pressurant blow-through (also termed suction dip or pull-through), the second of the major problems associated with tank draining, is characterized by a collapse of the free-surface of the liquid over the tank drain. It is aggravated by high drain rates and is worse when the liquid level in the tank is low. It goes almost without saying that pressurant blow-through happens only if vortexing can be avoided. If a large percentage of the propellant contained in a tank must be drained, vortexing must first be avoided, then steps can be taken to minimize pressurant blow-through.

Here, too, analysis has been of only marginal help. Although an apparently straightforward initial value problem can be formulated to describe tank draining, it has only been applied to tanks of very simple geometry (i.e. flat bottomed cylinders); further, too little experience has been accumulated in analysis of this problem. However, analysis, has given the important dimensionless modelling parameters required for experimental investigation of the problem: the Froude ($Fr = V^2/Rg$) and Bond ($\rho g R^2/\sigma$) numbers.

Rather than outline the initial value problem indicated earlier, it is more instructive to indicate the derivation of a simple expression which predicts the critical depth at which blow-through occurs. It is expected that inertial forces play an important role in determining when blow-through occurs. This is best illustrated by a simple analysis of the quasi-steady-state flow in the relatively flat region near the drain of a tank (not at all necessarily a flat bottomed tank).

The purpose of this analysis is to establish an engineering criteria including the influence of surface tension on the draining of a propellant tank. The analysis of Lubin and Hurwitz (7.2) is extended to include surface forces. The analysis is necessarily

approximate to preserve a measure of simplicity, but the results seem to be physically reasonable. Further, the high-g limit has been experimentally verified. Consider the layer of liquid over the drain as shown in Figure 7-1, Bernoulli's equation is applied to the surface streamline in the vicinity of the tank drain.

$$p_{\infty 1} + \rho gh = p_{01} + \rho gh_o + \rho \frac{u_o^2}{2} \tag{7.2}$$

$$p_{\infty 2} = p_{02} \tag{7.3}$$

Substracting (7.2) and (7.3) gives

$$p_{\infty 2} - p_{\infty 2} - \rho gh = p_{02} - p_{01} - \rho gh_o - \rho \frac{u_o^2}{2} \tag{7.4}$$

Application of the steady-state Bernoulli equation implies the assumption that velocities are not changing with time. This assumption is justified by the fact that the rate of fall of the free-surface toward the drain is small compared to the liquid velocity over the lip of the drain – at least until blow-through occurs.

The pressure difference between liquid and vapor is given by

$$p_2 - p_1 = \sigma J \tag{7.5}$$

where σ is the surface tension and J is the local surface curvature. Approximations to the curvature are necessary in view of the complex geometry. This point is treated in detail later.

The use of the hemispherical control volume yields better results when the liquid height is away from the drain. The hemisphere (see Figure 7-1) is constructed such that the

chord at the "dip" region has a length equal to the drain radius. This is arbitrary but serves the purpose. Fluid mechanically the hemisphere supplies a control surface more nearly orthogonal to the streamlines for application of mass conservation. The volumetric flowrate Q into the drain expressed in terms of the fluid velocity in the dip region becomes

$$Q = u_o \; 2\pi \, h_o \sqrt{h_o^2 + r_o^2} \tag{7.6}$$

which gives

$$h = h_o + \frac{\sigma}{\rho g}(J_\infty - J_o) + \frac{Q^2}{4\pi^2 \, h_o^2 \left(h_o^2 + r_o^2\right)(2g)} \tag{7.7}$$

when substituted into (7.4).

At this point the criteria for blow-through is taken for mathematical purposes, to be

$$\frac{dh}{dh_o} = 0 \tag{7.8}$$

(This is not precise but physically represents the fact that the level h moves much slower than the level h_o at the onset of blow-through.)

Before (7.8) can be applied to (7.7), an expression for the curvature in terms of the quantities h and h_o is necessary. To reduce the geometry to such a simple relation is an assumption but does seem to have some physical implication. The role of surface tension is a passive one until the surface starts to dip. At this point, the local curvature is increased giving the surface forces a chance to restore the system to minimum potential energy. Thus, the onset of a depression in the surface leads to a restoring force as a result of surface tension. This is no different from the case where the gravitational forces attempt to keep the system at a minimum potential energy shape by bringing more liquid to the drain region as the surface depresses in draining.

At these points away from the dip region, the curvature is given by

$$J_\infty \approx \frac{2}{R} \tag{7.9}$$

where R is the tank radius. This is only an order of magnitude estimate. Using this value as a reference, the curvature at the dip region is approximated by

$$J_o \approx \frac{1}{R - \epsilon (h - h_o)} + \frac{1}{R - \epsilon (h - h_o)} \tag{7.10}$$

where $\epsilon \sim 1$ and relates the curvature to the characteristic length $h - h_o$ for this part of the problem. Taking $\epsilon \equiv 1$, it follows that

$$\sigma (J_\infty - J_o) \approx \sigma \left[\frac{2}{R} - \frac{2}{R - (h - h_o)} \right]$$

$$\approx \sigma \left[- \frac{2}{R^2} (h - h_o) \right] \tag{7.11}$$

This expression is adequate for establishing criteria on the important dimensionless groups.

If (7.11) is applied to (7.4) and (7.8), there results

$$h = h_o + \frac{Q^2}{8g \pi^2 h_o^2 \left(h_o^2 + r_o^2 \right) \left[1 + \frac{2\sigma}{\rho g R^2} \right]} \tag{7.12}$$

This equation is suitable for applying the blow-through criterion, (7.8). The blow-through condition is,*

$$\frac{Q^2}{g\, h_c^5\, (1 + 2/B)} = \frac{4\pi^2\, (1 + \alpha^2)^2}{(2 + \alpha^2)\left[1 + \frac{(1 + \alpha^2)}{2\,(2 + \alpha^2)}\right]^5} \tag{7.13}$$

where $\alpha = r_o/h_c$ and $B = \rho g\, R^2/\sigma$

Two important limiting cases may be obtained from this. When the critical height is much greater than the drain radius ($\alpha \ll 1$)

$$\frac{Q^2}{g\, h_c^5\, (1 + 2/B)} = 6.5 \tag{7.14}$$

and when the drain radius is much greater than the critical height ($\alpha \gg 1$)

$$\frac{Q^2}{g\, h_c^5\, (1 + 2/B)} = 5.19 \left(\frac{r_o}{h_c}\right)^2 \tag{7.15}$$

These last two equations can be put in a possibly more familiar form by relating flow rate Q to the liquid flowrate in the drain, e.g., $Q = \pi r_o^2 V_d$.

When this is done, Equation (7.14) becomes, for high g:

$$\left(\frac{h_c}{r_o}\right)^5 = 1.5 \frac{V_d^2}{r_o\, g} \tag{7.14a}$$

*The critical height h_{oc}, over the drain has been replaced by h_c, the critical height away from the drain.

and for zero g:

$$\left(\frac{h_c}{r_o}\right)^5 = 0.76\,\frac{\rho V_d^2\, r_o}{\sigma}\left(\frac{R}{r_o}\right)^2 \qquad (7.14b)$$

Similarly, Equation 7.15 becomes, for high-g:

$$\left(\frac{h_c}{r_o}\right)^3 = 1.9\,\frac{V_d^2}{r_o\, g} \qquad (7.15a)$$

and for low-g:

$$\left(\frac{h_c}{r_o}\right)^3 = 0.95\,\frac{\rho V_d^2\, r_o}{\sigma}\left(\frac{R}{r_o}\right)^2 \qquad (7.15b)$$

where V_d is the liquid velocity in the drain pipe, r_o the drain radius, and R the tank radius.

Others have presented experimental results or arguments related to the critical depth h_c or critical draining velocity under zero-g conditions.

Gluck, et al[7.3] report that experimental data indicates blow-through occurs under high-g conditions when the following Frande number condition is satisfied.

$$\frac{h_c}{r_o} = 0.86\ \tanh\left[1.3\left(\frac{V_m^2}{2g\, r_o}\right)^{0.29}\right] \qquad (7.16)$$

where V_m is the mean velocity of the free-surface.

Reynolds (7.4) has suggested a critical draining velocity for zero-g

$$We_{max} = \frac{D V_d^2 \rho}{\sigma} \approx 10 \left(\frac{D}{d}\right)^4 \tag{7.17}$$

where D is the tank diameter, d the drain diameter, V_d liquid velocity in the drain, ρ the liquid density, and σ the surface tension of the liquid. Experiments reported by Derdul et. al.[7.5] indicate that this expression is of the correct form but that the limit should be lower because when

$$We_{max} = \frac{\rho V_d^2 D}{\sigma} < 0.4 \left(\frac{D}{d}\right)^4 \tag{7.18}$$

the meniscus in a draining tank in zero-g suffers negligible distortion.

All of the expression for gravity dominated draining indicated in this section are plotted in Figure 7-2. Equations (7.14a) and (7.16) have been tested in certain ranges by experiments.

The expressions appropriate for zero-g draining are not plotted, but it can be observed from (7.17) and (7.18) that small drain rates are required if enormous trapped residuals are to be avoided. For example, $We_{max} = \rho V_d^2/\sigma \approx 30 \times 10^4$ for $R/r_o = 30$. If the criterion set by (7.18) is exceeded by even one order of magnitude, the ullage gas will punch through the liquid leaving the tank walls covered with a thick layer of liquid. Even further, as the meniscus approaches the drain, flow rates must be even further reduced. According to (7.14b), for example, if h_c/r_o is to be limited to 1, the Weber number $W_e = \rho V_d^2 r_o/\sigma$ must be about 0.0013 for normal tank/drain geometry ($R/r_o \sim 30$) which requires that $W_e = \rho V_d^2 D/\sigma$ be about 0.1.

At least when the tank Bond number is large, blow-through results from high liquid velocities in the vicinity of the tank drain. This suggests that increasing drain diameter will help delay blow-through. The use of a baffle over the drain has also been suggested as a means of reducing the critical depth and thence the quantity of liquid trapped in the tank.

The insertion of a baffle over the drain region of a tank changes the flow patterns in such a way that the kinetic energy for the downward flow is distributed more evenly over the tank area. Consequently, the inertial forces are reduced and one expects that the critical height for the initiation of pull-through is reduced.

Figure 7-3 is a sketch for the flow problem. The baffle is viewed as a flat plate with an annular cut-out of width δ. The diameter of the drain region is denoted by D_b. Other configurations can be analyzed in an identical fashion.

As in the previous development, Bernoulli's equation is applied to the free streamline,

$$\rho g h = \rho g h_o + \rho \frac{u_o^2}{2} \tag{7.19}$$

where surface tension is neglected for the moment. The hemispherical control volume over the drain for applying mass conservation is impractical here except for the case where liquid is close to the baffle, say, $h \sim 5\delta$. Consequently, the control surface sketched in Figure 7-3 is adopted.

The flowrate through the baffle is

$$\begin{aligned} Q &= u_o \left\{ \pi D_b h_o + \pi (D_b + \delta) h_o \right\} \\ &= u_o (\pi h_o) (2D_b + \delta) \end{aligned} \tag{7.20}$$

which gives

$$h = h_o + \frac{Q^2}{2\pi^2 g h_o^2 (2D_B + \delta)^2} \tag{7.21}$$

when substituted into (7.22).

Applying the blow-through criterion, $dh/dh_o = 0$ gives

$$\frac{Q^2}{g h_c^3 D_b^2 \left(1 + \frac{\delta}{2 D_b}\right)^2} = 4\pi^2 \approx 40 \tag{7.22}$$

which is compared with the case where the baffle is absent.

When this is cast into the form of the equations compared in Figure 7-2 (Equations 7.14a, 7-15a, and 7.16), there results

$$\left(\frac{h_c}{r_o}\right)^3 = 0.062 \frac{v^2}{g r_o} \frac{(r_o/R)^2}{(1 - 3\delta/4R)^2} \tag{7.23}$$

This is also plotted (for the particular case $R/r_o = 30$, $R/\delta = 10$) in Figure 7-2 as a comparison with the nonbaffle formulas. Clearly, a device such as this is of considerable help in reducing trapped residuals in rocket propellant tanks.

REFERENCES

7.1 Abramson, H. N., Chu, W. H., Garza, L. R., and Ransleben, G. E., Some Studies of Liquid Rotation and Vortexing in Rocket Propellant Tanks. NASA TN D-1212., Jan 1962

7.2 Lubin, B. T., and Hurwitz, M., "Vapor Pull-Through at a Tank Drain With and Without Dielectrophoretic Baffling", presented at conf. on Long-Term Cryo-Propellant Storage in Space, Geo. C. Marshall Spaceflight Center, Huntsville, Ala., Oct 12-13, 1966

7.3 Gluck, D. F., Gille, J. P., Simkin, D. J., and Zukoski, E. E., "Distortion of the Liquid Surface During Tank Discharge Under Low-g Conditions", Aerospace vol. of the A. I. C. h. E. Symposium Series, 1965, p. 150 ff.

7.4 Reynolds, W. C. and Satterlee, H. M., "Liquid Propellant Behavior at Low and Zero-g", Ch 11 of the Dynamic Behavior of Liquids in Moving Containers, NASA SP 106 H. N. Abramson ed., 1966, p. 423-4.

7.5 Derdul, J. D., Grubb, L. S., and Petrash, D. A., "Experimental Investigation of Liquid Outflow from Cylindrical Tanks During Weightlessness, NASA TN D-3746, Dec. 1966.

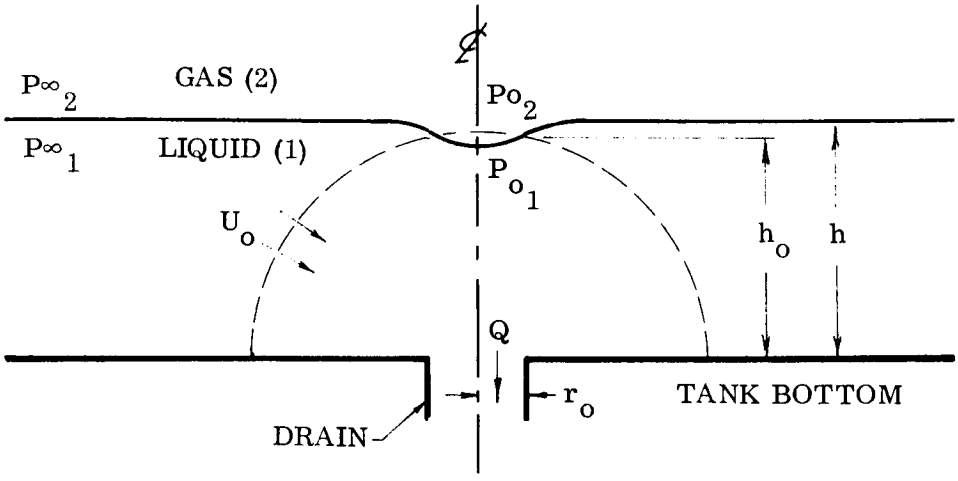

Figure 7-1 Blowthrough Analysis

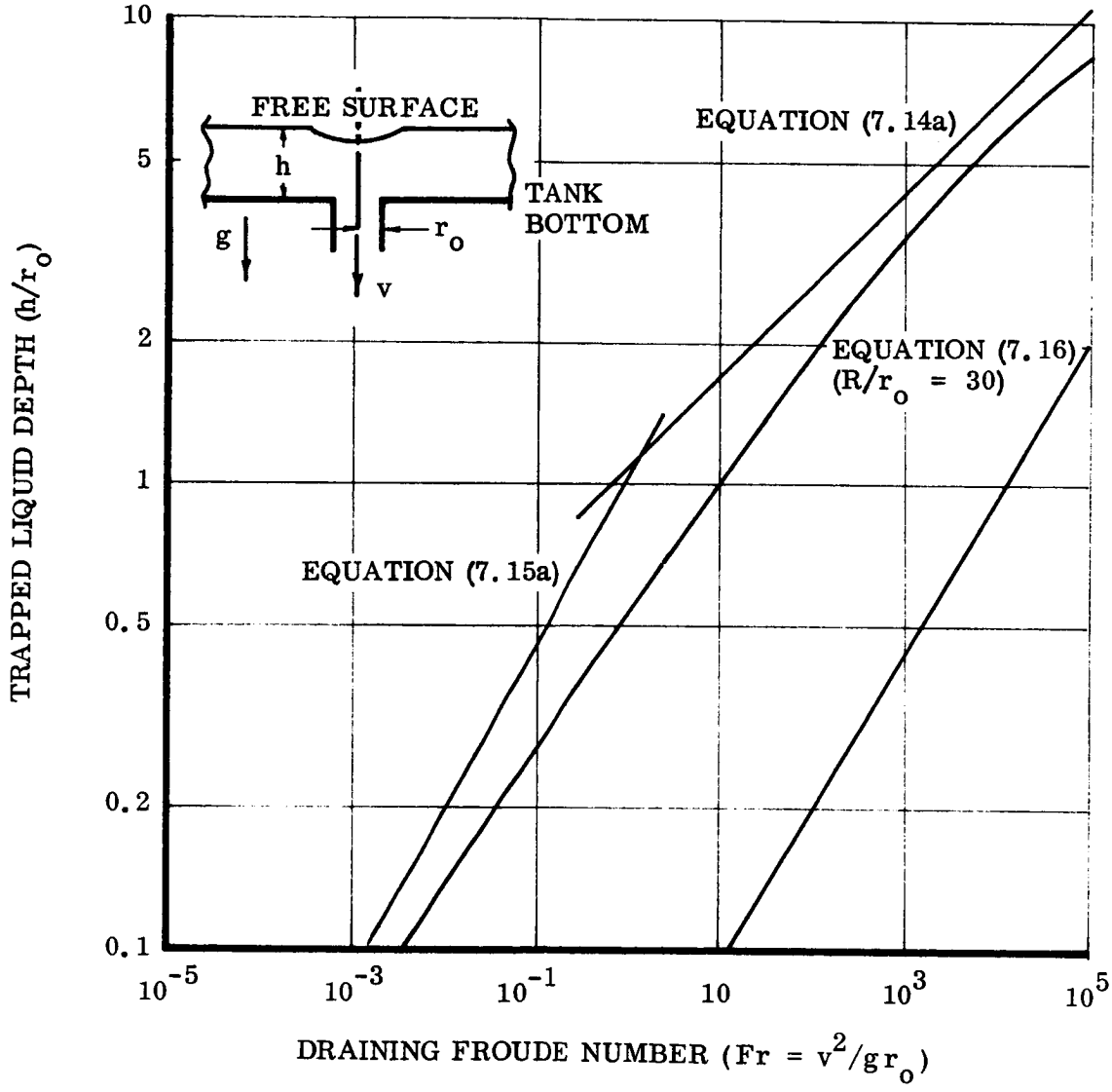

Figure 7-2 High-g Blowthrough Criteria

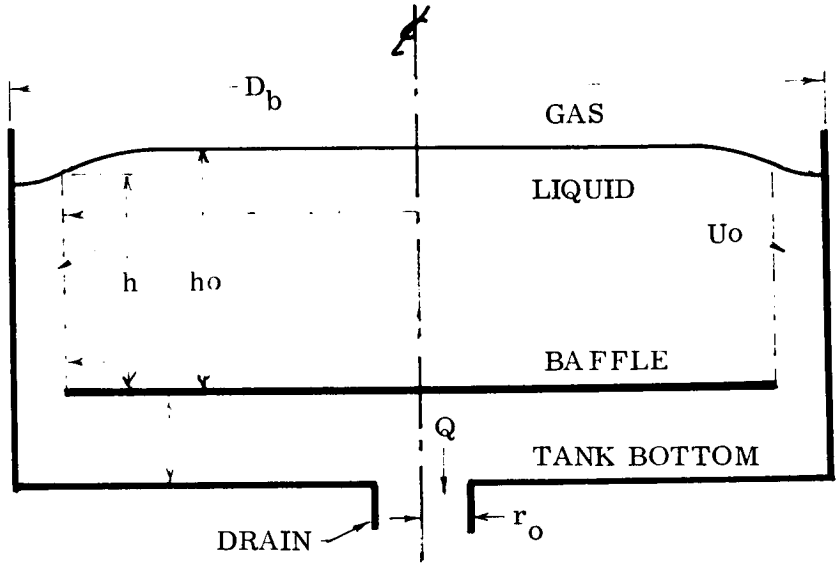

Figure 7-3 Blowthrough Analysis with Baffle

Section 8
HEAT TRANSFER TO SUBCOOLED PROPELLANTS

Rocket propulsion systems are subject to a wide variety of maladies which stem from improper temperature control of propellants or improper control over the flux of energy to or from the propellants. A few of these maladies are:

- Tank overpressure caused by too high a propellant temperature.
- Mixture ratio imbalance, especially in pressure-fed systems, caused by improper balance of temperature between propellant tanks.
- Gas generator malfunction due to poor propellant flow characteristics attributed, in turn, to the temperature imbalance.
- Propellant freezing.
- Propellant sludging or separation caused by poor temperature control, especially where the propellant is a mixture of two or more compounds
- Excess boiloff of cryogenic propellants
- Venting problems especially in cryogenic tanks under reduced-g conditions.
- Nonoptimal operation of pressurization system resulting from thermal stratification.

It is for these and a host of other problems that an understanding of heat transfer to and within propellant tanks is required.

Heat transfer and temperature control problems in space-borne rocket propellant tanks may be divided conveniently into two major classes depending on whether the propellant is space-storable or a cryogen. For these purposes, a space-storable propellant is one which, on the average, may be in thermal equilibrium with its environment, and a cryogenic propellant is one which may not. Cryogens, in this sense, are liquids whose temperatures are much lower than can be achieved by so-called passive temperature control techniques. The heat transfer and temperature control problem peculiar to each type of propellant will be discussed in turn.

HEAT TRANSFER IN STORABLE PROPELLANTS

In general, spacecraft, their tanks included, receive short wavelength thermal energy directly from the sun and reflected from other bodies such as the earth. They also receive longer wavelength thermal energy radiated from neighboring bodies (as the earth) by virtue of their temperature. Spacecraft, of course, reject thermal energy by radiation. Broadly stated, it is possible, through control the the absorptive and emissive properties of external surfaces of a spacecraft, to control its temperature.

An unprotected propellant tank may easily experience 150°F temperature variations from point-to-point and from time-to-time each orbit. Such temperature variations can give rise to motion of the liquids within storable propellant tanks and, for this reason, require discussion. Even further, the motions induced can affect the temperature distribution within the tank.

Very little specific work regarding the energy transport mechanisms acting within propellant tanks under low gravitational conditions has been accomplished. Assumptions valid under 1-g conditions might not be useful when the gravity level is reduced. The purpose of the following discussion is to illustrate the effects produced by the most likely energy transport mechanisms. It is hoped that this will aid the user in adapting other examples to cases of interest in the design of spacecraft propellant tanks.

The first energy transport mechanism requiring discussion is natural convection. The large temperature variations in the temperature of a tank wall would, under high-g conditions result in considerable natural convection inside the tank – in both the liquid and gas volumes. Under low-g conditions, natural convection will be much reduced, but not necessarily negligible. The dimensionless parameter governing the strength of the natural convection energy transport mechanism is the Rayleigh number.

$$Ra = \frac{g\beta L^3 \Delta T}{\nu^2} \frac{\mu C}{k}$$

where β is the volumetric coefficient of thermal expansion, ν, the kinematic viscosity, μ the dynamic viscosity, k the thermal conductivity, c the specific heat, and L the characteristic length for the system.

The Rayleigh number is as shown above, the product of the Grashoff number and the Prandtl number. The latter is a property of the fluid and does not vary widely among most liquids of interest. Thus, the Rayleigh number changes as the Grashoff number. In the context of heat transfer calculation for spacecraft propellants, the significant variation in the value of the Rayleigh number result from variation of g level, container size (or wetted tank length), and kinematic viscosity.

Natural convection within a propellant tank is more complicated than in other situations. The mechanism gives rise to important temperature nonuniformities inside the tank which complicate the use of standard natural convection heat transfer correlations. For example, the liquid in a container heated by the sun on one side and cooled on the other by radiation to space will circulate in a pattern resembling that shown in Figure 8-1a (assuming that the liquid is located as shown). Clearly, application of standard correlations is difficult, but in the absence of very specialized experiments or analysis, there is little choice.

The situation shown in Figure 8-1b is somewhat more complicated. When the heating takes place vertically as shown in this illustration, natural convection does not always occur. If the Rayleigh number based on tank radius is less than a critical value, natural convection circulation patterns doe not occur. Rayleigh numbers on the order of 500 to 2000 are required before circulation takes place.

The second energy transport mechanism of importance is associated with mass diffusion inside the tank. Consider the illustration shown in figure 8-2a. The tank shown has a thin layer at the hot end. The liquid will evaporate, its vapor will diffuse through the pressurizing gas filling the tank and will condense at the colder end of the tank. This process, of course, implies energy transport from the warm end to the

colder end. The diffusion process is expressed by rate equations drawn from Fick's law for diffusion plus the principle of conservation of mass for each species together with the rate equation for thermal energy. Theory is best obtained from texts such as that of Bird, Stewart, and Lightfoot[8.1].

Formulation of a problem of this sort is not difficult, but obtaining the solution is quite complicated unless the geometry is very simple. Further, natural convection in the gas can be induced by concentration gradients in the propellant vapor and ullage gas. This results from the fact that propellant vapors are usually very heavy compared to helium gas, the normal pressurant in storable propellant tanks.

A single example of the solution of the diffusion equations is offered. Consider the geometry in Figure 8-2b. A long thin tank is equipped with a capillary liquid locating device made from a porous material such as screen material. The ends are shown insulated (as would occur effectively by locating the tank between equipment sections at the same temperature as the propellants in the tank). Should the spacecraft now be shadowed from the sun, the tank wall will quickly cool causing evaporation of liquid from the standpipe, diffusion to the tank wall and condensation thereon.

The geometry shown in Figure 8-2 can be idealized as a cylinder with flat ends with all the liquid located along the tank axis such that the diffusion process is entirely radial. Solution of the governing equations for this case are approximately.

$$\frac{x_B}{x_{B1}} = \left(\frac{x_{B2}}{x_{B1}}\right)^{\frac{\ell n \frac{\rho}{\rho_1}}{\ell n \frac{\rho_2}{\rho_1}}} \tag{8.3}$$

where x_B is the mole fraction of helium gas with subscripts 1 and 2 denoting the appropriate value of x_B at the standpipe and at the tank wall where the propellant vapor is saturated at temperatures T_1 and T_2.

The molar flow of propellant vapor per unit length of cylinder is obtained from Fick's law

$$J_A = -2\pi r \frac{cD_{AB}}{1 - x_A} \frac{dx_A}{dr} = 2\pi r \frac{cD_{AB}}{x_B} \frac{dx_B}{dr} \qquad (8.4)$$

$$= 2\pi c D_{AB} \frac{\ln \frac{x_{B2}}{x_{B1}}}{\ln \frac{r_2}{r_1}}$$

where c is the concentration of the mixture. Typical values for physical constants and tank geometry sizes are

$D_{AB} = D_{He - N_2O_4} \sim 4.0 \times 10^{-4}$ ft^2/sec

$T_1 = 70°$ F

$T_2 = 40°$ F

$r_1 = 1/2$ ft

$r_2 = 2$ ft

The computed molar flow per unit length of tank is $J_A = 9.7$ lbm/hr. The approximate energy flow rate is given by

$$\vec{E} = J_A h_{fg_A}$$

where h_{fg_A} is the latent heat of vaporization of the propellant. For the example, $\vec{E} \approx 2000$ btu/hr for a tank 10 ft long. Even this moderate energy rate would tend to quickly cool the quantity of liquid held by the capillary retention standpipe. Reduction in total tank pressure would increase the importance of this mechanism.

The third mechanism for moving liquid propellants within their tanks involves the interaction of surface tension and temperature. The surface tension of liquids is a decreasing function of temperature, and disappears altogether at the critical point. Variation in the temperature of the free liquid surface gives rise to variations in the surface tension. This, in turn, results in a shear condition on the free surface. This is illustrated by the liquid layer shown in Figure 8-3. This problem is taken from the text by Landau and Lifshitz (8.2). Here, the temperature of the surface on which the liquid lies is nonuniform. If the layer is thin enough, the liquid temperature will not be a function of y and will have the same variation in x as does the underlying surface. The fluid pressure is

$$p = p_o + \rho g (h - y)$$

where p_o is the atmospheric pressure. The variation in pressure due to surface curvature can be neglected in this case. Considering that the fluid velocity is always parallel to the x axis, the Navier Stokes equation in the x direction may be used to determine the thickness of the layer as a function of x .

$$\mu \frac{\partial^2 u}{\partial y^2} = \frac{\partial p}{\partial x} = g \left[\frac{d}{dx} (\rho h) - y \frac{d\rho}{dx} \right]$$

subject to the boundary conditions at $y = 0$

$$u (x , o) = 0$$

and at $y = h$

$$\mu \frac{\partial u (x , h)}{\partial x} = \frac{d\sigma}{dx}$$

This equation may be integrated to obtain

$$\mu u = gy\left(h - \frac{y}{2}\right)\frac{d}{dx}(\rho h) - \frac{1}{6}gy\left(3h^2 - y^2\right)\frac{d\rho}{dx} - y\frac{d\sigma}{dx} \qquad (8.1)$$

For steady flow, the quantity of liquid passing a given section is zero

$$\int_0^h u\,dy = 0$$

Substitution of (8.1) here gives

$$\frac{\rho}{3}\frac{d^2h}{dx^2} + \frac{1}{4}h^2\frac{d\rho}{dx} = -\frac{1}{g}\frac{d\sigma}{dx}$$

which, when integrated assuming only small variations in σ and ρ with x

$$\left(\frac{h}{h_o}\right)^2 = \left(\frac{\rho_o}{\rho}\right)^{3/4} + 3\frac{\sigma_o}{\rho g h_o^2}\left(\frac{\sigma}{\sigma_o} - 1\right)$$

Note that the coefficient to the last term is the inverse of a Bond number based on liquid layer depth. For small Bond numbers, the variation can be great (to the extent of invalidating all the simplifying assumptions used).

Neglecting, for the moment, the fact that surface driven flows actually move liquids around within their tanks, it may be desirable to determine the effect of surface tension variation on the location of liquids in a tank. Here again, it is necessary to restrict attention to a specialized geometry, but one that is less special than that used in the previous example. Consider a small quantity of liquid located in a toroidal volume about the tank bottom. When the tank temperature is uniform, the liquid will

be uniformly distributed as shown by the solid curves. Assuming that the liquid temper- is a function only of angular location around the tank, the effect of temperature varia- tions on liquid location can be estimated. The pressure in the liquid must be constant, otherwise a net flow of liquid will occur. The pressure in the liquid is given by

$$p = p_g - \sigma J = p_g - \sigma\left(\frac{1}{r_1} + \frac{1}{r_2}\right)$$

where J is the curvature of the free surface and r_1 and r_2 are the principle radii of curvature of this meniscus. Assuming that these are approximately as shown in Figure 8-4. it is seen that variations in the free-surface curvature for this meniscus stem largely from variations in r_1. Equating liquid pressure at hot and cold locations, there obtains

$$\sigma_{Hot}\left(\frac{1}{r_1}\right)_{Hot} \approx \sigma_{Cold}\left(\frac{1}{r_1}\right)_{Cold}$$

and if the surface tension at the two locations is given by

$$\sigma = \sigma_{mean} - \frac{d\sigma}{dT}(T + \Delta T)$$

and if $r_{1_{Hot}}$ and $r_{1_{Cold}}$ are both reasonably close to $r_{1_{mean}}$

$$\frac{\Delta r_1}{r_{1_{mean}}} = \left|\frac{d\sigma}{dT}\right| \frac{\Delta T}{\sigma}$$

It is instructive to examine a numberical example: Propellant tanks of a typical space vehicle suffer a 150° F temperature difference from hot side to cold. Small

quantities of liquid remaining in a tank of the same geometry as shown in Figure 8-4 result in $r_1 \sim 1/2$ ft . The mean surface tension is typically 35 dynes/cm , and $|\, d\sigma/dT \,|$ about 0.1 dyne/cm-° C. Thus

$$\frac{\Delta r_1}{r_{1_{mean}}} = 0.12 \text{ ft}$$

Thus, this temperature variation can increase the radius r_i from 6 inches to about 7.5 inches on the cold side and reduce r_1 to 4.5 inches on the cold side. When it is recognized that the cross sectional area of the toroidal liquid volume varies approximately as the square of r_1 it can be seen that much of the liquid has been displaced toward the cold side of the propellant tank as in Figure 8-4.

HEAT TRANSFER IN CRYOGENIC PROPELLANTS

The temperature of cryogenic propellants are, as indicated, always below the lowest available temperature of external surfaces of the spacecraft. Consequently, heat is continuously transferred from the environment to the propellants through insulation and fixtures of a well designed cryogenic propellant tank. On the face of it, it might be assumed logically that the heat transfer to cryogenic propellants could be accurately estimated, and thus, for example, the pressure rise rate in the tank could be estimated as accurately. The first part of this is true to an acceptable degree, but it is not nearly as possible to accurately predict the pressure rise rate. The reason for this is that the pressure rise rate is influenced by the nonuniformity of temperatures within the liquid propellant and the gas or gases which fill the ullage volume in the tank. This nonuniformity makes it risky, at best, to use relations obtained from classical thermodynamics based on the assumption of thermodynamic equilibrium within the tank. The nature of the nonuniformity within the tank must therefore be examined in some detail. Consider the cylindrical tank shown in Figure 8-5. Here it is assumed that the heat being transferred to the tank enters only through the cylindrical

wall of the tank (this assumption will be examined a little later). A straightforward quasi-steady state analysis can be constructed which adequately described the state of temperature nonuniformity within the tank. based upon the assumption that all the heat entering the tank is entrained in a natural convection boundary layer which carries it toward the free-surface where it remains permanently in a stratified layer adjacent to the ullage space. Tellep and Harper (8.3) have presented such an analysis in the open literature and this has been amplified by Levy, et. al (8.4) They have used an integral boundary layer analysis to predict stratification within cryogenic propellant tanks. The basis idea is to write an expression for the rate of mass transfer toward the stratified layer at the free-surface. This is easily accomplished, because the mass flow rate in natural convection boundary layers may be obtained as a by-product of the standard analysis for predicting the natural convection heat transfer coefficients. This type of analysis can be used to predict the rate of growth of the stratified layer near the free-surface. The following relation has been obtained for laminar natural convection:

$$\frac{\Delta(t)}{H} = \left[1 - \frac{1}{1 - 0.62\left(\frac{H}{R}\right)\left(\frac{\nu t}{H^2}\right)\frac{Gr^{*1/3}}{Pr^{0.388}}}\right]^{+5}$$

This applies when the Prandtl number lies between 1 and 30 and when $\Delta(t) \leq H$. A corresponding relation is obtained for turbulent situations

$$\frac{\Delta(t)}{H} = 1 - \left[1 + 0.092\,\frac{H}{R}\left(\frac{\nu t}{H^2}\right)Pr^{-2/3}\left(\frac{Gr^*}{1 + 0.443\,Pr^{2/3}}\right)^{2/7}\right]^{-7}$$

In these relations, the Grashoff number has been defined as

$$Gr^* = \frac{g\beta R^4 q}{k\nu^2}$$

so that it is expressed in terms of the heat flux through the tank wall q rather than in terms of the temperature difference between the tank wall and the bulk liquid.

The dividing line between laminar and turbulent regimes occurs when the modified Rayleigh number is in the neighborhood of 10^{11} .

$$Ra^* = (Gr^*) Pr$$

The method suggested here is superior for most practical situations than the more elegant method of finite differencing the continuity, momentum, and energy equations and solving them numerically as an boundary-initial value problem. The utility of this method is limited to laminar situations and the computer time required for a solution which has been reported (8.5) appears excessive considering the accuracy of the more approximate method when compared with available experimental data.

Neither the integral-boundary layer analysis or the finite difference method predict the heat transfer situation within storable propellant tanks. The rate of growth of the stratified layer is so great that the whole liquid volume should be considered as a single lump rather than a stratified layer.

In the development of the relations just presented, it was assumed that the heat transfer to the tank occurred solely through the cylindrical wall of the tank. Heat transfer through the bottom of the tank can be easily superimposed on the foregoing results because bottom heating usually results in a mixing action. The heated liquid at the bottom of the tank is unstable if the Rayleigh number as previously defined exceeds 2000. The temperature distribution can be thus considered to be that predicted by the relationships for stratification resulting from sidewall heating added to the bulk temperature rise easily computed using the bottom heating alone.

Analyses of the types mentioned above are frequently adequate to evaluate a propellant tank-storage design. Where more definitive models are required, or possibly additional empirical data, these approaches can be useful in placing the problem in some perspective.

REFERENCES

8.1 Bird, R. B., Stewart, W. E., and Lightfoot, E. N.: Transport Phenomena, Wiley, New York, 1960, Ch. 16 and 17.

8.2 Landau, L. D., and Lifschitz, E. M.: Fluid Mechanics, Addison-Wesley, Reading, Mass., 1959, pp 236-7.

8.3 Tellep, D. W., and Harper, E. Y.: "Approximate Analysis of Propellant Stratification," AIAA Jour., Vol. 1, No. 8, Aug 1963, pp 1954 ff

8.4 Levy, A. M., Chin, J. H., Donaldson, J. O., Gallagher, L. W., Harper, E. Y., Hurd, S. E., and Satterlee, H. M.: Analytical and Experimental Study of Liquid Orientation and Stratification in Standard and Reduced Gravity Fields, Lockheed Missiles & Space Co., Rpt No. 2-05-64-1, July 1964 (prepared under contract no. NAS 8-11525 for NASA-MSFC, Huntsville, Ala.)

8.5 Clark, J. A., and Barakat, H. Z.: Transient, Laminar, Free-Convection Heat and Mass Transfer in Closed, Partially Filled, Liquid Containers. University of Michigan Dept. Mech. Engr., Rpt no. 04268-6-T, Jan. 1964 (prepared for NASA-MSFC, Huntsville, Ala., and contract no. NAS-8-825).

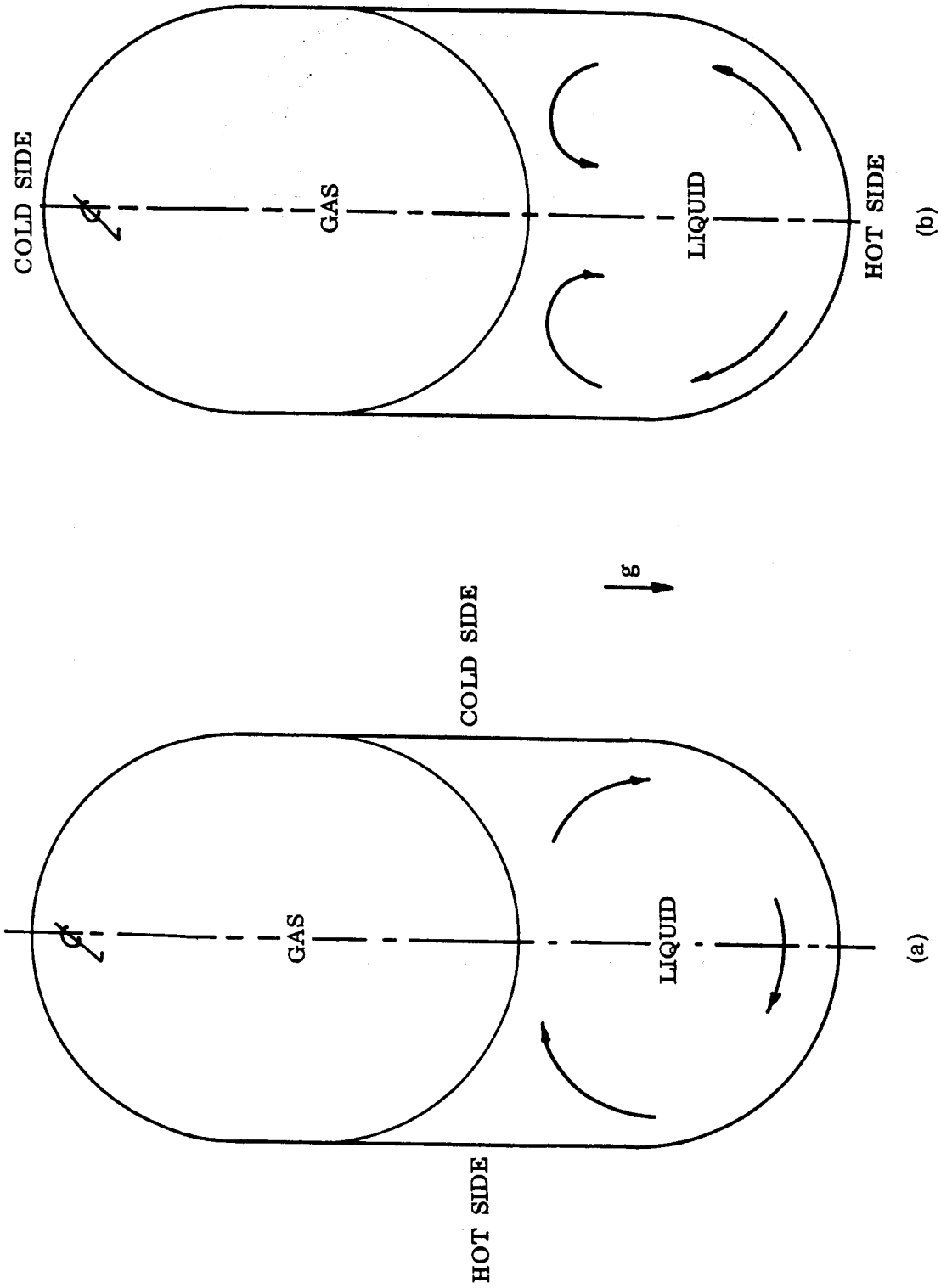

Figure 8-1 Natural Convection Patterns

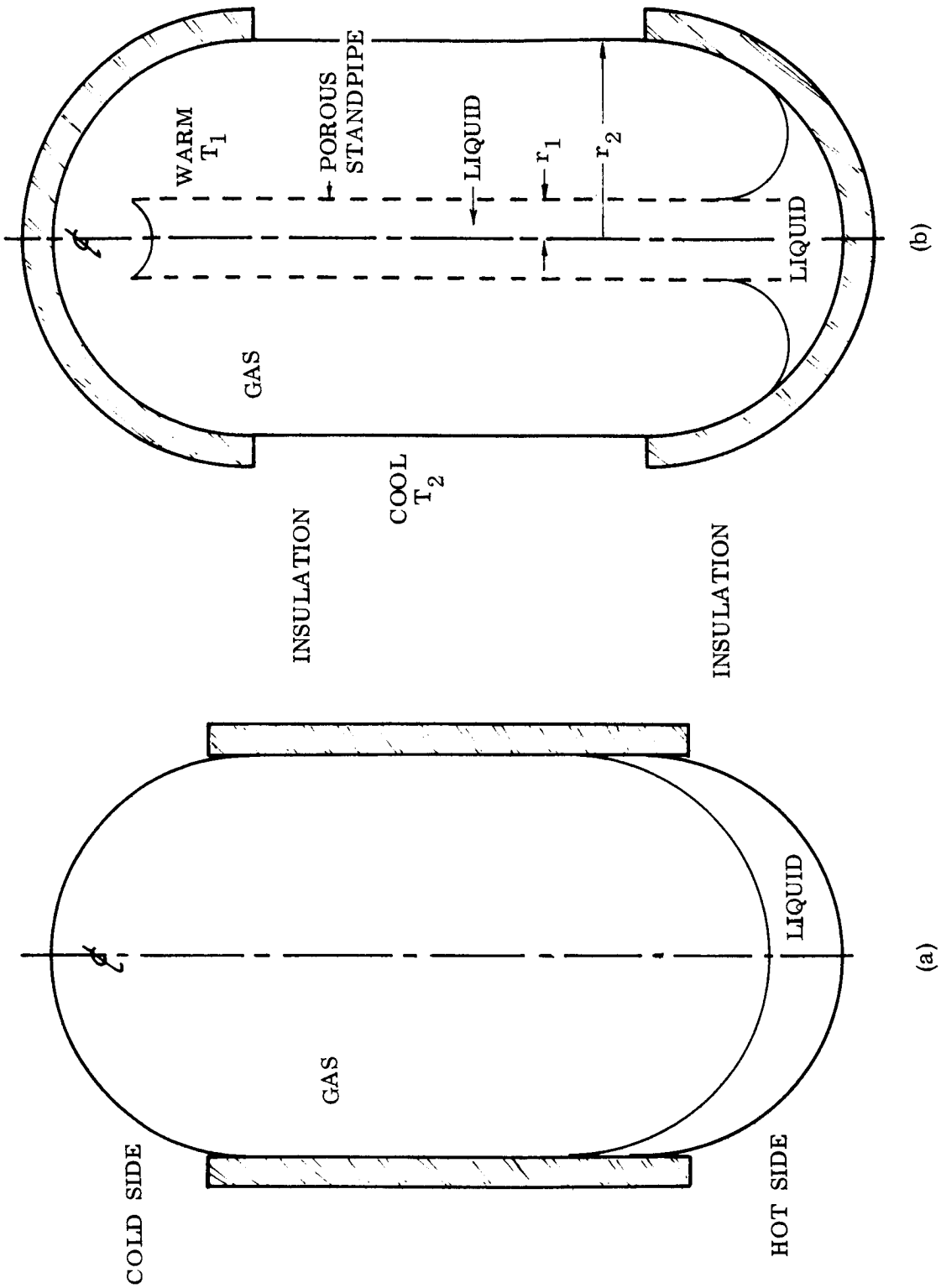

Figure 8-2 Diffusion Mass/Energy Transport Patterns

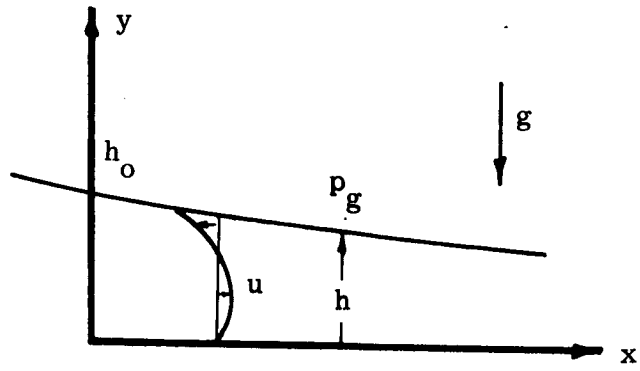

Figure 8-3 Liquid Motion Driven by Differential Surface Tension

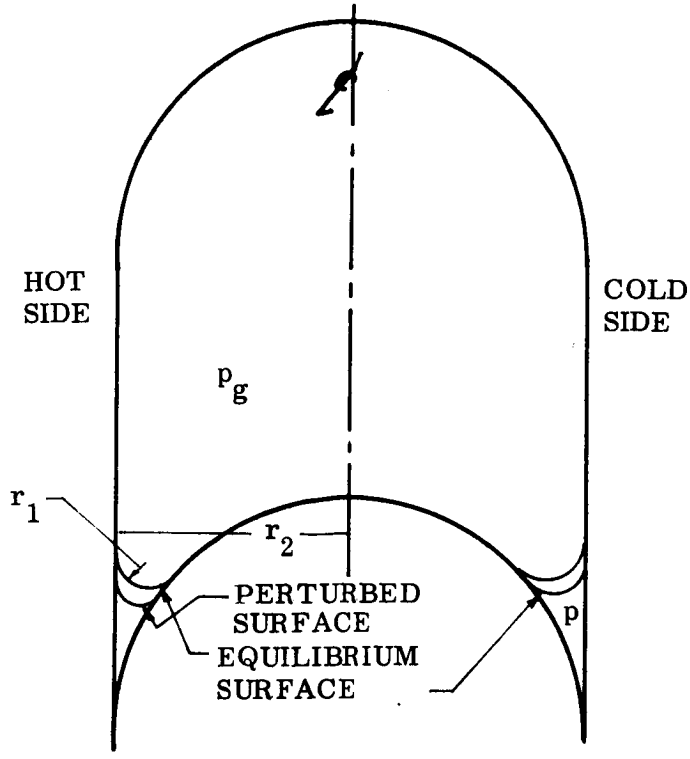

Figure 8-4 Free-Surface Displacement by Differential Surface Tension

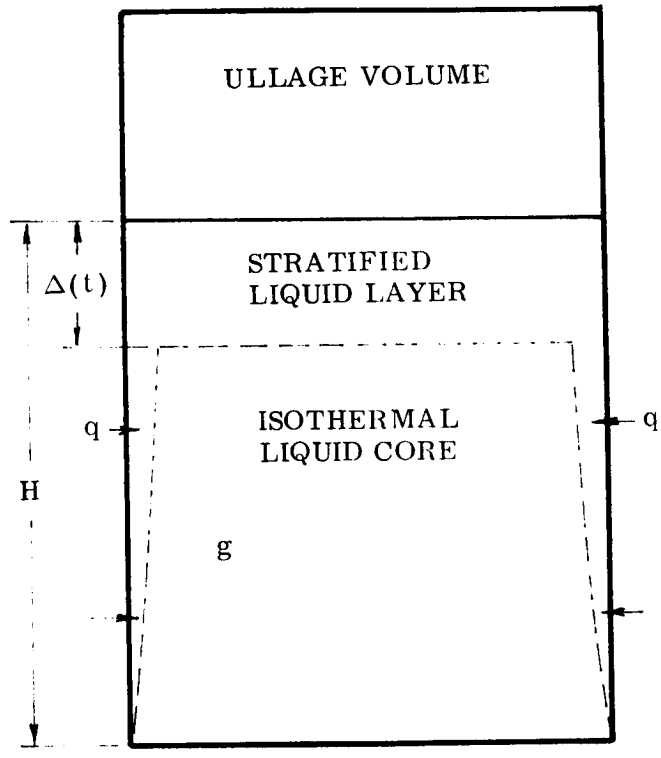

Figure 8-5 Geometry — Natural Convection Stabilization in a Cryogenic Propellant Tank

Section 9
LOW GRAVITY TESTING

As in other subjects, low gravity experimentation provides information that aids in three ways toward the understanding of a particular phenomena. Experimental simulation under controlled conditions can provide insight that serves as a guide to analysis. Having an analytic description of the phenomena, experimentation can then be used to check the validity of the predictions and the analytic model. Finally, in those instances where analytic tools are not available, experimental correlations in terms of modeling parameters that exhibit at least the gross characteristics of the particular phenomena can often be obtained. Aside from the obvious necessity to study liquid behavior at zero or low gravity this environment can also be used to condition the test liquid for an environment which is gravity dominated and in a full scale situation follows or precedes a period of low or zero gravity.

SIMILARITY

The proper modeling of a low gravity condition depends on the attainment of geometric and dynamic similitude between the model and the full scale prototype. Dynamic similitude is obtained by duplicating in the model the ratio of the forces governing the fluid behavior. These dimensionless force ratios become the governing parameters of the experiment. The essence of zero- or low-gravity testing is the attainment of a proper balance between weak interfacial tension forces, acceleration-induced body forces, inertia forces and viscous forces. The dimensionless ratio expressing the balance between surface tension forces and acceleration induced body forces is the Bond number written as $(\rho_1 - \rho_2)\, g\, L^2/\sigma$ where ρ_2 is the density of the upper fluid, ρ_1 the density of the lower fluid, σ the interfacial tension between the fluids, g the local acceleration, and L an appropriate container dimension.

In the case of spacecraft propellant tanks, the density of the upper fluid, being a gas, is significantly less than that for the lower fluid and is neglected in writing the Bond number. The Weber number We, expresses the ratio of the liquid inertia forces present to the surface tension forces and is written as

$$We = \frac{\rho V^2 L}{\sigma}$$

where V is the characteristic fluid velocity, and L a characteristic dimension. Finally the Reynolds number expresses the balance between the inertial forces in the liquid and viscous forces. Simulation of low gravity phenomena also requires that the contact angle between the test liquid and the container be maintained between the prototype and the model. For most spacecraft applications the contact angle between the propellant and the tank wall is very low, being 5° or less.

It is not generally possible to provide similarity in all of the areas above. Although a variation in fluid properties can be obtained by selecting a particular test liquid to provide simulation, the range of properties obtainable is not large when one is restricted to test liquids that can be handled in the laboratory and that have good wetting characteristics, i.e., low contact angle with the model containers. Generally, simulation of the Bond number is of primary interest. However, if the prototype Bond number is significantly low ($Bo > 0.01$) exact duplication from the prototype to the model is not necessary. In the range $100 > Bo > 0.01$, care should be taken to maintain Bond number simulation. Similarly in those situations involving fluid inertia maintenance of Weber number between model and prototype in the range $100 > We > 0.01$ is probably necessary. It is not generally possible with common test liquids to meet the requirements of Bond number and Weber number simulation and also satisfy Reynolds number simulation. Since most phenomena in large scale spacecraft propellant tanks are not viscous dominated it is sufficient in model testing to provide Reynolds numbers in the turbulent range.

The response time of the model relative to the prototype depends upon whether the phenomena is gravity or capillary dominated. In a gravity dominated regime ($Bo > 10$) time scaling is proportional to $\sqrt{L/g}$. For capillary dominated regimes response is proportionate to $\sqrt{L^3 \rho/\sigma}$. The above time scaling considerations are of particular importance in experiment design which will be discussed below.

TEST TECHNIQUES

The general techniques for providing or simulating a low gravity environment fall into two broad categories: bench tests at standard gravity conditions, and tests at reduced gravity conditions. Consideration of the Bond number indicates that characteristic dimension has a significant effect on the size and that a reduction in Bond number can be obtained even under standard gravity conditions by sufficiently reducing the size of the experiment. For example, suppose we are interested in studying the sloshing frequencies of a propellant in a large tank at 10^{-4} g_o. The dimensionless frequency, $\Omega = \omega \sqrt{\rho r^3/\sigma}$, in the absence of viscous effects is a function only of the Bond number. The Bond number will be maintained in a bench test in 1/100 scale model if a test liquid is employed having a value of σ/ρ equal to that of the prototype. If the general size of the prototype is of the order of 10 meters the model size is sufficiently large to be manageable. Generally, however, bench testing requires model sizes so small that goemetric similitude, contact angle maintenance and viscous effects become problems.

Since the form of the Bond number considers the effect of the density of a fluid above the interface, simulation of surface tension dominated phenomena can be obtained at standard gravity by replacing the gas with an immiscible liquid of nearly equal density to the liquid simulating the prototype. In this manner the hydrostatic pressure difference across the interface between the two liquids is reduced and the Bond number becomes a function of the density difference. For a given Bond number condition in this case the size of the experiment is limited by the density difference that can be measured and maintained in a test. Density differences of the order 10^{-4} gm/cc can be accurately measured using an analytic balance and a pycnometer. Measurement of

differences as low as 10^{-6} gm/cc by measuring the drift rate of a drop of one liquid in the other in a Stokes flow regime appears feasible. Major drawbacks of this test technique are concerned with the practical problem of simulating the low contact angle required and the introduction of viscous effects due to the upper liquid.

Testing at reduced gravities is accomplished in three ways: drop tower, aircraft, and orbital flights. Of these three by far the most useful tool in terms of economy, availability, and test control is the drop tower. Approximate test time can be calculated with relation below.

$$T = 0.248 \sqrt{h}$$

where h is measured in feet and T in seconds.

A test module encapsulated within a drag shield is usually employed. The drag shield, by virtue of its mass, is relatively unaffected by air drag. The test module is usually not attached to the drag shield and remains free to travel in a relatively drag free environment provided by the low relative velocity between the drag shield and the test module. The test module usually contains all of the test conditioning and measuring equipment. Test accelerations can be provided by applying a small force to the test module during free fall. To accomplish this such techniques as connecting the drag shield and the test module with constant force type springs have been employed. A small cold gas thrust system mounted on the test module provides the most flexibility. Such a system allows the experimenter to easily vary acceleration level from one test to another by changing the thrust system output as well as to vary the thrust initiation time and its duration during the free fall test period.

Test times in the drop tower are restricted by limitations associated with the drop tower height. A 100 ft. of free fall seems to be the practical compromise for a drop tower. This allows 2-1/2 seconds of test time. The small additional time obtained in towers with longer free fall distances is purchased at the expense of increased

problems associated with catching and arresting the drag shield and test module, and the increased effects of air drag.

Reduced gravity conditions can also be provided in an aircraft executing a Keplerian trajectory. In this method of free fall, testing times of the order of 32 seconds are theoretically possible with a jet transport type aircraft. Test capsules free floating in the aircraft cabin isolate the experiment from the aircraft. Because of the extended test times experiments of larger scale than those in drop towers are possible. However, aircraft testing has drawbacks. It is difficult for the pilot to keep the aircraft on precise trajectory required within the limits of the aircraft size. Thus collisions between the test module and the aircraft occur reducing the test time. This type of maneuver places large stress loadings on the aircraft and the costs per flight are high. Finally, the maneuvers of the aircraft prior to entering the Keplerian trajectory generate a great deal of agitation in the test liquid, reducing the control over the initial condition of the test.

Tests conducted on orbit offer the greatest opportunity for extended times in a zero or low gravity environment and in the future this will become the primary mode of testing. From a practical standpoint these tests should be conducted on manned orbital flights to reduce the problems associated with data recovery and remote test control.

EXPERIMENT DESIGN CONSIDERATIONS

The design of tests in a reduced gravity environment is primarily dependent upon the available test time. The time scaling considerations discussed earlier together with the properties of the test fluid provided an upper limit on the size of the simulated propellant tank. For example, suppose we desire to conduct a drop tower test composed of an initial period T_1 of zero gravity followed by a period of propellant motion T_2 at some low gravity condition. Further, suppose that we are performing a test in the drop tower in which three seconds is the available test time. The capillary response time for the reorientation liquids from the flat initial condition to the zero g condition

under capillary forces can be estimated from the relation $T = K\left(D^3/\beta\right)^{1/2}$

where

D = container diameter

β = ratio of kinematic surface tension to density

K = 0.17

T = period for 1/4 cycle of surface oscillation.

Allowing 3/4 of a cycle to obtain relative stable equilibrium we have

$$T_1 = 0.51 \sqrt{D^3/\beta}$$

The gravity dominated behavior to be studied following this period is scaled with the relation

$$T_2 = \sqrt{2L/g}$$

Combining these two relations we now have

$$T_1 + T_2 = 0.51 \sqrt{D^3/\beta} + 1.4 \sqrt{L/g} \geq 3$$

This together with the ratio of container length to diameter L/D sizes the test for a particular g level. If we desire to conduct a test with a liquid having $\beta = 30\ cm^3/sec^2$ and an acceleration level of $10^{-2}\ g_o$ in a container of 2.5-cm radius the above expression indicates that the container length L should be 14.3 cm.

Since the major portion of the information obtained from a low gravity test is obtained visually, generally on motion picture film, attention should be given to proper lighting in the design of the experiment. For most tests for which information about the interface shape and trajectory is desired, diffuse back lighting of the experiment with respect to the camera viewing axis usually provides excellent results in terms of contrast.

In many tests measurement of the level of acceleration is also desired. An economical technique for sensing acceleration level is to employ a bearing ball in an enclosed container. The trajectory of the ball provides an indication of the direction and level of acceleration. This technique is accurate within 10 percent for acceleration levels down to $10^{-2} g_o$. Below this acceleration level, accurate measurements become uneconomical. Acceleration information can also be obtained from calibrations of the spring force or thrust system employed on the test module.